Scuola Dottorale di Ateneo Graduate School

Università Ca' Foscari di Venezia

DOTTORATO DI RICERCA IN

Science and Management of Climate Change - *Dynamic Climatology*

Ciclo XXVIII - Anno 2016

Atlantic Multidecadal Variability in an ensemble of multi-century climate simulations

Settore scientifico-disciplinare di afferenza: FIS/06

Tesi di Dottorato di **Irene Mavilia** (matr. 955983)

Coordinatore del Dottorato:

Prof. Carlo Barbante

Tutor:

Dr. Alessio Bellucci

Co-tutor:

Dr. Silvio Gualdi

Abstract

The Atlantic Multidecadal Variability (AMV) is a coherent pattern of variability of the North Atlantic Sea Surface Temperature (NA SST) field affecting several components of the climate system in the Atlantic region and the surrounding areas. Our current knowledge of the AMV is based on a relatively short observational record, which severely limits our understanding of the mechanisms involved, as well as the characterisation of the low-frequency tail of the variability spectrum. In order to quantify accurately the contribution of anthropogenic forcings to the observed climatic changes, it is essential to understand better the natural climate variability occurring at long time scales. Here, AMV is examined in a set of multi-century preindustrial climate simulations performed with different coupled general circulation models. In these simulations the AMV exhibits a non-stationary behaviour, which is objectively assessed via a statistical test starting from the null hypothesis of a statistically stationary AMV, whose modulation is entirely random. The large-scale teleconnection patterns associated with the AMV evolution and the relationship between the detected AMV behaviour and the variability of the Atlantic meridional overturning circulation (AMOC) are inspected. A multi-model

analysis of the AMV allows us to investigate similarities and differences across an ensemble of state-of-the-art climate models and to identify the prominent simulated modes of variability involving different atmosphere-ocean interactions over decadal and longer time scales. In most of the models a shorter time scale mode ($\sim$20 years) seems to alternate with a longer time scale mode ($\sim$60 years) with a gradual shift from one to another across different epochs. The shorter time scale appears to be associated to a NA SST tripole pattern that corresponds to a NAO-like forcing; whereas the longer time scale features an AMV-like monopole for the SST spatial pattern, which corresponds to a weaker coupling with the atmosphere. Since these modes are particularly evident in the MPI-ESM-P model, this is chosen as a case study to deepen the dynamical explanation of AMV behaviour: its AMV spectrum presents two distinct peaks, corresponding to a short time scale (20-40-year band) and a long time scale (40-80-year band). Results show that the non-stationarity of the entire time series is mostly due to the long time scale, and that the difference between the two modes is due to the driving role of salinity on circulation that prevails at the long time scale. The non-stationary behaviour identified in most models suggests that the character of the observed AMV may undergo significant changes in the future. This ongoing analysis will provide further insight into the dynamics of the AMV variability.

Sommario

La variabilità multidecadale dell'Atlantico (Atlantic Multidecadal Variability, AMV) è un pattern coerente di variabilità della temperatura superficiale del Nord Atlantico (North Atlantic Sea Surface Temperature, NA SST), che incide su diverse componenti del sistema climatico nella regione dell'Atlantico e nelle aree circostanti. La nostra conoscenza attuale dell'AMV è basata su un record di osservazioni relativamente breve, che limita duramente la nostra comprensione dei meccanismi coinvolti, così come la caratterizzazione della coda a bassa frequenza dello spettro di variabilità. Allo scopo di quantificare accuratamente il contributo antropogenico ai cambiamenti climatici osservati, è essenziale capire meglio la variabilità climatica naturale che avviene a scale temporali lunghe. In questo studio, l'AMV è esaminato in un insieme di simulazioni climatiche multisecolari e preindustriali, ottenute da diversi modelli accoppiati di circolazione generale. In queste simulazioni l'AMV mostra un comportamento non stazionario, che è valutato oggettivamente mediante un test statistico. Sono analizzati i pattern di teleconnessione a larga scala associati all'evoluzione dell'AMV e la relazione tra il comportamento dell'AMV e l'Atlantic meridional overturning circulation (AMOC). Un'analisi multi-modello

dell'AMV ci permette di investigare le somiglianze e le differenze in un insieme di modelli climatici allo stato dell'arte e di identificare i modi di variabilità prevalenti che implicano diverse interazioni atmosfera-oceano su scale decadali e più lunghe. Nella maggior parte dei modelli, una scala temporale più corta (∼20 anni) sembra alternarsi a una scala temporale più lunga (∼60 anni) con un passaggio graduale da una all'altra attraverso le varie epoche. La scala più corta appare essere associata a un pattern di tripolo per le NA SST che corrisponde a un forzante di tipo-NAO; mentre la scala più lunga presenta un pattern monopolare per le SST, tipo-AMV, che corrisponde a un accoppiamento più debole con l'atmosfera. Poiché questi modi sono particolarmente evidenti nel modello MPI-ESM-P, questo è stato scelto come caso studio per approfondire la spiegazione dinamica del comportamento dell'AMV: il suo spettro dell'AMV presenta due picchi distinti, corrispondenti a una scala temporale corta (nella banda 20-40 anni) e una scala temporale lunga (nella banda 40-80 anni). I risultati mostrano che la non stazionarietà dell'intera serie temporale è dovuta principalmente alla scala temporale lunga, e che la differenza tra i due modi dipende dal ruolo della salinità come guida della circolazione, che prevale per la scala lunga. Il comportamento non stazionario identificato nella maggior parte dei modelli suggerisce che il carattere dell'AMV osservato potrebbe subire cambiamenti significativi in futuro. Quest'analisi, tuttora in corso, fornirà una nuova comprensione sulla dinamica della variabilità dell'AMV.

Acknowledgements

I would like to express my gratitude to my advisor Alessio Bellucci for his continuous help and guidance during the years of my PhD study, and to my co-tutor Silvio Gualdi for his advices and encouragement to my work, helping me to focus on the relevant research questions. Special thanks to Panos Athanasiadis who is always available for scientific discussions, stimulating ideas and motivating me to improve the research. I have been learning a lot also from other several people at CMCC, which brings together a wide range of competences on climate. Mutual support from my colleagues has been also very important to bring the thesis to completion. I would like to give many thanks to Rym Msadek for giving me the opportunity to visit GFDL in Princeton, which has been extremely valuable to me, and for her advices always accurate and comprehensive. I really appreciate the help and patience from Yohan Ruprich-Robert who has taught me a lot. The overall experience at GFDL makes me even more motivated and dedicated to this job. Thanks to my partner, my family and my friends to be always on my side.

Contents

Chapter 1

Introduction

1.1 Motivation

The climate system exhibits considerable variability on a wide range of temporal scales, ranging from interannual to millions of years. A better comprehension of mechanisms that determine natural internal climate variability occurring over multidecadal time scales is critical for the problem of anthropogenic signal detection: it is essential to understand the background natural climate variability on which external influences are superimposed, so as to better disentangle the relative contribution of anthropogenic and natural drivers of climate variability. Additionally, human-induced warming of the climate system in the future will be modulated by natural climate variability.

Due to the shortness of the observed record, variability on multidecadal time scales is poorly understood. Since observed records last 100-150 years at most, too few multidecadal variation cycles of climate variables or indices can be detected; as a result the multidecadal component of climate variability spectrum is only

marginally resolved. Moreover, records of observations must also deal with sparse and changing observing systems. Paleoclimatology provides a mean of assessing climatic variations before the beginning of instrumental records, but proxy data have some limitations: they are subject to dating errors and microenvironmental effects, they often remain limited to the proxy sites and they are also potentially limited in their ability to represent climatic variations over a range of different time scales [Jones et al., 1998].

An intriguing aspect of long-term climate variability is the non-stationarity: a time series is stationary if its mean is constant and its autocorrelation depends only on the lag (Wide Sense Stationarity WSS). In the climate context, continuous modifications in the processes influencing that variable potentially result in a non stationary behaviour where the statistical properties depend on the particular time in question. In literature various studies, using both models and data, reveal this aspect. Among others, two illustrative examples regard the El Niño/La Niña-Southern Oscillation (ENSO), that is a climate pattern that occurs across the tropical Pacific Ocean due to the coupled variations of surface sea temperature and air pressure; and the North Atlantic Oscillation (NAO), that is a fluctuation in sea level pressure difference between the Icelandic Low and the Azores High.

Based on a 2000-year simulation, performed with the global coupled GFDL-CM2.1 model, Wittenberg [2009] identifies different regimes of different durations, in ENSO modulations: see in Figure 1.1 multidecadal epochs with hardly any variability (M5); epochs with intense, warm-skewed ENSO events (M7); epochs with moderate, nearly sinusoidal ENSO events (M2); and epochs that are highly irregular in amplitude and period (M6). Occasional epochs mimic detailed temporal sequences of observed ENSO events (e.g. R2 and M6, R1 and M1), but a different

150-year interval may not contain the same oscillation. These results suggest that the observed ENSO over the past 150 years of measurements may be not truly representative of ENSO longer-term behaviour, since it is not sufficient to resolve the temporal variability of ENSO.

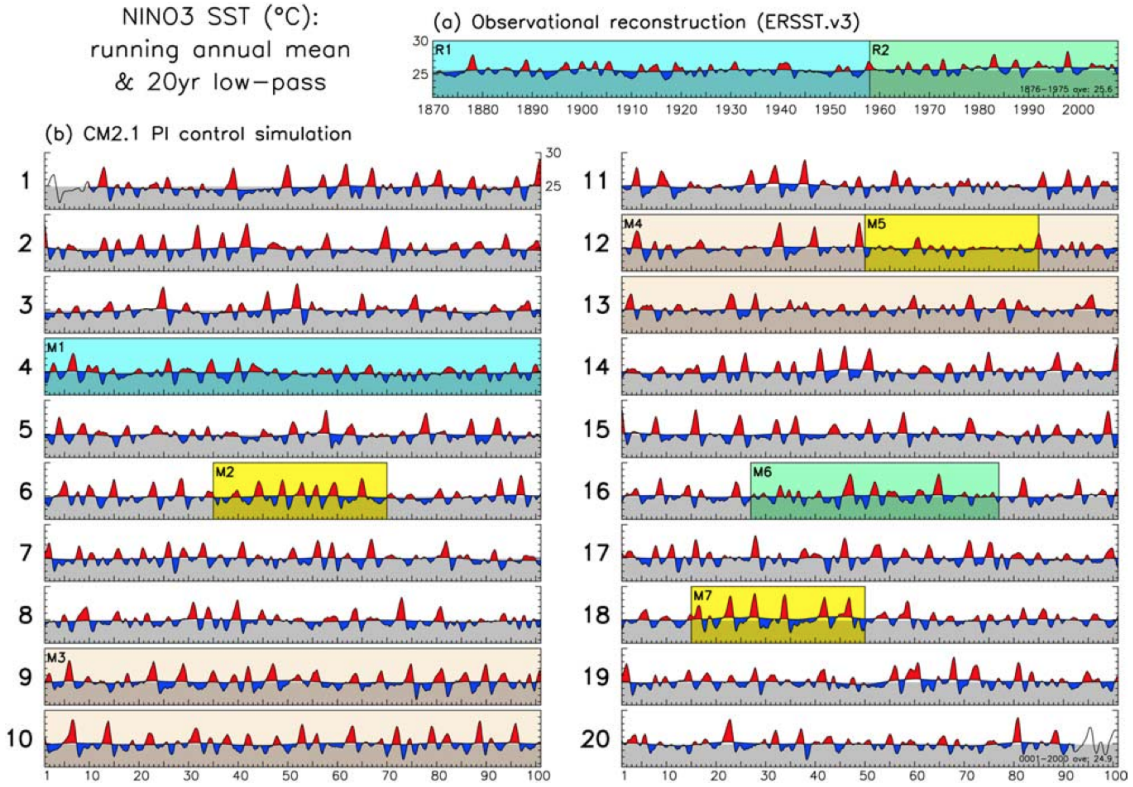

Figure 1.1: *SST (°C) averaged over the NINO3 region, for (a) observations and (b) the 20 consecutive centuries (numbered) from the GFDL-CM2.1 model [Wittenberg, 2009].*

With regard to NAO, Hurrell and Van Loon [1997] notice a non-stationary behaviour in the time evolution of the NAO over the 130 winters 1865-1994. In Figure 1.2 the time evolution of NAO is shown as a contour plot of the power spectra computed for running 60 years: large part of NAO variance at biennial periods comes from the early part of the record, while the variability between 6

and 10 years is more prominent over the latter half of the twentieth-century. There is a shift in the period associated to the largest variability.

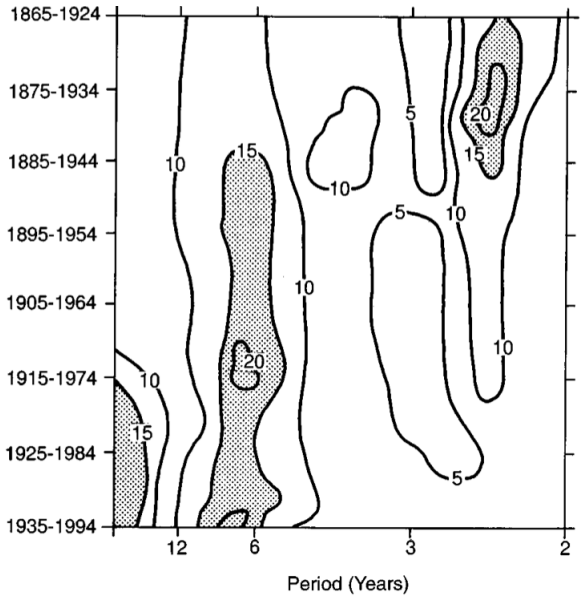

Figure 1.2: *Power spectra of the winter (December-March) NAO index for running 60-year intervals; variances greater than 0.15 mb^2 frequency^{-1} are stippled [Hurrell and Van Loon, 1997].*

Non-stationary behaviour in low-frequency internal variability appears, therefore, from studies based both on models and observations.

Another low-frequency mode of variability is the Atlantic Multidecadal Variability (AMV): it is identified as a coherent pattern of oscillatory changes in North Atlantic sea surface temperature; during positive (negative) AMV phases the sea surface temperature is anomalously warm (cold) over most of the North Atlantic. AMV was found to be a natural mode, internal to the climate system, with a period of the order of 60-80 years [Schlesinger and Ramankutty, 1994; Kushnir, 1994]. These multidecadal variations have been observed in instrumental data [Enfield et al., 2001; Trenberth and Shea, 2006; Deser and Blackmon, 1993] and paleo-proxy

records [Delworth and Mann, 2000; Gray et al., 2004; Kilbourne et al., 2014; Saenger et al., 2009]. A number of studies have demonstrated the connection between the AMV and other components of the climate system both within and outside the Atlantic region. The AMV can, for instance, affect climate multidecadal variability over both North America and western Europe; it can be linked to worldwide precipitation (in Sahel, India, North America and North Eastern Brazil) and to Atlantic hurricane activity [Sutton and Hodson, 2005; Knight et al., 2006; Sutton and Dong, 2012; Ting et al., 2011; Zhang and Delworth, 2006; Enfield et al., 2001; Goldenberg et al., 2001; Latif and Keenlyside, 2011]. The AMV is also related to the Mediterranean sea surface temperatures: Mariotti and Dell'Aquila [2012] find that Atlantic multidecadal variability is transmitted to the Mediterranean/European region via atmospheric processes, and analysis by Marullo et al. [2011] reveals a period of about 70 years in the Mediterranean sea surface temperature time series, strongly correlated to the AMV.

Besides, AMV is important because its phases of oscillation have alternately obscured and exaggerated the effects of global warming, and made attribution of global warming more difficult to ascertain. For example, Keenlyside et al. [2008] suggest that global surface temperature may not increase over the next decade, as natural climate variations in the North Atlantic and tropical Pacific temporarily offset the projected anthropogenic warming.

Despite its relevance for the climate variability over the Atlantic sector and adjacent regions, the precise nature of AMV needs to be clarified and its underlying mechanism remains little known. An in-depth examination of the AMV long-term behaviour in a comprehensive way, i.e. investigating its possible non-stationarity, is currently missing. The non-stationarity associated with the natural variability

modes should not be overlooked in order to understand whether the current spectral features of the AMV variability are potentially subject to major changes in the future.

1.2 Objectives and methodology

Aim of this study is to analyse the possible existence of non-stationary aspects of the Atlantic multidecadal variability. Since long time scales variations of Sea Surface Temperature (SST) exhibit large-scale organization owing to both atmosphere and oceanic processes, particular emphasis is placed on changes in the relationship between AMV and the variability of the Atlantic Meridional Overturning Circulation (AMOC); and, in order to explain these changes, large-scale teleconnection patterns associated with AMV evolution are also examined. Attention is paid on the possibility that AMV may change in different regimes with different time scales (periodicities), amplitude and teleconnection patterns with respect to the present ones.

A climate model is a useful tool to reconstruct the physical mechanisms behind low-frequency climate variability, suitable for an analysis of the internal variability because it can run under fixed radiative forcing conditions. Moreover, a model can provide long multi-century integrations necessary to resolve the multidecadal time scale of North Atlantic SST variability. Due to the large inter-model differences in terms of physical parametrizations, numerical schemes, resolution, etc., it is preferred to resort to different models rather than relying on one single climate model. A multi-model approach for AMV analysis allows us to investigate similarities and differences across a large ensemble of state-of-the-art climate models and to identify

the prominent simulated mechanisms. In this study, eleven multi-century preindustrial simulations are used mainly from the Coupled Model Intercomparison Project Phase 5 (CMIP5) ensemble. In order to better constrain the multidecadal variability, only the longest simulations are used (allowing a minimum of 500-year-long integrations). To isolate the internal, unforced variability, only simulations performed under preindustrial forcing conditions were selected.

Spatial description of AMV, as simulated by this set of models, is obtained using maps of correlation coefficients; while its evolution in time is given by spectral analysis of the North Atlantic SST time series with a specific focus on significant peaks at multidecadal time scale. The AMV time series is often subdivided in intervals to detect different regimes of variability and look at their characteristics. Moving these temporal windows allows us a better understanding of how the different regimes evolve in time and how the transitions among regimes occur. Since this approach reveals the non-stationarity as a prominent feature of AMV time series, which can vary in both amplitude and frequency over long periods of time, an objective assessment of this aspect is required: the eleven models undergo a statistical test to check the AMV stationarity. The starting null hypothesis refers to a statistically-stationary AMV, whose modulation is entirely random, and several analytical time series with the same spectrum than the true one are generated by the bootstrap method and used to show that a model simulates a non-stationary AMV when there are periods that do not keep the same statistical properties of the entire time series.

Regressions and cross-lagged correlations are performed between AMV and AMOC indices, to investigate long-term changes in their relationship. Furthermore, Maximum Covariance Analysis (MCA) is applied to study the role of the atmosphere-

ocean interactions, since it reveals changes in teleconnection patterns associated to the AMV index. It is especially used here to show how global sea level pressure anomaly field can be derived from North Atlantic sea surface temperature anomaly field.

A dynamical explanation for AMV regimes requires then the computation of lagged regression maps of several fields onto the AMV index chosen in this study as reference. This in-depth examination distinguishes the physical mechanisms underlying different preferred AMV time scales, corresponding to different variability modes.

The thesis is organised as follows. Chapter 2 introduces the framework within which this thesis takes place, with a literature review of the Atlantic Multidecadal Variability, its link with the large scale ocean circulation and its coupling with the atmosphere; a validation of the models that participate in this study is given in chapter 3, which presents also the evidence of non-stationary AMV behaviours, using a time-evolving approach for spectral analysis; therefore the models undergo to a statistical test for AMV stationarity described in chapter 4. Chapter 5 addresses how the different regimes exhibit by the model AMV are related to long-term modulations in the oceanic and atmospheric components of climate system; an in-depth analysis of dynamical mechanisms underlying different modes of variability is performed in chapter 6 for one model as case study; finally a summary and discussion of the results are debated in chapter 7.

Chapter 2

Overview of Atlantic Multidecadal Variability (AMV)

2.1 Definition and impacts

Sea surface temperatures play a key role in regulating climate and its variability and are governed by both atmospheric and oceanic processes. In the North Atlantic SSTs multidecadal (10 to 90 years) fluctuations are well documented by studies based on observations, proxy-reconstructions and numerical simulations [Schlesinger and Ramankutty, 1994; Kushnir, 1994; Enfield et al., 2001; Trenberth and Shea, 2006; Deser and Blackmon, 1993; Delworth and Mann, 2000; Gray et al., 2004; Kilbourne et al., 2014; Zhang and Delworth, 2006; Zanchettin et al., 2010; Ting et al., 2011]. Kerr [2000] named these pronounced multidecadal North Atlantic SST variations as Atlantic Multidecadal Oscillation (AMO): oscillation because the climate swings one way then the other, multidecadal because they take roughly 60 years to complete an oscillation, and Atlantic because they are most evident in

and around the North Atlantic. Other authors suggest that Atlantic Multidecadal Variability (AMV) is a more appropriate term to indicate any repeating fluctuation in the time series, regardless of whether the fluctuation repeats on a regular basis or not.

Many differently-constructed indices of AMV are used in literature: most of them are based on the spatially-averaged North Atlantic SSTs and they can differ according to the selected North Atlantic domain and to the time window used to low-pass filter the SSTs; other authors define the AMV index as the principal component of the leading Empirical Orthogonal Function (EOF) of North Atlantic SST. Zanchettin et al. [2014] conclude that indices based on the spatial averaging are more closely related to tropical regions, while EOF-based indices generally appear more closely related to extra-tropical variability. Figure 2.1 shows on top the observed AMV index, calculated as the areal-averaged SST over the [0°-60°N; 75°-7.5°W] domain, low-pass filtered with a 37-point Henderson filter (that is approximately equivalent to a 19 year running mean), detrended, also removing the long-term mean; this index explains 53% of the variance in the detrended unfiltered index. The corresponding SST regression pattern obtained by regressing the detrended SST data on a normalized (unit variance) version of the index is shown at the bottom [Sutton and Hodson, 2005]. Observed AMV appears to have a time scale of around 60-70 years; AMV warm phases occur in the late 19th Century and from 1931 to 1960, while cold phases occur from 1905 to 1925 and from 1965 to 1990. Anomalies of the same polarity are visible over most of the North Atlantic basin, featuring a typical "comma-shaped" pattern with largest values east of Newfoundland. From this regression map it is also important to notice that North Atlantic SSTs co-vary with the North Pacific and the Mediterranean

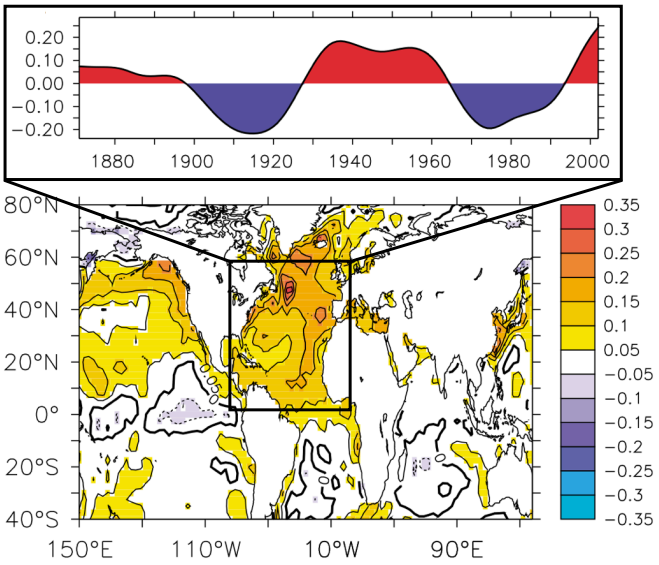

Figure 2.1: *(Top) Index of the AMV, 1871 to 2003. The units on the vertical axis are* °C*. (Bottom) Spatial pattern of SST variations associated with the AMV index shown on top: shown are the regression coefficients (*°C *per standard deviation) [Sutton and Hodson, 2005].*

Sea SSTs; indeed, AMV influences climate also outside the Atlantic region: it has been linked to summer temperatures in western Europe and precipitation variations in the continental United States [Sutton and Hodson, 2005; Enfield et al., 2001]; to the occurrence of Sahel drought and Atlantic Hurricane activity, [Knight et al., 2006; Sutton and Dong, 2012; Ting et al., 2011; Zhang and Delworth, 2006; Goldenberg et al., 2001; Latif and Keenlyside, 2011]; to the Mediterranean sea surface temperatures [Mariotti and Dell'Aquila, 2012; Marullo et al., 2011], and to North East Brazilian rainfall [Folland et al., 2001].

An ongoing debate concerns the nature of the 20th Century evolution of the AMV: the issue is whether AMV is driven by internal variations or is predominantly externally-forced. Traditionally, the AMV is thought to describe the internal contribution to North Atlantic SST variability [Schlesinger and Ramankutty, 1994].

Also more recently, works by Latif et al. [2006] and Ting et al. [2009] show that the multidecadal variability in North Atlantic SST is not driven by external forcings but arises basically from internal variability. Same point is supported by who relates AMV to the intrinsic multidecadal variability of the North Atlantic thermohaline circulation [Delworth and Mann, 2000; Medhaug and Furevik, 2011]. However, other studies indicate that external factors, such as changes in greenhouse gas concentrations, aerosol concentration, volcanic activity and solar insolation, could also play a role. Otterå et al. [2010] find that volcanism has a strong influence on Northen Hemisphere climate, not only for short-term changes, but also for multidecadal AMV-type changes; while Saenger et al. [2009] indicate that variations in solar activity, volcanism, greenhouse gases and tropospheric aerosols externally force the background component of SST variability at a lower frequency with respect to the multidecadal one. Booth et al. [2012], show that models that represent indirect aerosol effects, as the Hadley Centre Global Environmental Model, version 2, Earth system configuration (HadGEM2-ES), capture more of the observed AMV than those that represent only direct aerosol effect, so they conclude that aerosol emissions and periods of volcanic activity explain 76% of the simulated multidecadal variance in detrended 1860-2005 North Atlantic sea surface temperatures. However they are questioned by Zhang et al. [2013], since there are major discrepancies between the HadGEM2-ES simulations and observations in the North Atlantic Ocean, that are largely attributable to what appears to be excessively strong aerosol effects.

2.2 The Atlantic Meridional Overturning Circulation (AMOC) and its link with AMV

A widely accepted candidate to explain the detected AMV is the Atlantic Meridional Overturning Circulation (AMOC): a prominent ocean circulation system. The low-frequency fluctuations of the AMOC are shown to be the main precursor for the model AMV [Delworth et al., 1993; Timmermann et al., 1998; Latif et al., 2004, 2006; Jungclaus et al., 2005; Knight et al., 2005; Dong and Sutton, 2005; Delworth and Mann, 2000; Collins et al., 2006; Msadek and Frankignoul, 2009].

AMOC consists of four main branches (Figure 2.2): upwelling processes that transport water from depth to near the ocean surface, surface currents that transport relatively light water toward high latitudes, deep water formation regions where waters become denser and sink, and deep currents closing the loop. These four branches span the entire Atlantic on both hemispheres, forming a circulation system that consists of two overturning cells, a deep one with North Atlantic Deep Water (NADW) and an abyssal one with Antarctic Bottom Water (AABW) [Kuhlbrodt et al., 2007].

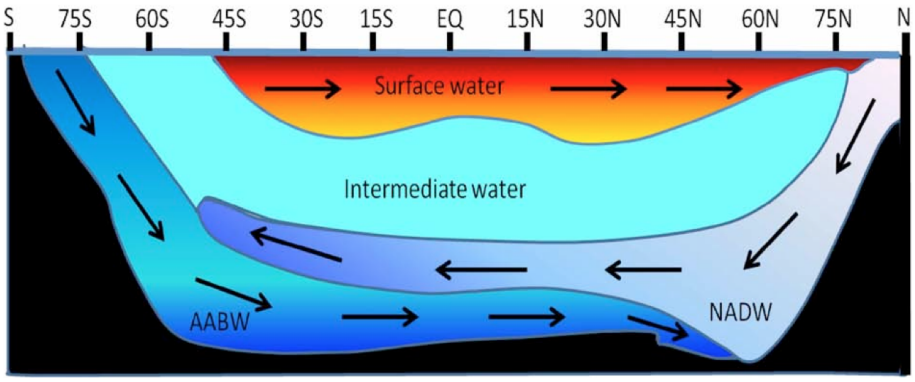

Figure 2.2: *Schematic representing a zonally averaged picture of the Atlantic Ocean [Wang et al., 2014].*

In Figure 2.3, estimates of total, atmospheric and oceanic heat transports are presented (left panel), jointly with the relative contribution of each oceanic basin (right panel), based on reanalyses from the National Centers for Environmental Prediction-National Center for Atmospheric Research (NCEP-NCAR).

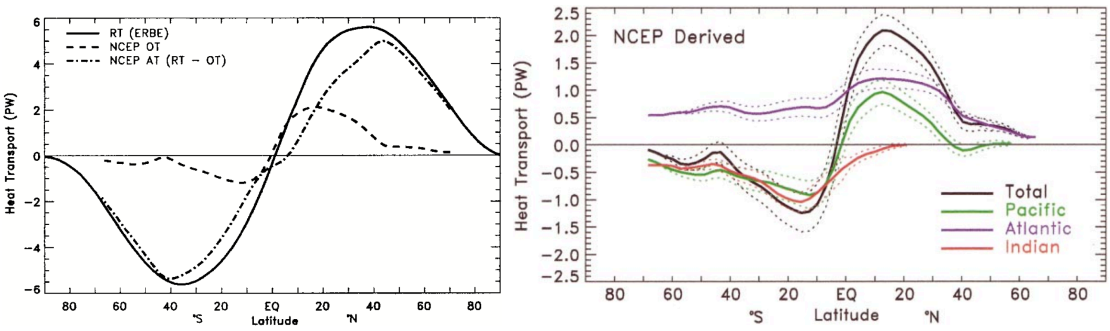

Figure 2.3: *(Left) Total heat transport RT (solid line), ocean heat transport OT (dashed) and atmospheric transport AT estimated from NCEP reanalyses. (Right) Zonal annual mean ocean heat transports for the total, Atlantic, Indian, and Pacific basins from NCEP reanalyses. The 1 standard error bars are indicated by the dashed curves [Trenberth and Caron, 2001].*

The global oceanic contribution dominates the atmospheric contribution at low latitudes in the northen hemisphere. In the Atlantic ocean, the relative contribution of the ocean heat transport to the atmosphere is larger than for the global average [Medhaug and Furevik, 2011]. There is a northward heat transport in the entire basin related to the overturning circulation, which is exclusive for the Atlantic, see right panel in Figure 2.3. The AMOC contributes to around 25% of the total (atmosphere and ocean) poleward heat transport and thus plays a key role in the global Earth climate, with a maximum 1.3 PW oceanic heat transport occurring at 24°-26°N [Srokosz et al., 2012]. Both vertical mixing in the ocean's interior and wind-driven upwelling are likely contributing to drive the observed circulation [Kuhlbrodt et al., 2007]. The first one is the traditional thermohaline driving

mechanism: it is that part of the ocean circulation determined by changes in temperature and salinity, related to the term "Thermohaline Circulation (THC)" that, therefore, is not synonymous with the AMOC. The AMOC is a descriptive, geographic term that does not refer to any particular driving mechanism; whereas the THC is related to one of the mechanisms involved in the overturning. While THC is not directly measurable, AMOC can be determined in practice, as a zonal integral of the meridional velocity as a function of depth. Deeper currents and upwelling in particular are extremely difficult to measure; therefore, although the AMOC plays a key role in the ocean/climate system, it can be at best indirectly estimated from sparse observations, and only the mooring array of the 'Rapid Climate Change' (RAPID) Research Programme of the Natural Environment Research Council (NERC) has now observed the AMOC at 26°N continuously for 10 years. More details on AMOC quantitative definition and measurement are provided in section 5.1.

According to a dominant paradigm, AMV is driven by coordinate multidecadal changes in the AMOC strength, via the AMOC modulation of the Atlantic ocean heat transport. Using a multi-model approach, Zhang and Wang [2013] find the following AMV/AMOC relationship: a strengthening (weakening) of the AMOC leads to a warm (cold) phase of the AMV by an anomalously larger (weaker) heat transport, which in turn determining a slowdown (an acceleration) of the AMOC by changes in the meridional density gradient, after some time-lag due to dynamical adjustment. Delworth et al. [1993] authored one of the earliest studies investigating the relationship between the AMOC and SST changes in the North Atlantic. They show that the density anomalies in the sinking region of the overturning circulation drive the (midlatitude) multidecadal or longer time-scale

AMOC oscillations. Reduced heat transport associated with a weak AMOC leads to a cold, dense pool throughout the upper 1 km in the central North Atlantic (30°-60°N). This cold pool has an associated cyclonic circulation that transports salt into this sinking region, thus increasing further the density there. As a result, AMOC strengthens, leading to the transport of warmer, less dense waters into the sinking area. In turn, AMOC weakens again, accompanied by reduced heat transport. In Delworth et al. [1993], the existence of the oscillation crucially depends on the phase lag between the temperature and salinity contributions to the total density in the deep-water formation regions, see also Danabasoglu [2008]. Applying the multi-taper frequency-domain singular value decomposition (MTM-SVD) approach [Mann and Park, 1999] to a 1400-year simulation, Knight et al. [2005] find that the maximum of the AMOC is associated to a coherent large-scale temperature pattern with widespread warm anomalies in the Northen Hemisphere, considerably similar to the observed positive AMV pattern. Figure 2.4 shows that this pattern first diminishes, then re-establishes in the opposite sense at the AMOC minimum, when much of the Northern Hemisphere is anomalously cold: the simulated AMV/AMOC variability evolves coherently. Recently, Ba et al. [2014] analyse the key elements of the Delworth et al.'s (1993) mechanism in a multi-model ensemble of coupled general circulation models. They find a certain degree of cross-model consistency: in most models the mid-latitude SST variations in the North Atlantic are significantly correlated with fluctuations in the AMOC, salinity variations control density changes in the convective regions where mixed layer deepening precedes AMOC strengthening, and the subpolar gyre variations significantly lead AMOC changes.

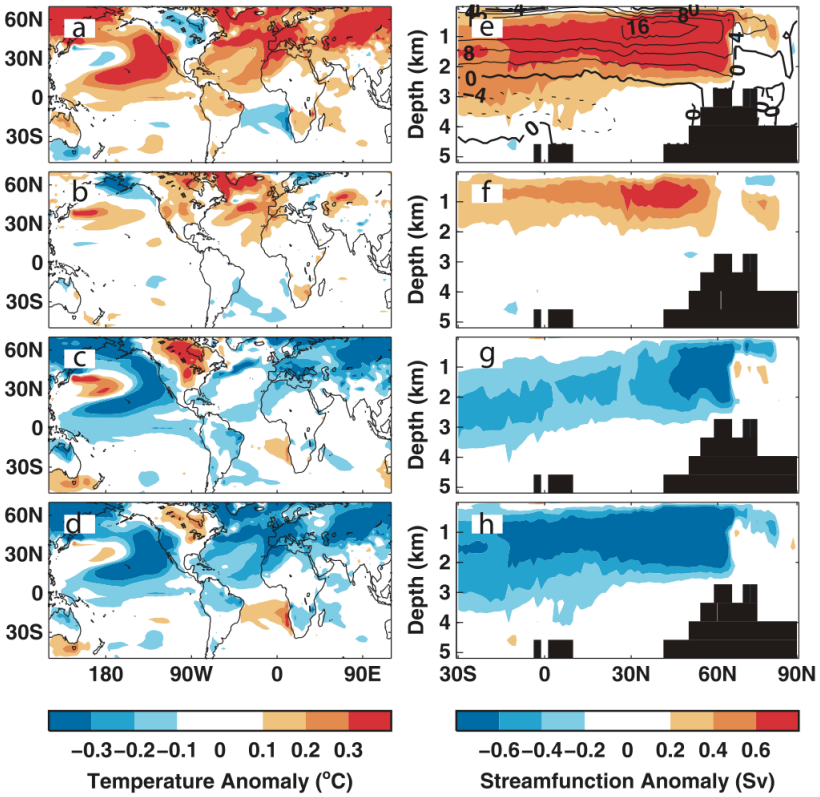

Figure 2.4: *Joint MTM-SVD analysis of simulated multidecadal mean surface temperature and AMOC. Panels a-d show the signal in surface temperature anomaly in the frequency band from (70 years)$^{-1}$ to (180 years)$^{-1}$, at phases of 0°, 60°, 120°, 180° respectively. Zero phase corresponds to maximum mean Northern Hemisphere temperature. Panels e-h show the corresponding phases of the covarying signal in AMOC anomaly in the same band. In panel e, the climatological AMOC is shown by contours [Knight et al., 2005].*

2.3 The role of ocean-atmosphere coupling

We have seen that the multidecadal portion of North Atlantic SST variability is thought to reflect, at least partially, natural internal variations in the Atlantic meridional overturning circulation. However, AMV is also influenced by direct atmospheric forcing and other oceanic changes [Msadek and Frankignoul, 2009]. Multidecadal climate variability can be also a coupled ocean-atmosphere system.

In fact, for a steady Earth's climate, large anomalies in oceanic heat transport should be balanced by opposite variations in the atmospheric heat transport on decadal and longer time scales (Bjerknes's (1964) compensation); and the character of large-scale air-sea interaction over the midlatitude (30°-60°N) North Atlantic Ocean differs with time scales. Gulev et al. [2013] confirm this conjecture providing observational evidence that in the mid-latitude North Atlantic and on time scales longer than 10 years, surface heat fluxes are driven by the ocean and may force the atmosphere, whereas on shorter time scales the opposite is true.

Farneti and Vallis [2011] categorise air-sea interactions that take place at the middle latitudes at decadal and longer time scales. They start from the classical Hasselmann's (1976) stochastic model of climate variability: slow changes of climate are explained as the integral response to continuous random excitation by short period "weather" disturbances; the atmosphere varies essentially as white noise and the ocean, of a much higher heat capacity, passively integrates this variability, producing a red noise spectrum. However, in the presence of internal oceanic variations, some spectral peaks emerge from the red noise (departures from the Hasselmann's (1976) noise paradigm): the ocean dynamics makes the system more predictable. The ocean circulation can indeed modulate the spectrum of variability in the overlying atmosphere: the ocean circulation introduces a delay and modulates SST variability on decadal time-scales. Other authors inspect the possible coupled ocean-atmosphere interactions in the extra-tropical North Atlantic, analysing in particular the mechanisms behind coordinated changes between SST and the North Atlantic Oscillation (NAO), which refers to the pressure gradient between Iceland and Azores and is associated with changes in the surface westerlies across the Atlantic onto Europe. Bellucci et al. [2008] suggest that the ocean is not

passively responding to the atmosphere, showing the existence of significant lead-lag correlations between NAO index and SST, so that changes in the SST may feed back on the NAO; and the hypothesis that the ocean acts as a damped oscillator that is excited by atmospheric variability is expressed by Delworth and Greatbatch [2000]; Czaja and Marshall [2001]; Johnson and Marshall [2002]; Marshall et al. [2001].

Chapter 3

Multi-model characterization of AMV

3.1 Model data

In this chapter the behaviour of AMV is investigated in a multi-model set of simulations. As the focus of this study is the unforced internal component of climate variability, preindustrial simulations have been selected. They estimate the unforced variability of the model, imposing constant pre-1850 conditions: greenhouse gases, aerosols, ozone and solar irradiance are fixed at the year 1850, CO_2 concentration is 286.3 ppm, CH_4 concentration is 805.25 ppb and N_2O concentration is 276.4 ppb. Since this study is focused on the multidecadal time scales, multi-century simulations with a minimum length of 500 years are required to properly resolve the low-frequency range of the spectrum. Based on this criteria, 11 simulations performed with as many models were selected (Table 3.1). Out of these, ten models come from the fifth phase of the Coupled Model Intercomparison Project Phase 5 (CMIP5) archive, which promote a framework of coordinated climate experiments, providing a freely available state-of-art multimodel dataset.

model name	**length (years)**	**Resolution (Ocn)** (lon × lat)	**Resolution (Atm)** (lat × lon)
MPI-ESM-P	1156	1.5° L40	T63/1.9° L47
CCSM4	1051	1.11°×(0.27°÷0.54°) L60	1.25°×0.9° L26
MPI-ESM-LR	1000	1.5° L40	T63/1.9° L47
CanESM2	996	1.41°×0.94° L40	T63/2.81° L35
NorESM1-M	501	1.125° L53	1.9°×2.5° L26
GFDL-ESM2M	500	1°×(1°÷$^1/_3$°) L50	2°×2.5° L24
MRI-CGCM3	500	1°×0.5° L50	T159 L48
ACCESS1-0	500	1°×(1°÷$^1/_3$°) L50	1.25°×1.875° L38
ACCESS1-3	500	1°×(1°÷$^1/_3$°) L50	1.25°×1.875° L38
CESM1-BGC	500	1° L60	1.25°×0.9° L26
GFDL-CM2.1	3500	1° L50	2°×2.5° L24

Table 3.1: *Eleven multi-century preindustrial simulations that partecipate in this study.*

In Taylor et al. [2009] the protocols for all the CMIP5 experiments are detailed. Specifically, preindustrial experiments have the following features:

- Prescribed non-evolving atmospheric concentrations of:
  - all well-mixed gases (including CO_2),
  - some short-lived (reactive) species.
- Prescribed non-evolving emissions or concentrations of:
  - natural aerosols or their precursors,
  - some short-lived (reactive) species.
- Unperturbed land use: fixed agriculture disturbance mask.

In addition to the selected CMIP5 models, a 3500-year long integrations performed with the GFDL-CM2.1 model, not available in the CMIP5 archive, is analysed.

3.2 Observed data

Met Office Hadley Centre's sea ice and sea surface temperature (SST) data set, HadISST [Rayner et al., 2003], is used to validate the model results. HadISST is a combination of monthly globally-complete fields of SST and sea ice concentration on a 1 degree latitude-longitude grid from 1870 to date. The SST data are taken from individual ships' observations from the Met Office Marine Data Bank (MDB), which from 1982 onwards also includes data received through the Global Telecommunications System (GTS). In order to enhance data coverage, monthly median SSTs for 1871-1995 from the Comprehensive Ocean-Atmosphere Data Set (COADS) (now ICOADS) were also used where there were no MDB data. HadISST dataset has been made globally complete, since gaps in the SST data have been interpolated using the reduced space optimal interpolation (RSOI). For 1982 onward, the RSOI technique was applied to the in situ/satellite SST combination using a two-stage procedure: first reconstructing the global pattern of long-term change and then the residual interannual variability, followed by superposition of quality-improved gridded observations onto the reconstructions to restore local detail.

3.3 Simulated AMV

In order to understand the variability of North Atlantic SST (NA SST), spectral analysis of the unfiltered NA SST time series is performed via multi-taper method (MTM) [Thomson, 1982]. Ghil [2002] explains that this method provides useful tools for the spectral estimation of a time series whose spectrum may contain

both broadband and line components. MTM is non-parametric, since it does not use a priori model of the process that generated the time series under analysis and it attempts to reduce the variance of spectral estimates by using a small set of tapers rather than the unique data taper or spectral window used by the classical methods. The data are pre-multiplied by orthogonal tapers constructed to minimize the spectral leakage due to the finite length of the time series, and a set of independent estimates of the power spectrum is computed. The spectrum is computed via multi-taper method also because it relaxes some of the strict stationary assumptions, so it is particularly well-suited for the spectral analysis of climatic time series [Mann and Lees, 1996]. In Figure 3.1 the MTM power spectra of the simulated and observed NA SST time series are shown in colours and the corresponding red noise spectra are overlapped as thin black lines.

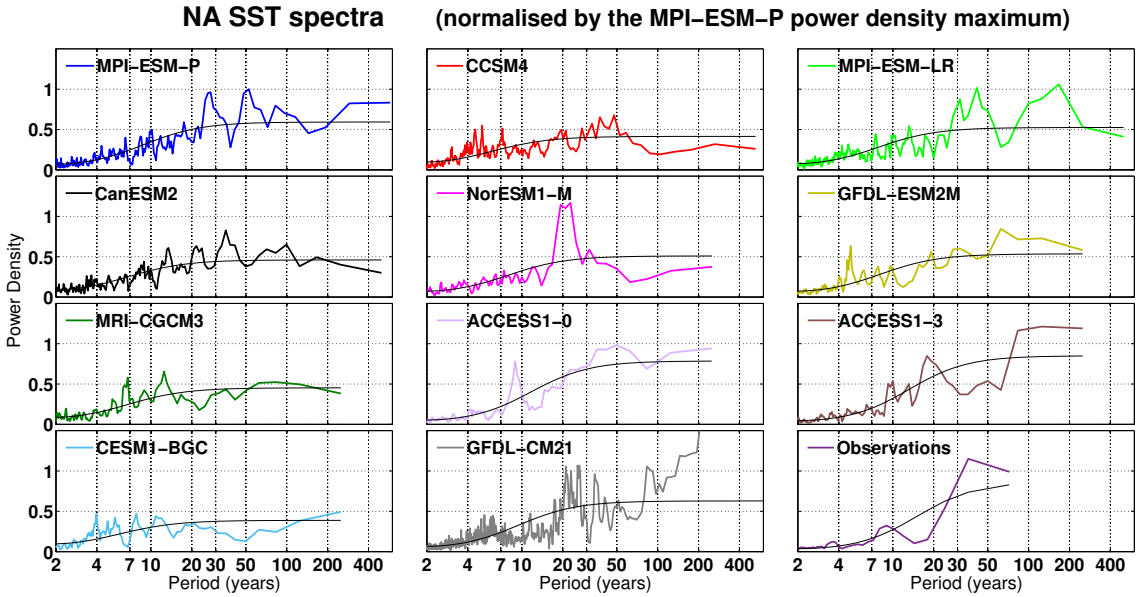

Figure 3.1: *MTM spectrum of North Atlantic SST for the analysed models and the HadISST observations from 1870-2014. The black thin lines are the AR1 red noise fits.*

Red noise is used to describe noise with enhanced low-frequency fluctuations arising from the interaction of white noise forcing with the slow-response components of a system. We have seen in section 2.3 that there is a theoretical justification for a red noise description of the noise background in climatic time series, since the thermal inertia of the oceans provides memory. The frequencies with significant power above red noise indicate that SSTs significantly deviate from the red noise null-hypothesis postulating that the low-frequency variance is entirely determined by the integration of the atmospheric white noise [Hasselmann, 1976]. Focusing on periodicities longer than 10 years, at multidecadal time scale, significant variability above the red noise can be seen in all the models and in the observations. The observations have a band of enhanced power between 30 and 50 years, which is not very well resolved because of the shortness of the record. Flat low-frequency tails of the spectra are seen in CCSM4, MRI-CGCM3 and CESM1-BGC models, while peaks are more distinguishable for the rest of models. Depending on the model considered, power spectrum of AMV index shows peaks at different frequencies and with different amplitudes. This wide range of variability is found also in Ba et al. [2014] multi-model comparison.

For each model the AMV index is calculated by averaging annual mean SST over the region 0°-60°N and 75°-7.5°W, as in Sutton and Hodson [2005]. The spatial mean is weighted by grid cell area according to the equation: $\frac{\int_A SST(\vec{x}) \cdot dA(\vec{x})}{\int_A dA(\vec{x})}$. Prior to the analysis, the long-term mean is removed and the resulting time series of SST anomalies is detrended in order to remove spurious long-term changes associated with residual model drifts, which are not physically meaningful. In order to isolate the decadal scale, SSTs are low-pass filtered with a 10-year running mean.

Figure 3.2 illustrates the spatial patterns of SST associated with the AMV index for the models and the HadISST observations. Shown are the point-wise correlation between global SST field and AMV index.

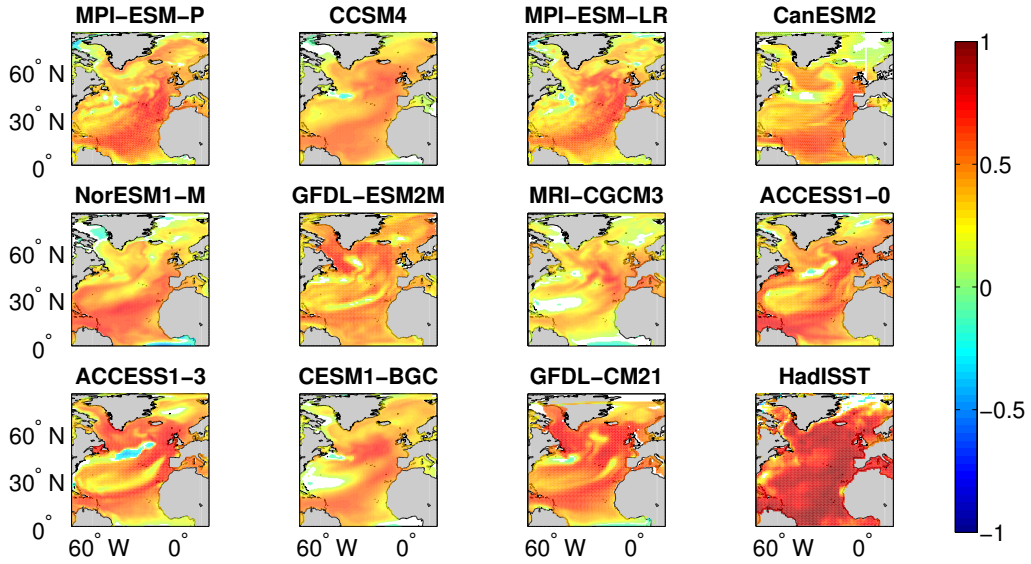

Figure 3.2: *Spatial patterns of SST associated with the AMV index for the models and the HadISST observations from 1870-2014. Shown are the 95% significant correlations between normalised AMV index and 10-year running mean filtered, detrended global SST.*

The observed AMV index is calculated in the same manner as for the models; nevertheless the comparison with models is not completely consistent because observed record is comparatively short and it accounts for external forcings, which are instead excluded in models. From observations, there is an overall high positive correlation between the SST and the AMV index for the entire AMV region (as in others studies [Medhaug and Furevik, 2011]). Although there are some differences among the models, their spatial SST patterns resemble the typical basin-scale pattern of the same positive sign with largest values in the east and midlatitude region (comma-shaped patterns). The majority of models also show little or slightly

negative correlations in the Gulf Stream and the Nordic Seas areas. Most of commonalities among the models and observations come from the strong correlations shown in the tropical Atlantic, except for MRI-CGCM3 model; while north of 30°N the patterns differ more.

These patterns evolve in time: next, we visually inspect the individual AMV time series (Figure 3.3); note that the GFDL-CM2.1 AMV index is divided in 1000-year-long segments in order to better discern its features and compare with the other models.

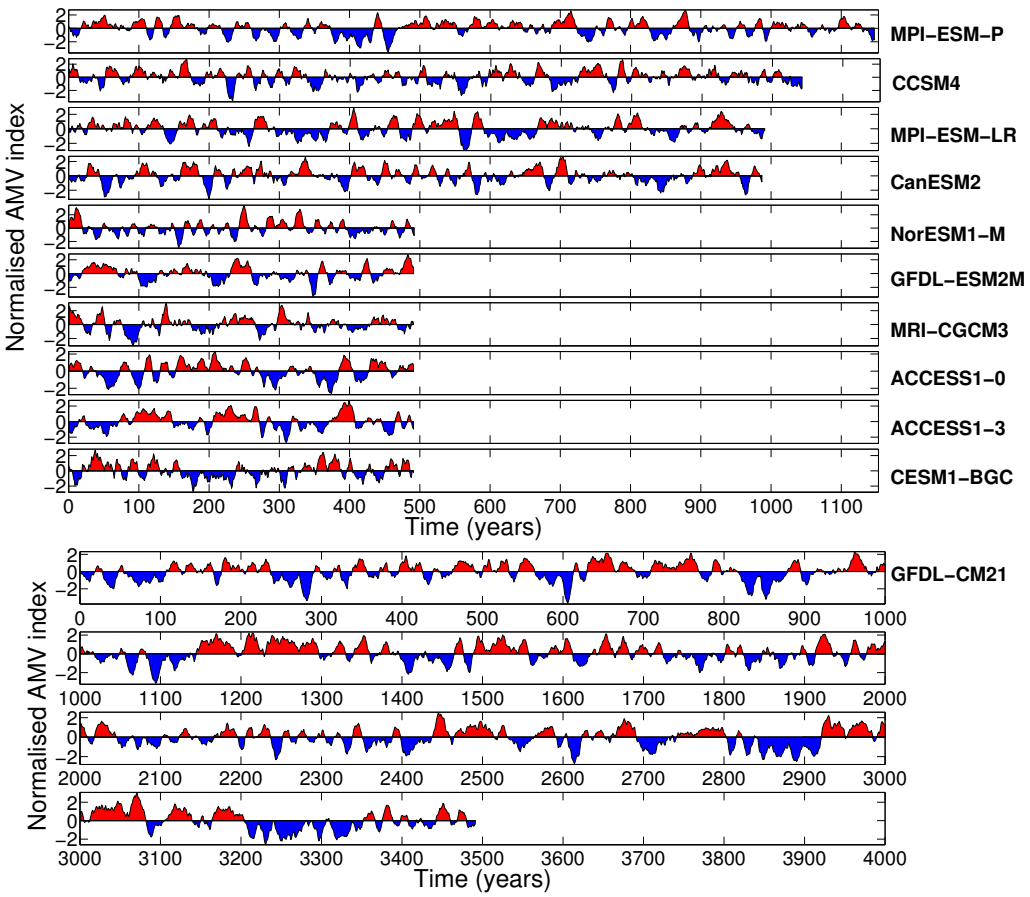

Figure 3.3: *Normalised AMV index in the CMIP5 preindustrial simulations (top) and in the GFDL-CM2.1 model (bottom).*

The non-stationarity appears to be a prominent feature of AMV index time series. Different epochs of different characteristics and duration can be identified in the evolution of AMV index time series: there are multidecadal epochs with mostly warm-skewed events; with moderate, nearly sinusoidal events; with intense and longer-period events; and with small amplitude. Not only the spectral features display non-stationarity, but also the amplitude of the AMV signal. Analogously to the epochs found by Wittenberg [2009] for ENSO, these different regimes are illustrated in Figure 3.4 for MPI-ESM-P model and in Figure 3.5 for CCSM4, MPI-ESM-LR and CanESM2 models, as an example.

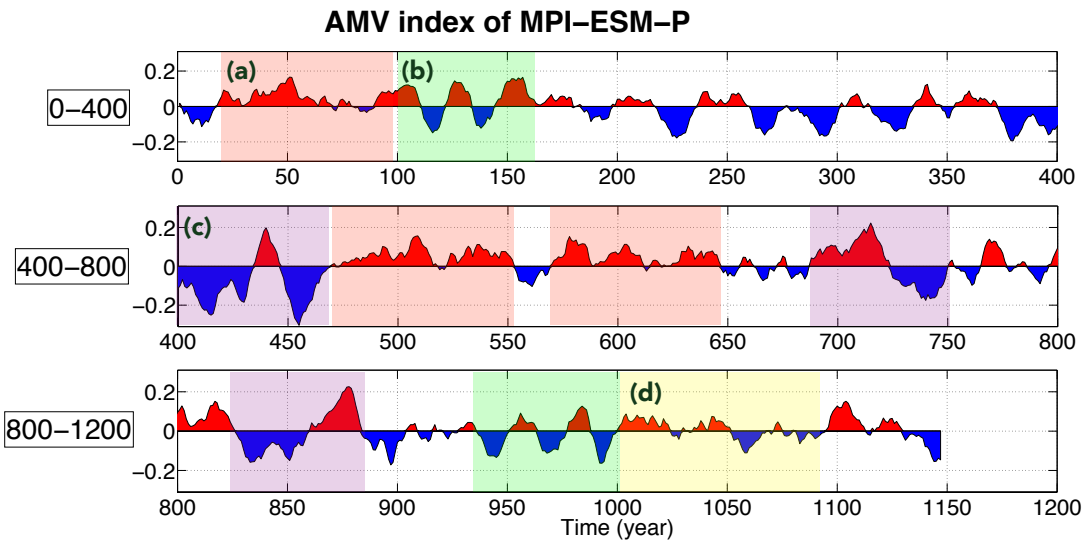

Figure 3.4: *AMV modulation shows epochs with different characteristics. (a) RED: mostly warm-skewed events; (b) GREEN: moderate, nearly sinusoidal events; (c) PURPLE: intense and longer-period events; (d) YELLOW: small amplitude.*

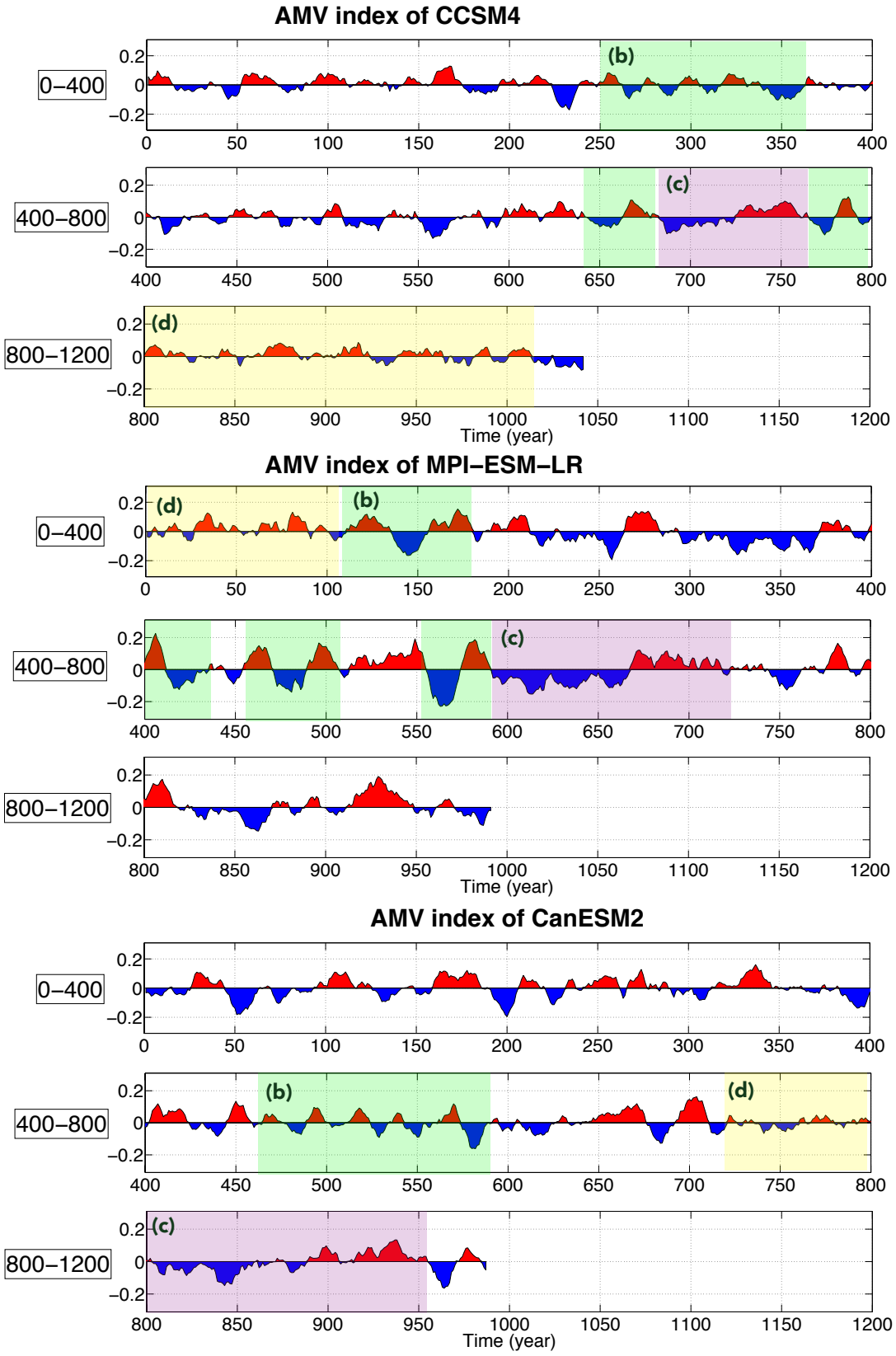

Figure 3.5: *As in Figure 3.4, but for CCSM4, MPI-ESM-LR and CanESM2.*

3.4 Evidence of non-stationarity

In the light of Figure 3.4 and 3.5, North Atlantic SST variability is analysed for different epochs. An objective method to select epochs consists in dividing the AMV index time series into equal-length intervals. The length of these intervals is chosen to be 200 years just to be comparable with the length of observations. In order to underline the AMV non-stationarity, multi-taper method spectral analysis is carried out for chunks of consecutive, overlapping 200-year-long intervals, shifted by 50 years; for both models and observations. Figure 3.6 and 3.7 show the results for the four longest CMIP5 models, for illustrative purposes, since the other models present an analogous non-stationary behaviour. Spectral analysis is performed for each interval, for the entire time series and for the observations taken from HadISST data. Each power spectral density is normalised by its maximum. First interval refers to the period from year 1 to year 200, second interval refers to period [50-250] years, third to [100-300], and so on.

This time-evolving view of AMV spectral features highlights a strong dependence to the selected time interval, emphasizing the non-stationarity of AMV. For example, looking at the MPI-ESM-P model, we can see that the AMV during the [450-650] time interval, central year 550, displays almost no variability for periods shorter than 20 years, while during the [900-1100] time interval the the maximum of variability is seen at 20 years. Therefore, the preferential periodicity can differ a lot among the intervals. The spectrum of observations resembles, for example, the [200-400] time interval spectrum because both show enhanced power in the 30-50 years band. However, the observed spectrum differs substantially, for example, from the [900-1100] time interval spectrum, which presents the highest power

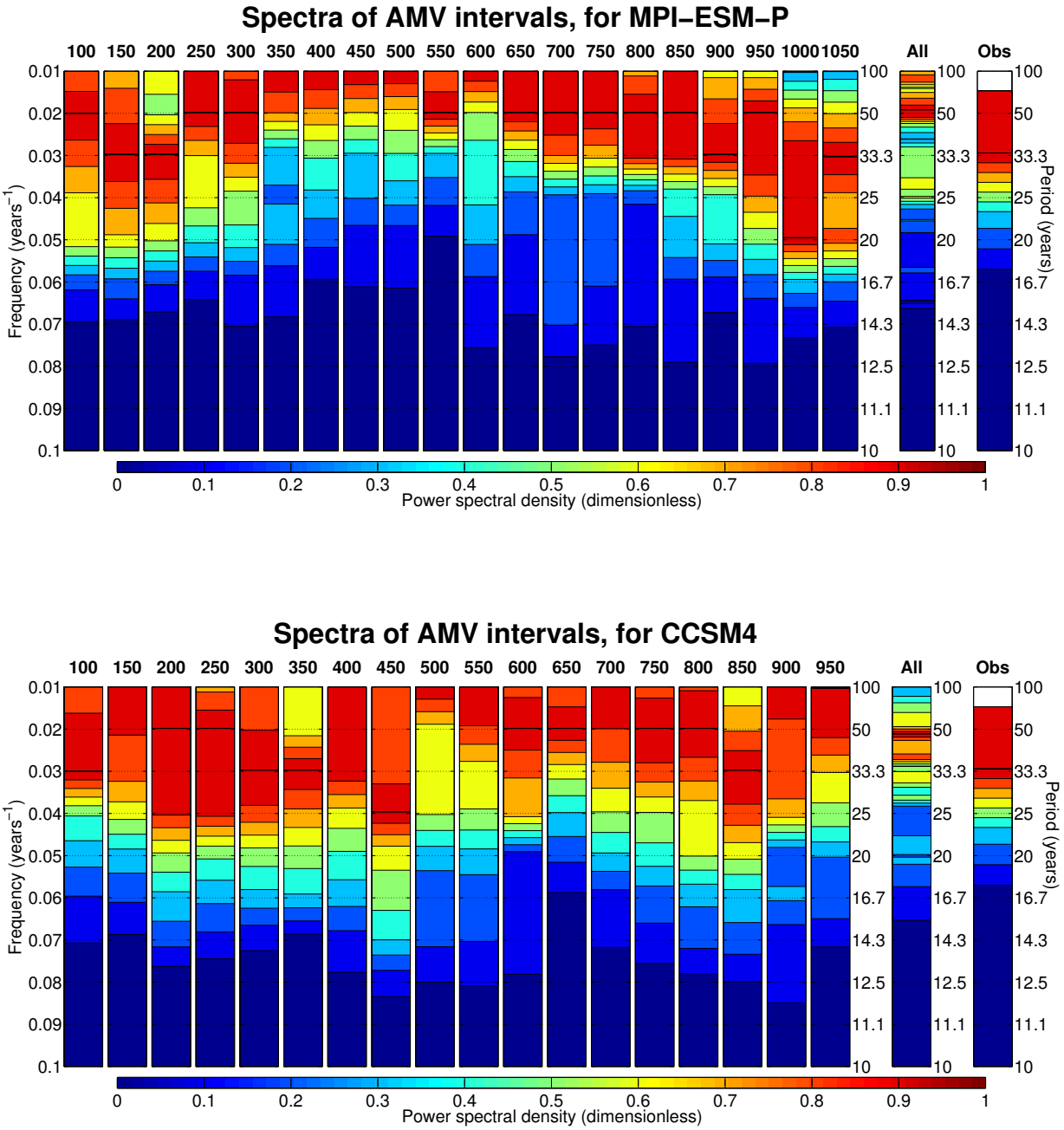

Figure 3.6: *Spectral signature of AMV index by using the multi-taper method for 200-year-long intervals labelled with the central year (shown on top) and for the entire time series (indicated with "All" on top), for (top) MPI-ESM-P and (bottom) CCSM4. "Obs" bin refers to HadISST data from 1870-2014.*

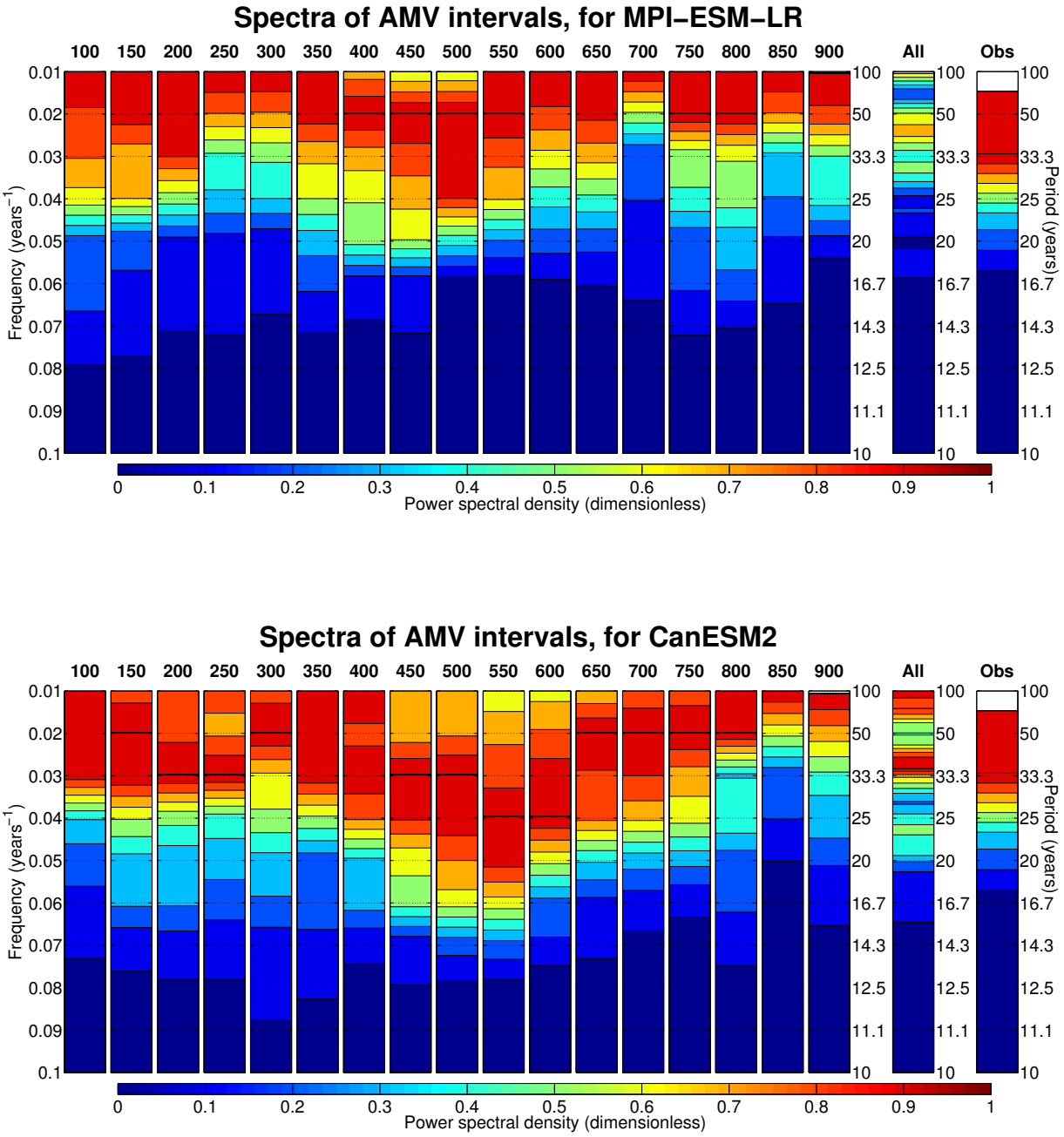

Figure 3.7: *As in Figure 3.6, but for (top) MPI-ESM-LR and (bottom) CanESM2.*

at higher frequencies (periods shorter than 30 years). It is therefore possible to understand that the observed AMV spectrum represents only one of the several possible behaviours that emerge looking at long datasets, suggesting that in the future AMV might enter a regime remarkably different from the 20th Century. This method is used by Saenger et al. [2009] in order to characterise changes in the dominant periodicities of Atlantic SST variability. They analyse a 440-year reconstruction of Atlantic SST anomalies, based on the Bahamas coral growth rate measurements, and they find that some periods show multidecadal power similar to the currently observed AMV, whereas no significant multidecadal power is evident in other past epochs.

Transitions among these regimes of different variability also emerge from the AMV autocorrelation, diagnosed with a moving window framework (Figure 3.8). For all the analysed models, the AMV time series is split again in 200-year-long intervals, shifted by 50 years, and the autocorrelation function is computed for each interval.

For most of the models, the dominant time scale of the autocorrelation function changes with the time interval, revealing a modulation of AMV that is irregular and interval-dependent. For MPI-ESM-LR model is noticeable that a $\sim$ 50-year time scale characterises initial part of the record, later shortening down to $\sim$ 25 years, as indicated by the sloping contours. Other models display no preferred time scales for long segments of their evolution, see in particular CCSM4 and ACCESS1-3 models. On the other hand, NorESM1-M model shows an almost stationary autocorrelation throughout the whole length of the model record. This kind of spectral analysis allows to observe the variance peaks in the frequency domain and to verify how those peaks vary in time. The present results are consistent with Zanchettin et al.'s (2010) work based on Global Surface Temperature (GST). They show that

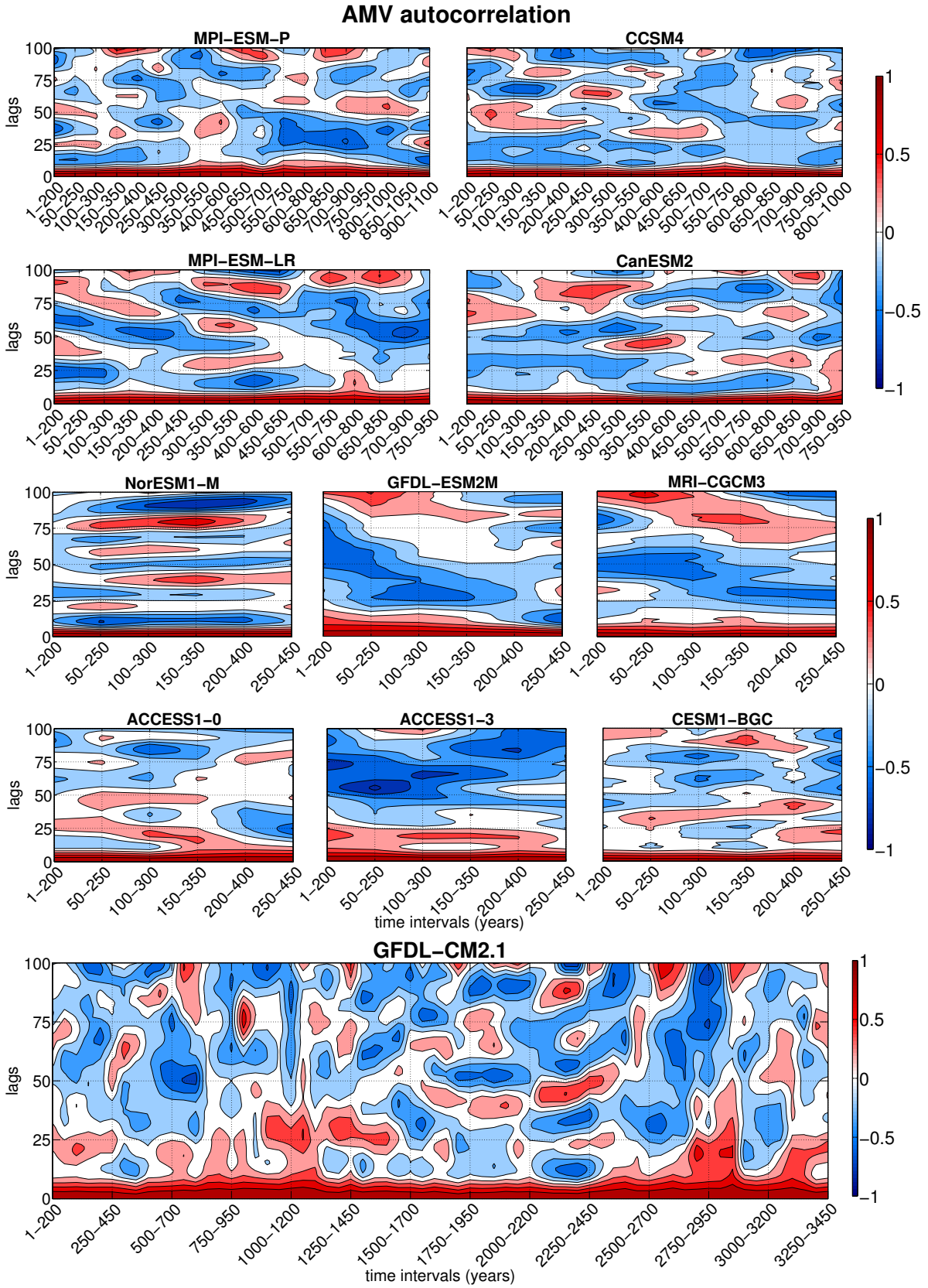

Figure 3.8: *Autocorrelation function of AMV index for moving and overlapped 200-year-long time windows, for the analysed models.*

observed (Central England Temperature, CET) and simulated (MPI-ESM) climate time series covering several centuries are often characterized by fluctuations on time scales that are not homogeneously distributed in time: they appear within irregularly intermittent temporal intervals, whose duration varies, in general, with the signal fluctuation frequency.

To conclude, the preferred variability time scales depend not only on the model, but also on the period considered: this indicates a non-stationary AMV behaviour. Does this modulation arise by chance? We will address this question in the next chapter (chapter 4), where the AMV non-stationary behaviour exhibited in these eleven simulations is objectively assessed, via a statistical test.

Chapter 4

A statistical test for AMV stationarity

The analysis of AMV in the multi-model set of preindustrial integrations, illustrated in the previous chapter, revealed the alternation of epochs characterized by different spectral characteristics.

Here, a statistical test to rigorously check the AMV stationarity is described. The starting null hypothesis (H_0) refers to a statistically-stationary AMV, whose modulation is entirely random and with limited memory. In such a system, apparent "transitions" would have no underlying "cause" any more than does a long run of heads or tails when flipping a fair coin. Theoretically, stationarity is defined as a quality of a process in which the statistical parameters (mean and standard deviation) of the process do not change with time. The most important property of a stationary process is that the auto-correlation function depends on lag alone and does not change with the time at which the function is calculated. Therefore a practical definition of non-stationarity indicates that the entire time series is not stationary if there are intervals that do not keep the same statistical properties (e.g. autocovariance) of the entire time series. This is what the test checks.

First the method is explained for MPI-ESM-P model and then the results for the entire set of models are presented.

4.1 A detailed explanation, using MPI-ESM-P

4.1.1 True AMV index and analytical AMV indices

The starting point is the AMV index time series, taken in this case from the MPI-ESM-P model: the index of AMV is calculated by averaging annual mean simulated sea surface temperature (SST) over the region 0°-60°N and 75°-7.5°W. The spatial mean is weighted by grid cell area. The raw time series is only detrended, while the low-pass filtered time series is also filtered by 10-year running mean and then normalised by its standard deviation.

The resampling methods are useful to generate random time series that have similar properties of the members of the population from which the simulated AMV time series is taken. "Random-phase" test is applied to the analysed AMV time series. This technique is considered "resampling" in the frequency domain, as it do not preserve the distribution of values but rather the power spectrum. Therefore the resampled series retains the same autocorrelation as the original series [Ebisuzaki, 1997]. Basically, after computing the Fourier transform of the original time series, the following step creates a large number of new Fourier series with random phases and the same power spectrum as the original series. Inverse Fourier transforms give the new series that differ from the original series because they have random phases in each of their Fourier modes. With the bootstrap we are able to find a number of time series with the same length of the true time series (in this case 1156

years), and use them to compute confidence intervals in order to robustly assess the non-stationarity of the true time series. In Figure 4.1, the 1000 bootstrap time series, in green, share the same spectrum (left plot) and autocorrelation (right plot) of the original time series (superimposed as a thick black line).

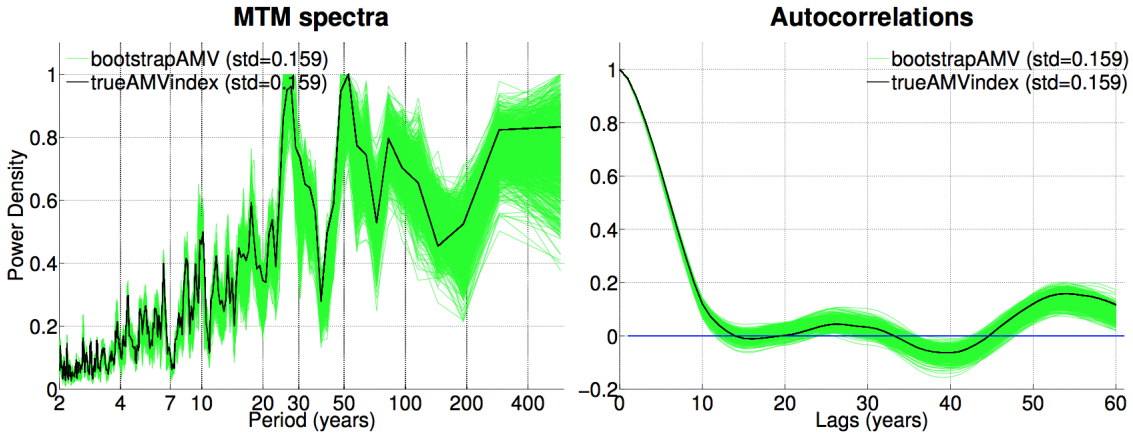

Figure 4.1: *(left) Original unfiltered time series spectrum in black and 1000 spectra associated to the 1000 analytical time series in green, via multi-taper method. (right) Original time series autocorrelation in black and 1000 autocorrelations associated to the 1000 analytical time series in green. For autocorrelation, the original and analytical time series are low-pass filtered by 10 years for plotting issues.*

4.1.2 The confidence interval

Having checked, in Figure 4.1, the effectiveness of the bootstrap method, it is possible to compute a band of confidence for a significance α=10% for the autocovariance function. In order to have a reasonable number of intervals to plot all together, here the intervals are shifted by 50 years. Each of the 1000 bootstrap time series is 10-year low-pass filtered, split in 19 intervals of length equal to 200 years, and shifted by 50 years. Therefore there are 19000 intervals in total. The autocovariance function is computed for all them, spanning 60 lags. For each lag there are 19000

autocovariance values. They are sorted in ascending order and, for each lag, the inferior limit for the confidence interval is set equal to the autocovariance value corresponding to the 950th element ($0.05 \cdot 19000 = 950$): the 5% of the total number of values, and analogously the superior limit for the confidence interval is set as the value related to the 18050th element ($0.95 \cdot 19000 = 18050$): the 95% of the total number of values. In parallel, also the original 10-year low pass filtered AMV time series is divided in nineteen 200-year-long intervals and the autocovariance is computed for all of them.

In Figure 4.2 each plot refers to a different 200-year-long interval, the black line is the true autocovariance function for that interval, the grey shading is the confidence interval and the red curve represents the mean behaviour of the original intervals.

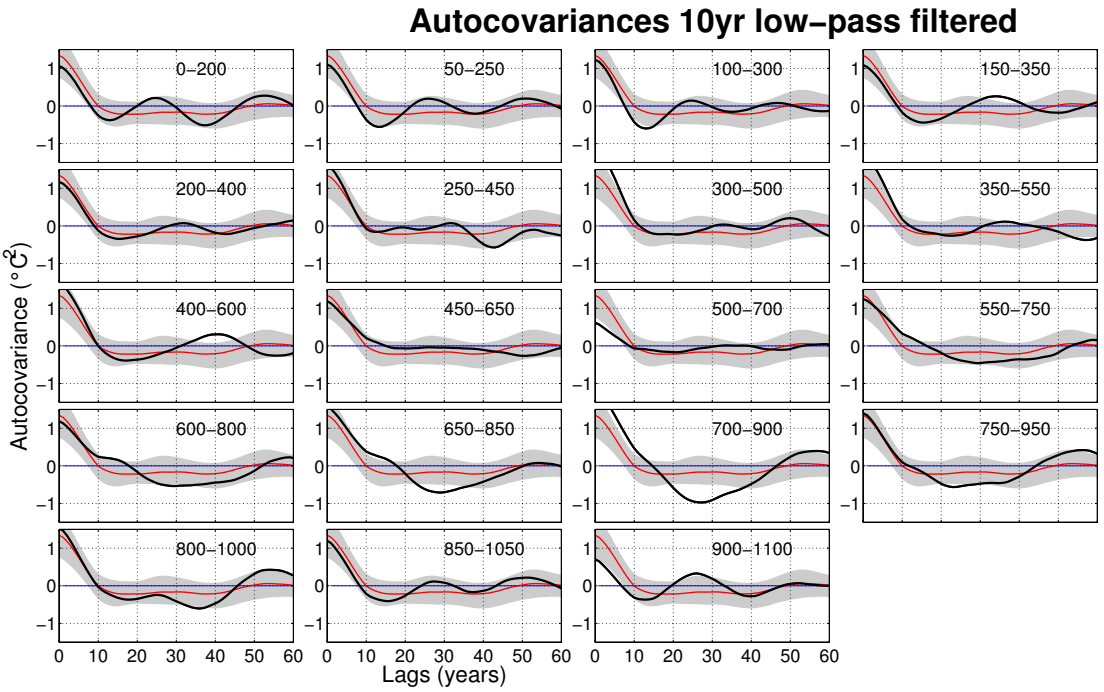

Figure 4.2: *Autocovariances for the 10-year low pass filtered time series split in 200-year-long intervals shifted by 50 years (black thick lines). The gray shading indicates the confidence interval at 90% and the red curve represents the average of the autocovariance functions of the the original intervals.*

Already from a visual inspection, it is possible to find periods where the autocovariance function falls outside the shading, so they do not have the same statistical characteristics of the whole time series. Instead of looking at the intervals, a rigorous approach is counting the number of autocovariance values that fall outside the confidence interval. Taking into account all the 19 intervals, we have 1140 values (that is 19 intervals multiplied by 60 lags). The result is 176 points out, that corresponds to 15.44 % of the total. Concluding: the 15.44% of the total number of values falls outside the confidence interval, it is more than the significance 10% level, so we can reject the null hypothesis and state that the AMV time series for MPI-ESM-P model is not stationary, where AMV is defined as the 10-year low-pass filtered North Atlantic SST time series.

Generalising the method, more robust results are obtained using the raw unfiltered time series and more intervals, shifting the 200-year-long intervals only by 1 year instead of 50 years. In this manner, the MPI-ESM-P time series contains 957 intervals, corresponding to 57420 total autocovariance values, 6981 of which exceed the confidence interval, that is a percentage of 12.16, again we can reject the null hypothesis because the percentage is bigger than the significance 10% level.

4.2 Summary of method and results

The test applied to check the stationarity in the AMV time series is summarized as follows, the method involves:

- Generation of 1000 analytical time series with the same spectrum as the original time series (bootstrap method) [Ebisuzaki, 1997].
- Division of the 1000 analytical time series in 200-year-long intervals (length similar to the observations) shifted by 1 year.
- Computation of the autocovariance function for all these 200-year-long intervals, for all the 1000 analytical time series, with a maximum lag equal to 60 years.
- Use of their distribution to compute the confidence interval at 90% level, finding the inferior (superior) threshold as the lowest (highest) 5% of the total autocovariance value for each lag.

The original NA SST time series are raw, only detrended, and they are also divided in 200-year-long intervals, which are shifted by 1 year. For all the models, each autocovariance value of NA SST index for each interval and for each lag, is compared to the corresponding threshold value for that lag. The number of values outside the threshold are counted. As a result, taking into account the total number of autocovariance values for the original time series (60 lags multiplied by the number of intervals), all models present values that exceed the confidence interval, and 9 out of 11 models exceed the 10% significance level, see Table 4.1 and Figure 4.3. Concluding, two models (NorESM1-M and MRI-CGCM3) out of eleven do not

model	length	n of intervals	tot points	points out	%
MPI-ESM-P	1156	957	57420	6981	12.16
CCSM4	1051	852	51120	5877	11.50
MPI-ESM-LR	1000	801	48060	6268	13.04
CanESM2	996	797	47820	5439	11.37
NorESM1-M	501	302	18120	1693	9.34
GFDL-ESM2M	500	301	18060	2750	15.23
CESM1-BGC	500	301	18060	2497	13.83
MRI-CGCM3	500	301	18060	1612	8.93
ACCESS1-0	500	301	18060	3085	17.08
ACCESS1-3	500	301	18060	1916	10.89
GFDL-CM2.1	3500	3301	198060	21896	11.06

Table 4.1: *Number of autocovariance values that exceed the 90% confidence interval (points out) and their percentage with respect to the total number of points (%), for NA SST time series.*

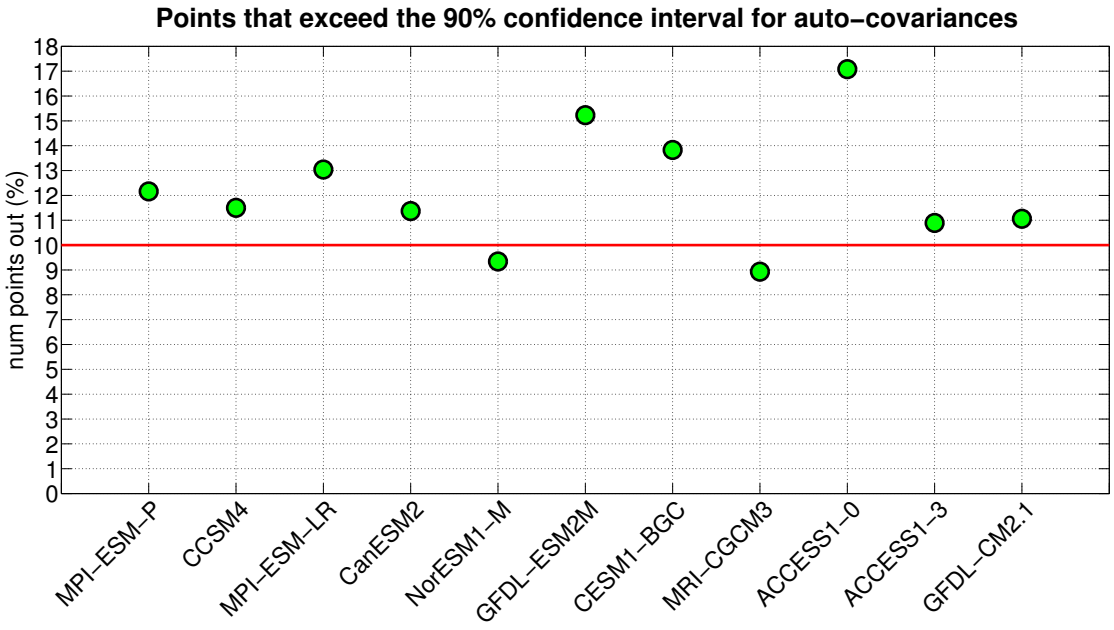

Figure 4.3: *Percentages of autocovariance values that exceed the 90% confidence interval, for all the NA SST time series. Red line defines the 10% significance level.*

pass the test, even if they are very close to the 10% threshold. For the remaining nine models (MPI-ESM-P, CCSM4, MPI-ESM-LR, CanESM2, GFDL-ESM2M, CESM1-BGC, ACCESS1-0, ACCESS1-3 and GFDL-CM2.1) we can reject H_0: the time series are not stationary.

Next, the objective is to understand whether the non-stationarity of the NA SST time series is present also isolating the multidecadal time scales of NA SST variability, through a 10-year running mean. Before the division in 200-year intervals, both the analytical time series and the original NA SST time series are 10-year low-pass filtered, obtaining AMV time series. Since the high-frequency noise contribution to the non-stationarity is removed, fewer models pass the test: seven instead of nine. For 7 models out of 11 the AMV time series results to be non-stationary at 90% level of confidence; they are MPI-ESM-P, CCSM4, MPI-ESM-LR, GFDL-ESM2M, CESM1-BGC, ACCESS1-0 and GFDL-CM2.1 (Table 4.2 and Figure 4.4).

model	**length**	**n of intervals**	**tot points**	**points out**	**%**
MPI-ESM-P	1147	948	56880	8218	14.45
CCSM4	1042	843	50580	5810	11.49
MPI-ESM-LR	991	792	47520	5818	12.24
CanESM2	989	788	47280	4142	8.76
NorESM1-M	492	293	17580	1614	9.18
GFDL-ESM2M	491	292	17520	3757	21.44
CESM1-BGC	491	292	17520	3017	17.22
MRI-CGCM3	491	292	17520	1443	8.24
ACCESS1-0	491	292	17520	3843	21.93
ACCESS1-3	491	292	17520	412	2.35
GFDL-CM2.1	3491	3292	197520	20319	10.29

Table 4.2: *As in Table 4.1, but for AMV time series.*

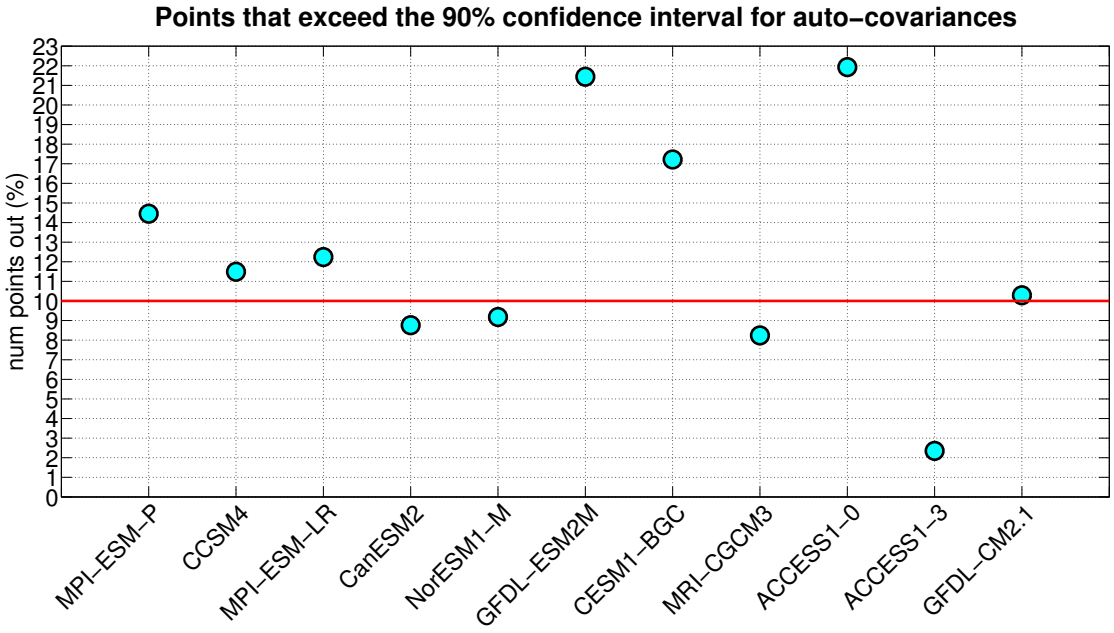

Figure 4.4: *As in Figure 4.3, but for AMV time series.*

The other four models are the NorESM1-M and MRI-CGCM3, that do not pass the test already in the unfiltered case, plus CanESM2 and ACCESS1-3. In particular, NorESM1-M model shows less pronounced evidence of non-stationarity already in Figure 3.8, revealing an almost stationary autocorrelation through time. However, they are only marginally stationary because they are again very close to the 10% threshold, except for ACCESS1-3 which do not show preferred time scales for long segments of its evolution (see Figure 3.8).

The statistical test is affected by the length of model records, since short records provide fewer intervals, and by the number of lags for the autocovariance functions. Each model may require different numbers of lags (not necessarily 60 years) according to each preferred AMV time scales, however a common parameter is needed in multi-model comparison and the test should be robust for whatever number of lags for autocovariances are used.

Chapter 5

The role of AMOC and ocean-atmosphere mechanisms

Having underlined the non-stationarity that characterises the natural, internal, low-frequency variability in the North Atlantic sea surface temperatures, this chapter deals with the related long-term modulations in the oceanic and atmospheric components of climate system.

5.1 Simulated AMOC

A widely accepted mechanism for AMV invokes coordinated changes in the Meridional Overturning Circulation (MOC) strength, which in turn lead to multidecadal changes in the meridional heat transport [Delworth et al., 1993; Timmermann et al., 1998; Latif et al., 2004, 2006; Jungclaus et al., 2005; Knight et al., 2005; Dong and Sutton, 2005; Delworth and Mann, 2000; Collins et al., 2006; Msadek and Frankignoul, 2009]. MOC is quantified by the meridional overturning stream-

function, $\psi(y, z, t)$, calculated integrating the meridional velocity $v(x, y, z, t)$ across longitude x and depth z, at time t and at any given latitude y:

$$\psi(y, z, t) = \int_{-z}^{0} \int_{x_{east(y,t)}}^{x_{west(y,t)}} v(x, y, z, t) dx \cdot dz$$

Units for MOC are Sverdrups (Sv), where 1 Sv is equal to a volume flow rate of $10^6 m^3 s^{-1}$. The mean state of MOC in the Atlantic Ocean is the long-term mean of the Atlantic meridional overturning streamfunction and is represented in Figure 5.1, as simulated by different models. Positive values (negative values) denote clockwise (anticlockwise) circulation.

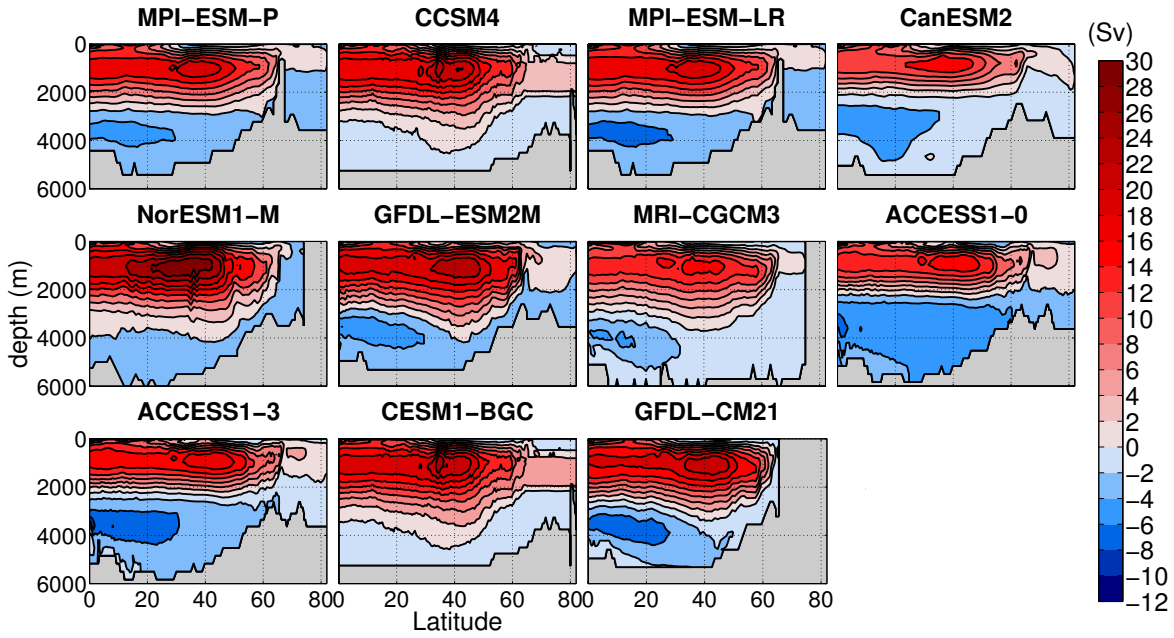

Figure 5.1: *Vertical mean profile of AMOC streamfunction (Sv) in the models.*

All models generally capture the basic structure of the AMOC climatology, with a northward current in the upper ocean, a downwelling around 60°N, and the

southward returning flow in the lower layer (around 3000 m). Beneath this depth, the northern extension of the Antarctic Bottom Water (AABW) cell can be seen in almost all the models. However, the largest differences are seen in how models reproduce this lower overturning cell: CCSM4, NorESM1-M and CESM1-BGC models show a very weak or absent cell. These are also the models that present an AMOC southward returning flow that penetrates to the bottom of the basin below 4000 m.

In models, an AMOC index is usually defined as the maximum Atlantic meridional overturning streamfunction either at a specific latitude [Mahajan et al., 2011; Zhang and Delworth, 2006] (in particular 30°N [Ba et al., 2014; Jungclaus et al., 2005]), or within a depth-latitude box, e.g. Msadek et al. [2010]; Escudier et al. [2012]; Wang and Zhang [2013]. Otherwise it is also defined by projecting in space the yearly MOC onto the low-pass filtered pattern given by EOF1 of MOC anomalies [Msadek and Frankignoul, 2009]. According to Otterå et al. [2010], these alternative formulations yield very similar results.

Different models can have the maximum of the meridional overturning circulation at different locations in the latitude-depth plane: Table 5.1 reports the locations of the maxima detected in the analysed models. These values of simulated AMOC maxima can be compared to the observed data from RAPID MOC time series [Smeed et al., 2015], keeping in mind that they refer to different latitudes, while RAPID array is displaced across the Atlantic at 26°N. RAPID MOC monitoring project provides 10-year time series of observed MOC transports at 26°N for the period 1-April-2004 to 22-March-2014, defined as the streamfunction at the depth of its maximum (z_{max}), at each time: $AMOC(t) = \psi(t, z_{max})$. RAPID time series has a mean strength of 17.2 Sv with a 10-day filtered root mean square

model name	depth (m)	latitude (°N)	value (Sv)
MPI-ESM-P	1020	38.5	27.0
CCSM4	1041	34.6	29.7
MPI-ESM-LR	1020	34.5	28.4
CanESM2	661	36.7	20
NorESM1-M	1100	42.0	35.1
GFDL-ESM2M	1007	45.0	31.3
MRI-CGCM3	1050	45.0	19.5
ACCESS1-0	813	42.6	22.2
ACCESS1-3	813	42.6	26.0
CESM1-BGC	1041	34.6	30.8
GFDL-CM2.1	1176	43.5	29.0

Table 5.1: *Location of the maximum of Atlantic meridional circulation, for each model.*

variability of 4.6 Sv [McCarthy et al., 2015]; therefore, models overestimate the AMOC maximum.

In order to compare different models, the AMOC index is here defined as the maximum of Atlantic meridional overturning streamfunction in the range of latitudes between 30°N to 50°N, so as to include the detected maxima (Table 5.1). Therefore, the index represents the fluctuations in the intensity of the AMOC. Long-term mean is subtracted to obtain anomalies, then the resulting AMOC index is filtered by a 10-year running mean and detrended as for AMV index, since the time scale of interest is the multidecadal one.

5.2 AMV/AMOC relationship

In order to understand the mechanisms underlying the non-stationarity of the AMV, the relationship between the AMV behaviour and the large-scale ocean circulation (AMOC) is inspected.

Figure 5.2 shows the AMV index plotted against the AMOC index in the eleven preindustrial simulations.

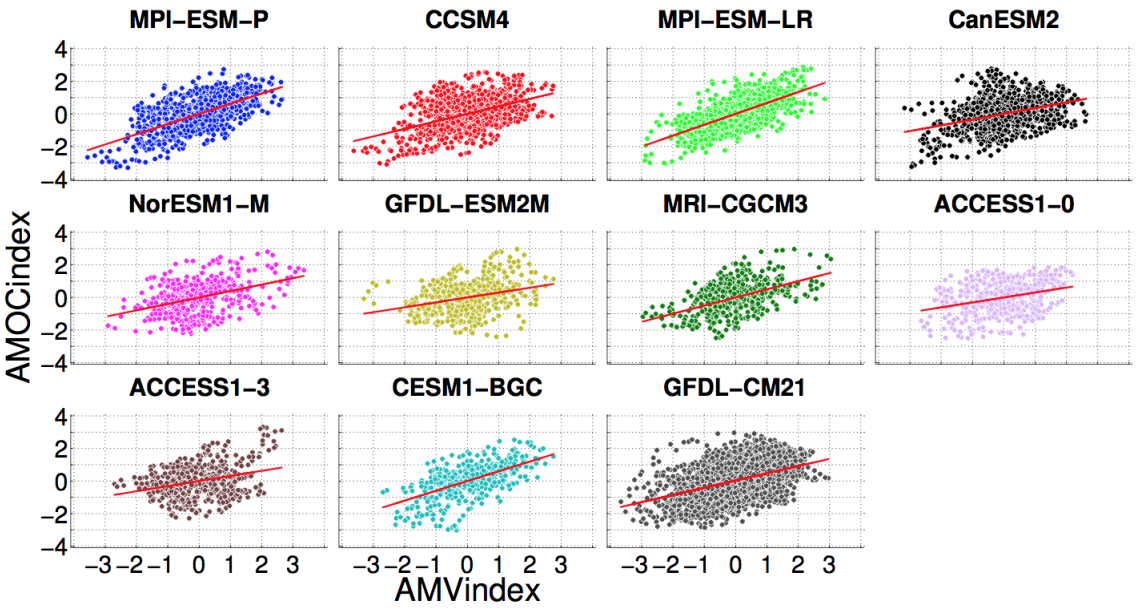

Figure 5.2: *AMV index versus AMOC index scatter plot and linear fit.*

Both indices are standardized by subtracting the mean and dividing by the standard deviation. Therefore the indices become dimensionless, with zero-mean and unit standard deviation. In the scatter plots, AMV index is presented as the independent x variable, so the regression analysis infers the change in the AMOC starting from North Atlantic SST variations. The slope a of the fitted line, describing linear regression $y = ax$, varies across models, ranging from 0.3 to 0.7, and is equal to the AMV/AMOC correlation. All models show a positive correlation between their corresponding AMOC and AMV indices. The highest correlation is shown by the MPI-ESM-LR model, while the two ACCESS models exhibit the lowest correlations. For all the models, the range of correlation values indicate that the AMV explains less than a half of the AMOC variance.

However, this analysis considers only the zero-lag relationship between AMOC and AMV. To explore their lagged covariability, the lagged correlation between AMV and AMOC index has been computed (Figure 5.3).

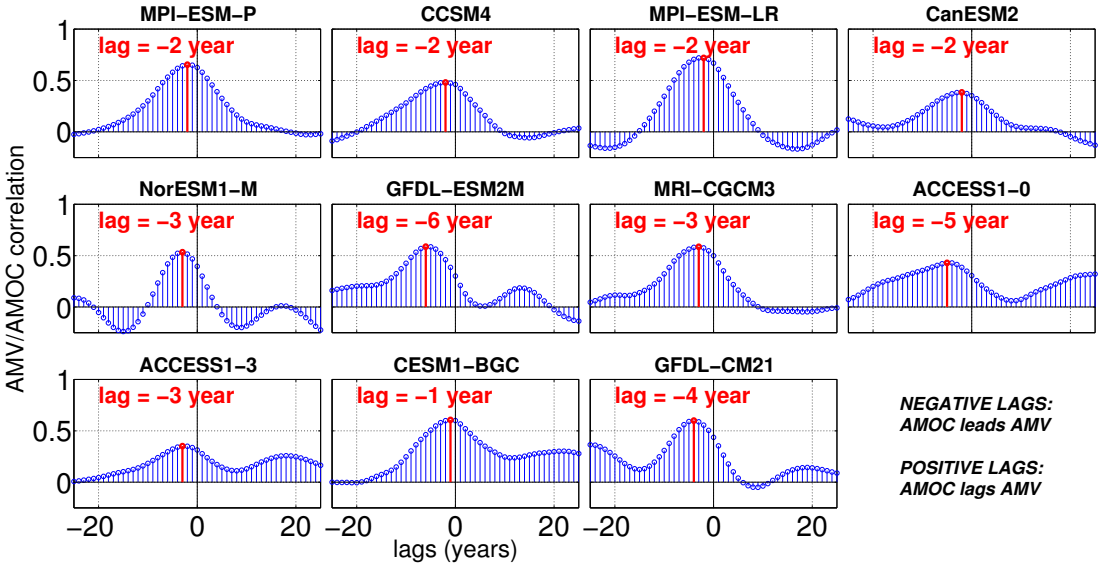

Figure 5.3: *Lagged correlation between AMV and AMOC indices: negative (positive) years in x-axis mean the AMOC leads (lags) the AMV. Maximum lagged correlation is highlighted in red.*

Lead-lag correlation patterns vary across the models, but some commonalities can be found. All models present the maximum of lagged correlation when AMOC leads AMV by a few years (from 6 to 1 year before the AMV maximum), indicating that North Atlantic SSTs increase a few years after a strengthening of the Atlantic MOC. The phase relationship is consistent with an increase in the overturning leading to a warming of the North Atlantic. The different lags of maximum correlation may arise from different adjustment time scales of the AMOC to the northern Atlantic deep convection [Wang and Zhang, 2013]. Most of the models show an asymmetric AMV/AMOC correlation function that increases slowly for negative lags, implying strong AMOC influence on AMV, but the subsequent decrease is steeper for positive

lags, suggesting a weaker impact of AMV on AMOC. AMOC drives AMV more than the opposite. In fact, on long time scales, AMV is regarded as a passive response to the AMOC in some studies [Delworth and Mann, 2000; Knight et al., 2005; Medhaug and Furevik, 2011]. Two models (MPI-ESM-LR and NorESM1-M) display a self-sustained oscillatory behaviour. The oscillation is consistent with the following mechanism, described by Zhang and Wang [2013]. When the AMOC leads the AMV, a strengthened AMOC produces a heat transport convergence in the North Atlantic Ocean and thus generates a warm phase of the AMV. After some time delay, the warm phase of the AMV tends to reduce the meridional density gradient over the North Atlantic Ocean, which weakens the AMOC strength. After some adjustment, the negative AMOC anomaly generates an anomalous, cold phase of AMV which will in turn feed back onto the AMOC a few years later, and so on. This relationship is consistent with the delayed advective oscillation mechanism reviewed by Vallis [2010]: the oscillation arises because of a delay in the response of the AMOC and the associated transport of heat to the meridional temperature gradient; the detailed manifestation of the oscillation seems to differ somewhat from model to model, with varying roles for salinity playing an important role in some simulations and less so in others. Other models primarily exhibit a positive correlation for all time lags (ACCESS1-0, ACCESS1-3, CESM1-BGC). This means that there is a positive feedback between the AMOC and AMV, so if there are no other feedbacks, the AMOC and AMV will not oscillate. Finally, some models displays less clear AMV/AMOC correlations. Since the surface warming in the North Atlantic subpolar gyre following an increase of the AMOC is a robust feature in a variety of coupled climate models, the predictability of the AMOC could lead to predictability of North Atlantic surface temperatures on decadal time scales.

However, the time scales and spatial patterns of SST predictability will be model dependent [Roberts et al., 2013]. Also Medhaug and Furevik [2011] underline that, although individual models show potential for decadal prediction based on the relationship between the AMV and AMOC, the models strongly disagree both in phasing and strength of the covariability. This makes it difficult to identify common mechanisms and to assess the applicability for predictions.

Next we investigate low-frequency changes in the relationship between Atlantic surface temperatures and overturning circulation, looking at how their correlation changes as a function of time. While the previous analysis was based on the entire time series, now the AMV/AMOC correlation is computed for a moving 200-year-long time window. At each step, this time window slides one year forward and the correlation is computed again, until reaching the end of the time series: as an example, the value of correlation coefficient at T=1 corresponds to the correlation in the interval from year 1 to year 201; the value at T=2 refers to the interval from year 2 to year 202, and so on (Figure 5.4).

Moving window AMV/AMOC cross-correlation shows highly varying patterns among the models, with alternating periods with higher and lower correlation. From a visual inspection, transitions into periods of strong AMV/AMOC link seem to be more moderate than the transitions into periods of weak AMV/AMOC link, which can be also abrupt. The detected decrease in AMV/AMOC correlation, evident for example during the last part of the model record for GFDL-ESM2M and MRI-CGCM3 models, also implies that even if the AMOC does generally play an important role in the AMV variability, there are other factors that may contribute to the AMV.

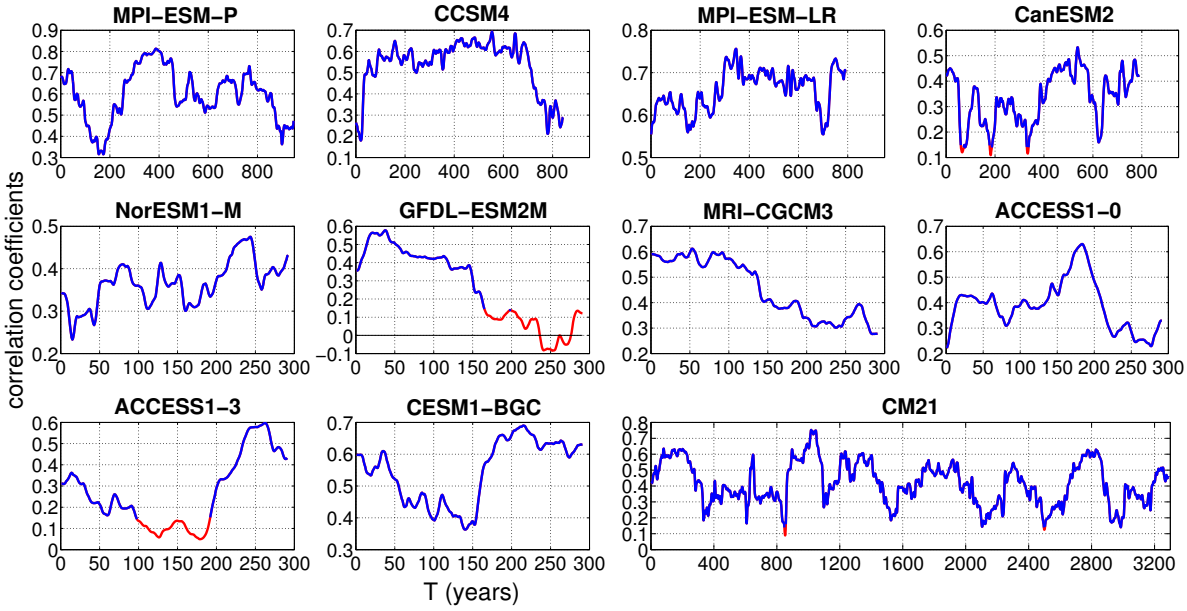

Figure 5.4: *AMV/AMOC correlation in moving 200-year time windows, for all the models. Not significant values (95% confidence level) are indicated in red.*

5.3 Ocean and atmosphere interactions

In the previous section it was shown that, at multidecadal time scales, the link between North Atlantic SSTs and Atlantic MOC undergoes significant fluctuations with time. In order to understand what causes this non-stationarity, next we consider the role of the atmosphere/ocean interactions on the AMV signal.

The dominant patterns of co-variability between the ocean and the atmosphere are studied with a Maximum Covariance Analysis (MCA) approach [von Storch and Zwiers, 1999]. MCA performs a Singular Value Decomposition (SVD) of the cross-covariance matrix between atmospheric and oceanic fields. SVD identifies structures in a given variable that are best correlated with structures in another variable. They are structures that 'explain' the maximum amount of covariance between two data sets in a similar way that EOFs and PCs are the structures

that explain the most variance in a data set. The matrices of the two fields of interest are the starting point of the analysis: the first field is $X = (\vec{x}_1|...|\vec{x}_t)$ and the second field is $Y = (\vec{y}_1|...|\vec{y}_t)$. The matrices X and Y are the $[space \times time]$ matrices of the anomalies obtained removing the time mean and normalised by the standard deviation in time, to allow a comparison. The cross-covariance matrix between the two fields is computed as $C_{XY} = \frac{1}{t}XY^\top$, since normalised anomalies are used, the elements of C_{XY} are correlation coefficients. SVD is applied on C_{XY} to produce $C_{XY} = U\Sigma V^\top$. Matrices $A = U^\top X$ and $B = V^\top Y$ of the expansion coefficients, represent the data in the new bases formed by singular vectors. Following the procedure summarized by von Storch and Navarra [1999], heterogeneous (homogeneous) correlation maps are generated correlating at each grid point the expansion coefficients time series of one field, with the time series of the other (the same) field in that grid point. Therefore, the homogeneous correlation map is a useful indicator of the geographic localization of the co-varying part of the field itself, and the heterogeneous correlation map indicates how well the pattern of anomalies in one field can be derived from the other field [Bretherton et al., 1992]. In this study, 10-year running mean filtered North Atlantic SST and global Sea Level Pressure (SLP) are used. Global SLP is chosen as representative of atmospheric circulation at the ocean surface and it allows us to study the teleconnection patterns not only over the North Atlantic ocean, but also over all the other basins. Only the first MCA mode is considered, as the fraction of cross-covariance explained by the higher-order modes vanishes quickly (not shown). For illustrative purposes, we will consider here the four longest CMIP5 models: MPI-ESM-P, CCSM4, MPI-ESM-LR and CanESM2. First of all the correlation maps for the entire time series are shown, and then we focus on periods of decrease and increase of AMV/AMOC correlation.

Figure 5.5 shows the two heterogeneous maps (on the left) and the two homogeneous maps (on the right), for each model. All panels refer to the entire time series.

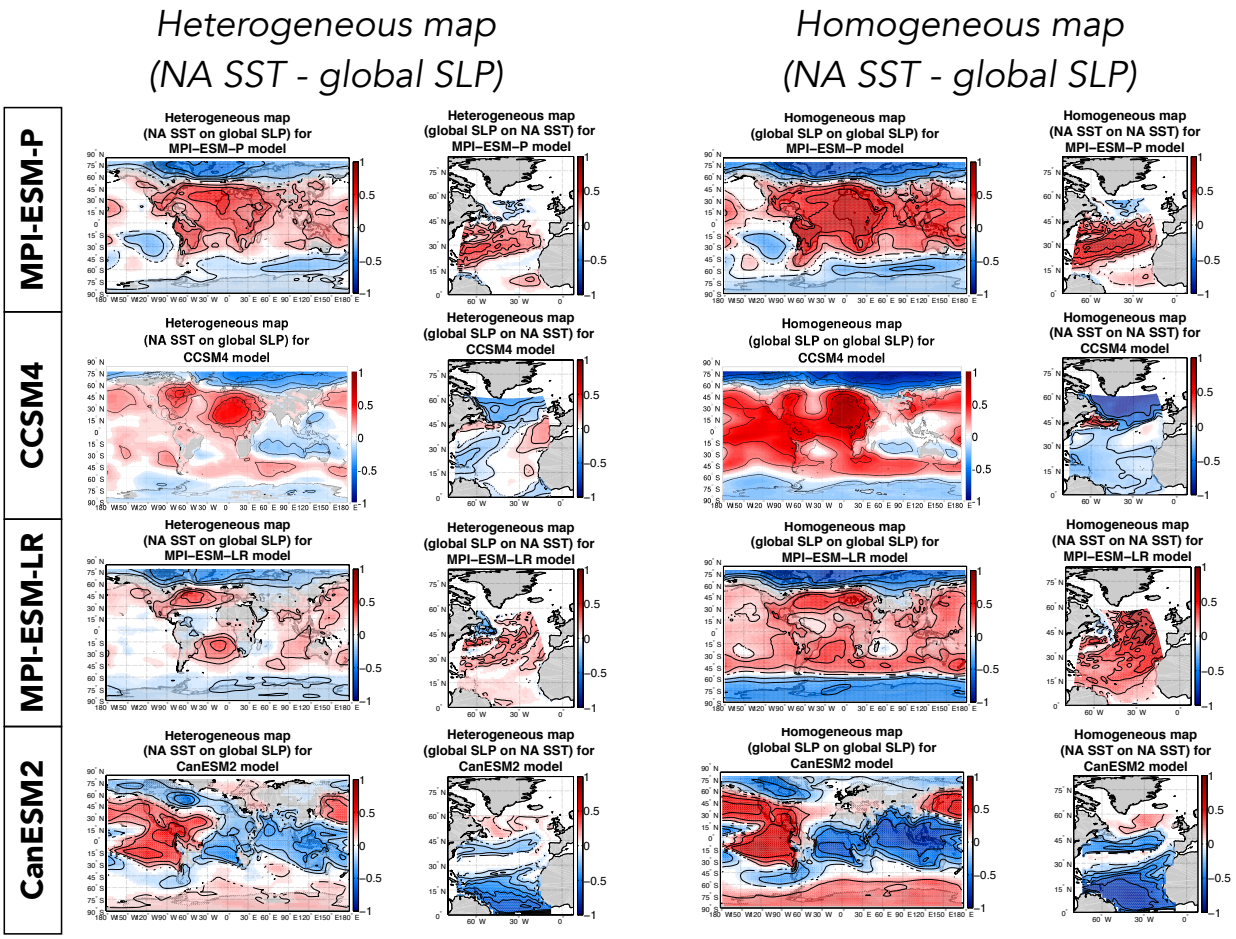

Figure 5.5: *MCA heterogeneous and homogeneous maps between North Atlantic SST and global SLP fields, computed for the whole time series, for MPI-ESM-P, CCSM4, MPI-ESM-LR and CanESM2 models.*

We compare the first column with the third column (global domain), and the second column with the fourth column (North Atlantic domain), because difference in the shapes of the patterns on the heterogeneous and homogeneous correlation maps for the same field provides insights into the nature of the cause/effect linkages between the fields [Wallace et al., 1992]. As expected, the shape of patterns on the

corresponding maps are similar, but the heterogeneous correlations are weaker than the homogeneous correlations. Similar patterns are seen in SLP heterogeneous maps for MPI-ESM-P, CCSM4 and MPI-ESM-LR models, even though MPI-ESM-P presents a wide area of large covariance covering the entire North Atlantic, CCSM4 positive centres of action are displaced more over land (American and European continents), and MPI-ESM-LR shows two separated large covariance areas in the North and South Atlantic, with very low covariances in the other oceans and in the tropical band. Very different is the CanESM2 case, where the large covariance between SLP and North Atlantic SST is shifted west and the teleconnection is stronger in the tropical band instead of the high latitude band. Regarding the NA SST heterogeneous maps, the pattern differs even more across models, being also very fragmented.

Next, we apply the MCA analysis, focusing on specific time windows, characterised by a concomitant "strong" or "weak" AMV/AMOC correlation, whereby strong/weak are defined as follows. When AMV/AMOC correlation is lower (higher) than the correlation averaged over the whole model record, that period is defined weak (strong). The averaged correlation is 0.42 for MPI-ESM-P model, 0.43 for CCSM4, 0.40 for MPI-ESM-LR and 0.34 for CanESM2, as indicated by the dashed line on each top panel in Figure 5.6.

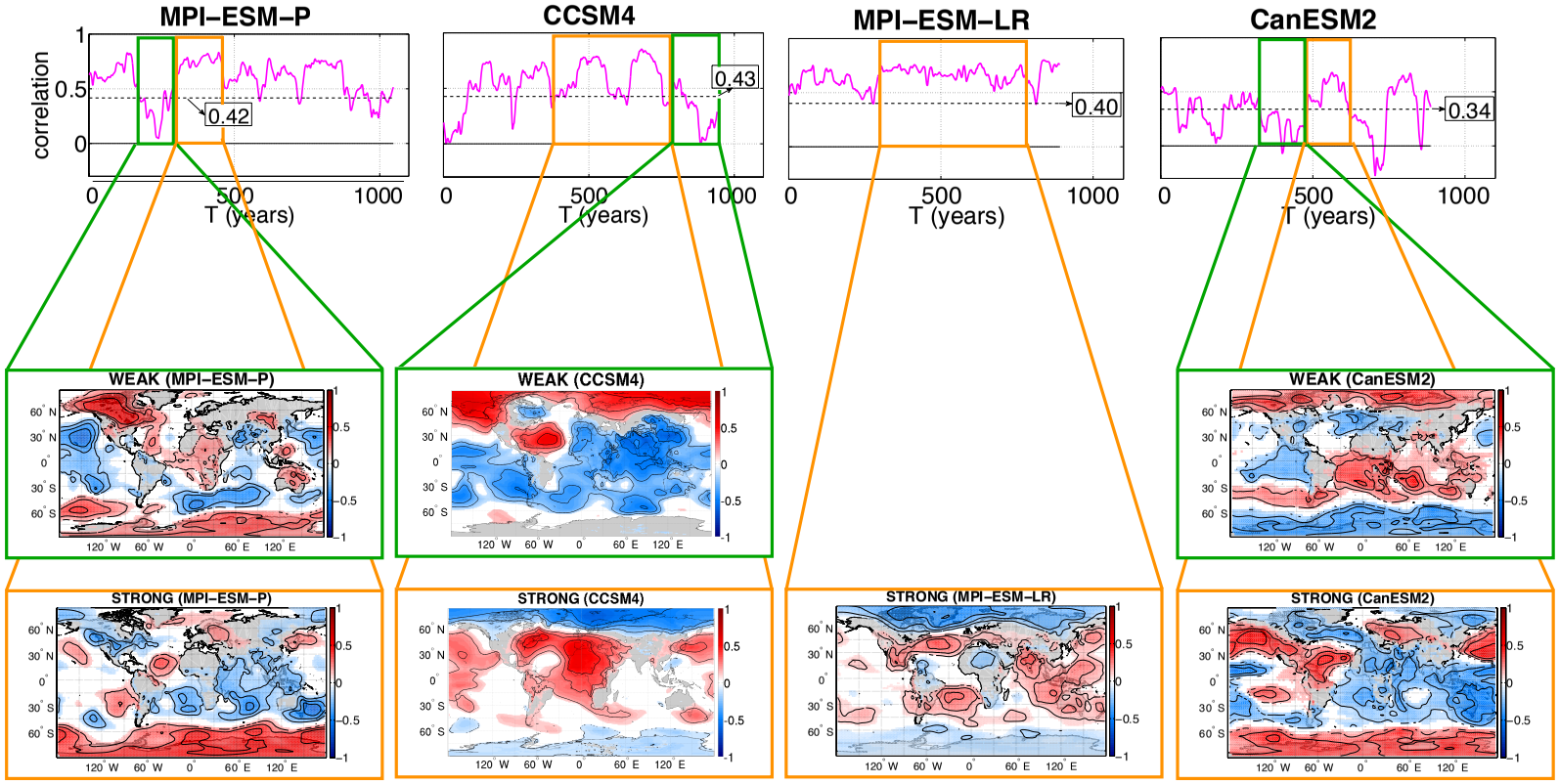

Figure 5.6: *Fig: (top) Correlations computed in 100-year time windows, moving them 1 year forward each step. (bottom) MCA teleconnection patterns: impact of North Atlantic SST over global SLP, in period of weak AMV/AMOC relationship (green boxes) and in period of strong AMV/AMOC relationship (orange boxes).*

For all the models, but MPI-ESM-P, periods of strong AMV/AMOC correlation seem to have more persistent teleconnection patterns, since they resemble the heterogeneous map related to the entire time series. On the other hand, during periods of weak AMV/AMOC correlation, North Atlantic sea surface temperatures have largely different atmospheric impacts, with no apparent consistency across the models. This may be due to the fact that periods selected in this manner have different lengths, affecting MCA analysis and making MCA patterns not consistently comparable. In order to overcome this problem, in Figure 5.7, 5.8, 5.9 and 5.10 equal-length intervals are selected to show changes in teleconnection patterns associated to the AMV index. For each model, the corresponding AMV time series is displayed on the top, as a reference, and at the bottom the heterogeneous correlation map is computed for each 400-year interval shifted by 50 years starting from the top left corner. Looking at MPI-ESM-P case (Figure 5.7), the high positive correlation over the North Atlantic Ocean during the period 1-400, gradually shrinks until it almost disappears during the period 350-750; then it appears again and reaches the shape we have seen for the entire time series during the period 500-900. This feature means that different regimes in the AMV index time series correspond to different atmosphere-ocean interactions. It is not clear which kind of AMV regime (mostly warm or mostly cold, moderate or intense, nearly sinusoidal or irregular, shorter-period or longer-period, etc.) may be associated to a different MCA pattern. Values reported in the yellow box on the top-right of each heterogeneous map are the correlations between AMV and AMOC for each period: low AMV/AMOC correlations seem to be associated with heterogeneous maps where large positive SLP/NA SST covariance is centred in the North Atlantic; while highest AMV/AMOC correlations seem to correspond to weaker SLP/NA SST

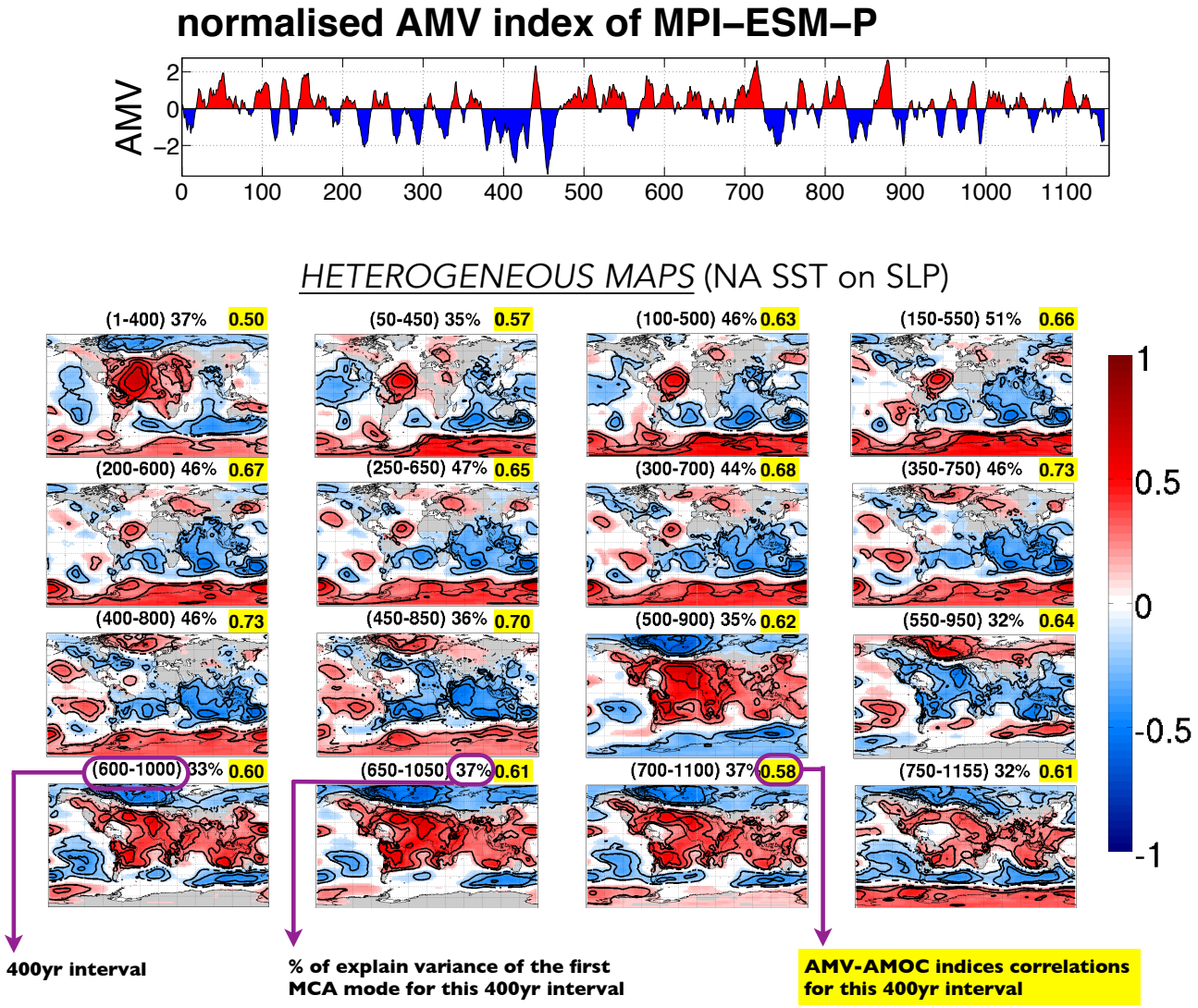

Figure 5.7: *MCA heterogeneous maps between North Atlantic SST and SLP fields, computed for 400-year-long intervals shifted by 50 years, for MPI-ESM-P model. Titles of each map include the limit years of that interval in brackets, then the percentage of explain covariance of the first MCA mode and lastly the AMV/AMOC correlation for that interval, inside a yellow box.*

covariances that are localised particularly outside the North Atlantic area. This result fits with the expectation of a stronger involvement of ocean-atmosphere interaction associated to a weak AMV/AMOC relationship: in those periods the

atmospheric forcing could prevail as a driver of AMV, compared to the ocean internal dynamics, and teleconnections with other basins could break the coupling. In Figure 5.8, CCSM4 shows almost the same pattern from the first interval until period 150-550, after that this pattern starts to change becoming similar to the entire time series pattern, then it changes again spreading the SLP/NA SST covariance signal also outside the Atlantic, reaching the last interval 650-1050, which is characterised by the lowest AMV/AMOC correlation value.

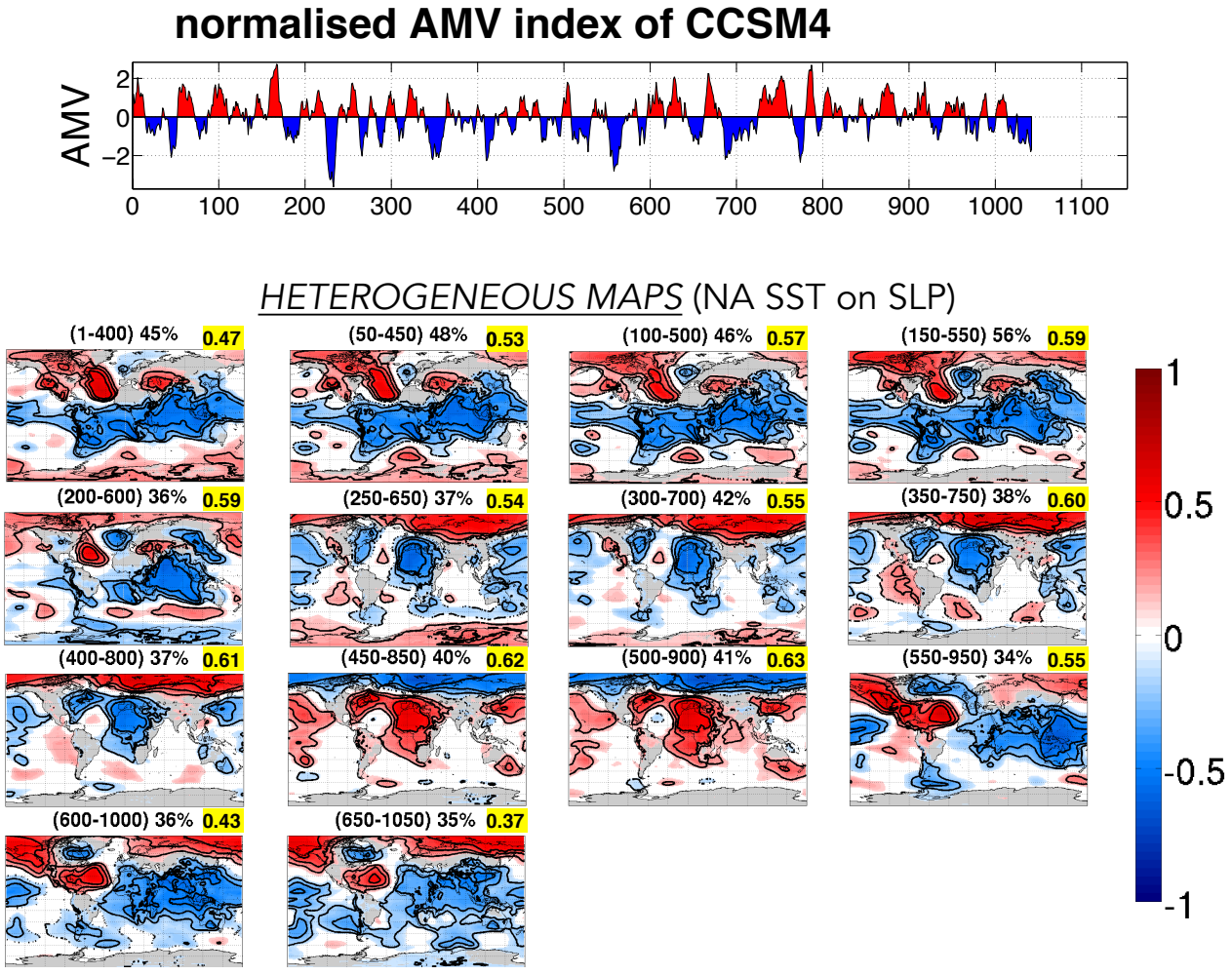

Figure 5.8: *The same as Figure 5.7, but for CCSM4 model.*

The dipole shown by the MCA heterogeneous map for the entire MPI-ESM-LR time series (seen in Figure 5.5) is built and then destroyed again, looking at the time series by subsequent intervals (Figure 5.9).

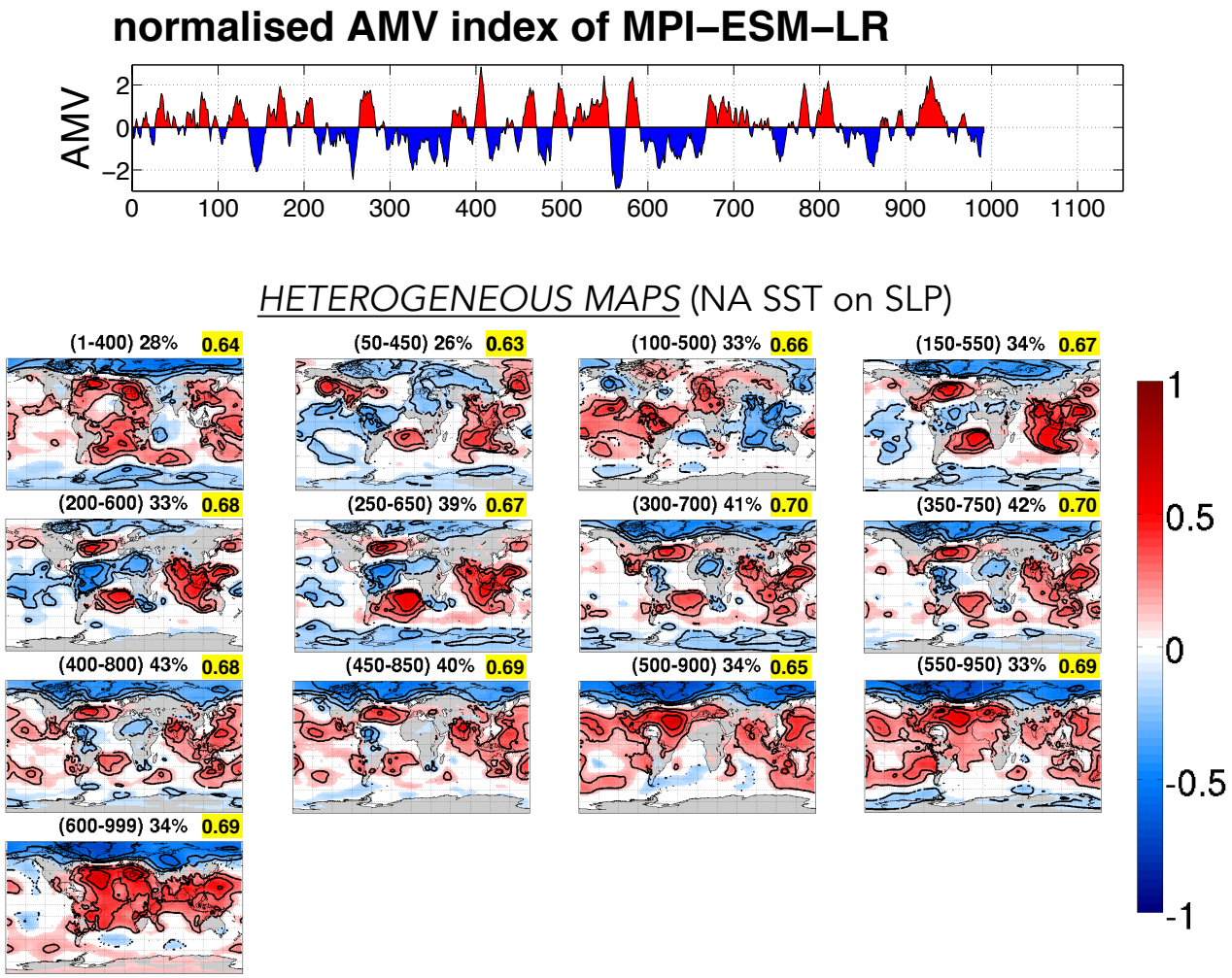

Figure 5.9: *The same as Figure 5.7, but for MPI-ESM-LR model.*

Also CanESM2 model in Figure 5.10 presents an evolution in teleconnection patterns according to different AMV regimes of variability, included the tendency to have large positive SLP/NA SST covariances over the North Atlantic region when the

AMV/AMOC correlation is low. It is noticeable that the teleconnection between tropical Pacific and extra-tropical North Atlantic undergoes a modulation looking at period 350-750 versus period 1-400.

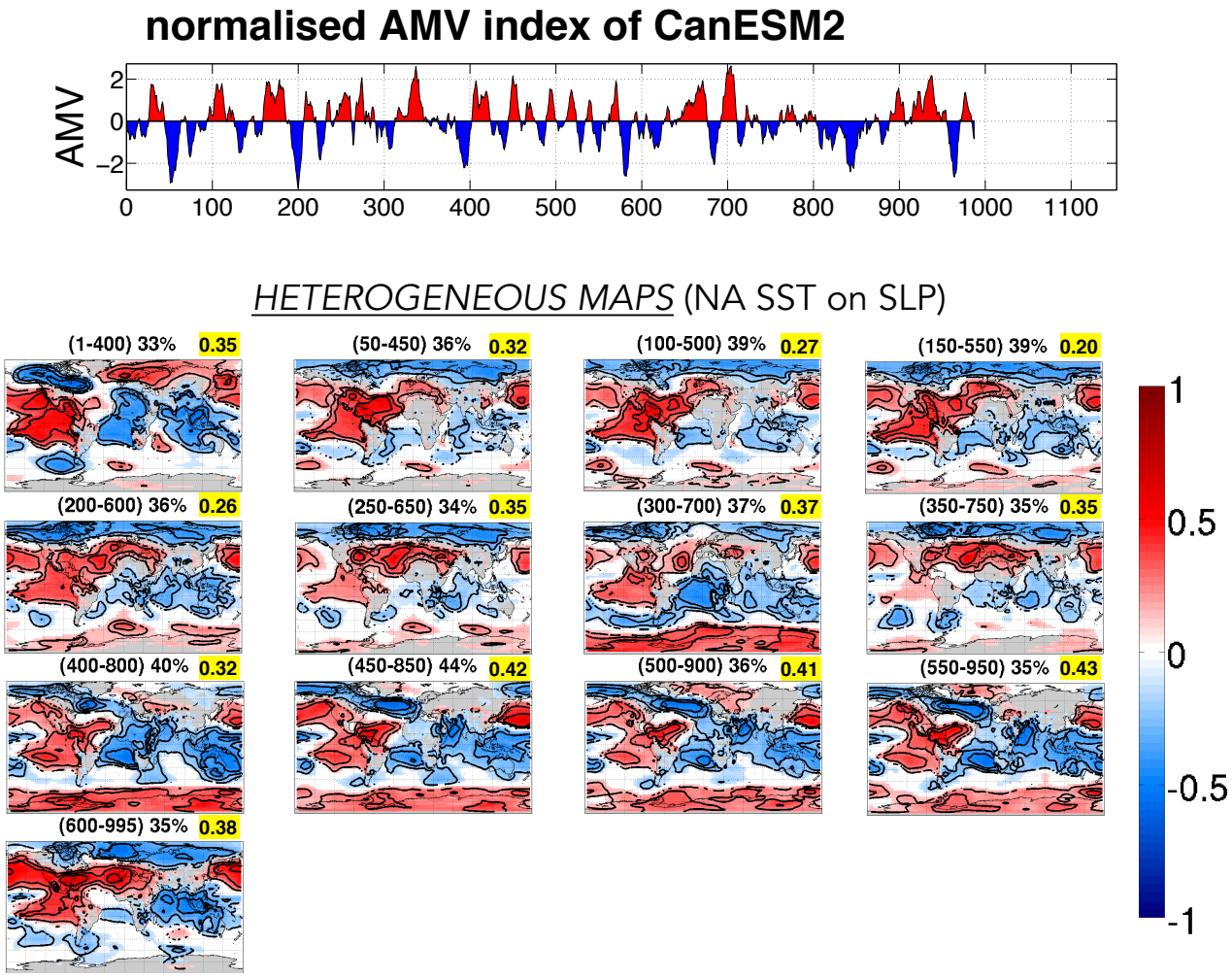

Figure 5.10: *The same as Figure 5.7, but for CanESM2 model.*

5.4 Modes of variability

The analysis presented in the previous section revealed that ocean-atmosphere covariability patterns are subject to a high non-stationarity, suggesting that the overall variability results from many different processes.

Further characterization of AMV regimes is done here, including at the same time information about: periodicity (AMV autocorrelation function), North Atlantic SST co-varying pattern (MCA homogeneous correlation map) and North Atlantic SST impact on global SLP (MCA heterogeneous correlation map). The approach is again to look at individual time intervals within the AMV time series: the analysis is done by epochs selecting 200-year time intervals (shifted by 50 years) from each of the multi-century AMV index time series.

Different time scales are detected for different periods: in Figure 5.11, 5.12 and 5.13 intervals characterised by a shorter time scale ($\sim$ 20 years) alternate to longer time scale periods ($\sim$ 60 years); analogously to Figure 3.8, but making explicit each single interval. Note that for GFDL-CM2.1 model, intervals are shifted by 100 years instead of 50 years because of the length of the model record.

Corresponding to these preferential periodicities, different MCA homogeneous and heterogeneous maps of the first MCA mode between North Atlantic SST and global SLP for the same 200-year intervals are shown in Figure 5.14, 5.15, 5.16, 5.18 and 5.19, for the longest models, ordered by length.

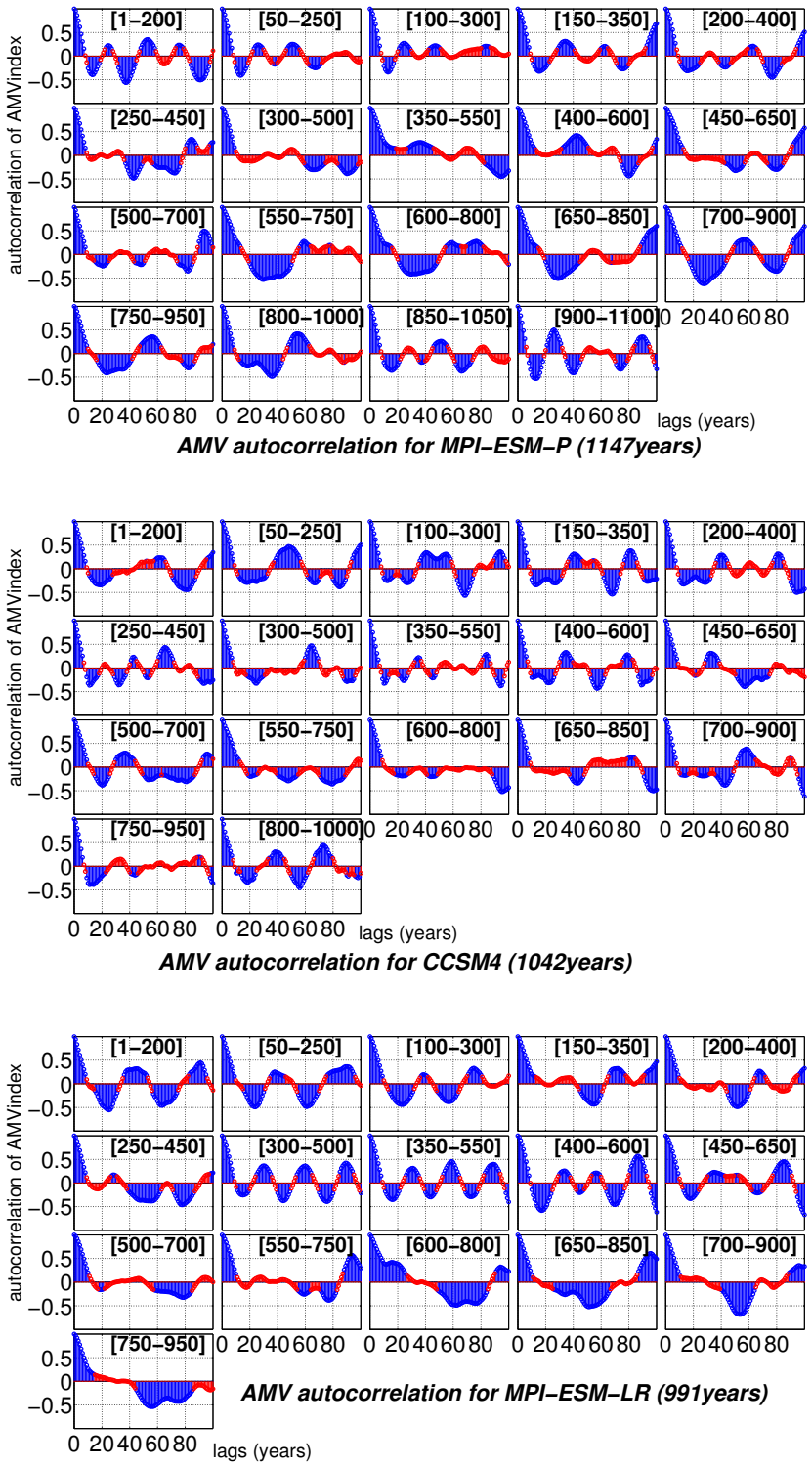

Figure 5.11: *AMV autocorrelation for MPI-ESM-P, CCSM4 and MPI-ESM-LR, for 200-year intervals shifted by 50 years (indicated inside the square brackets), red values are non-significant values.*

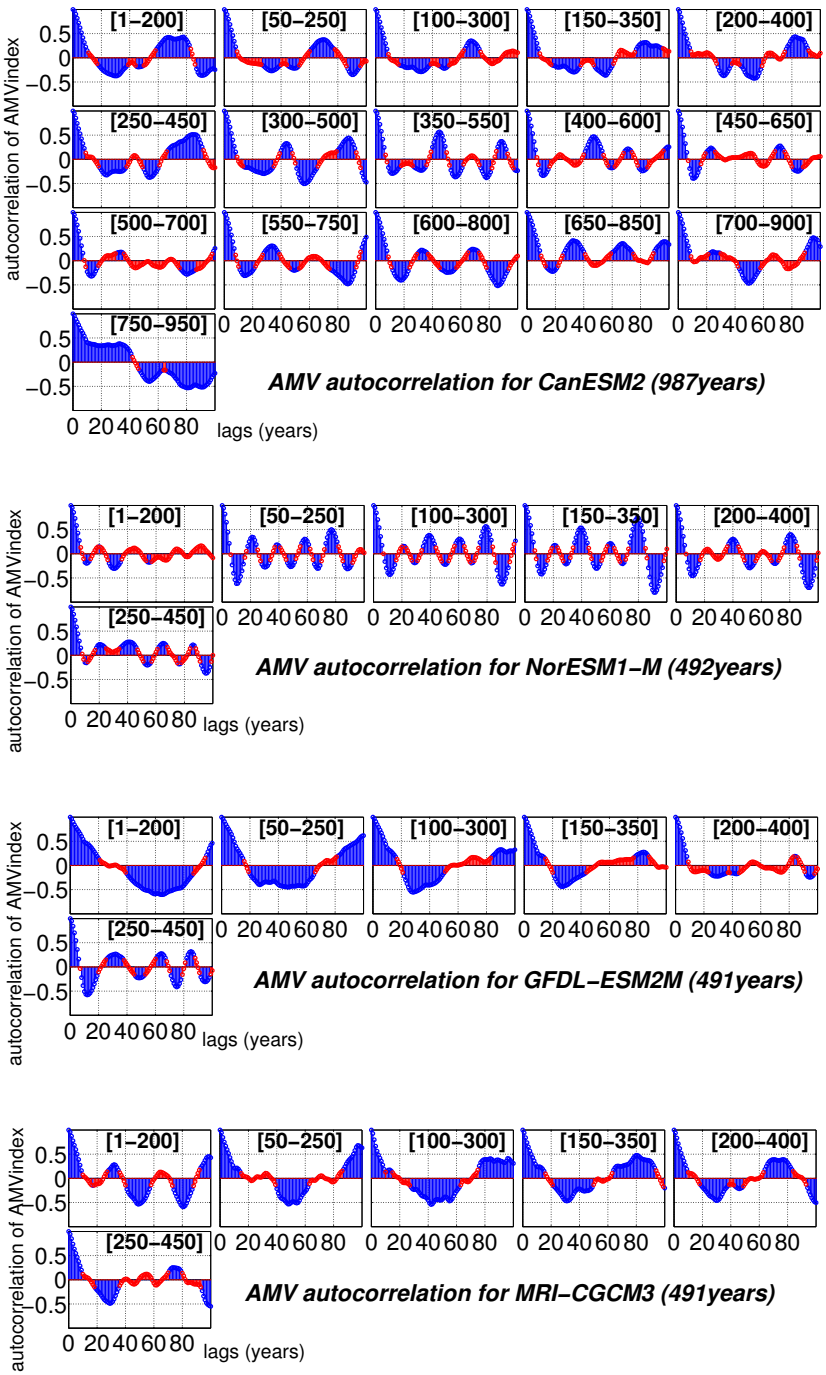

Figure 5.12: *As in Figure 5.11, but for CanESM2, NorESM1-M, GFDL-ESM2M and MRI-CGCM3.*

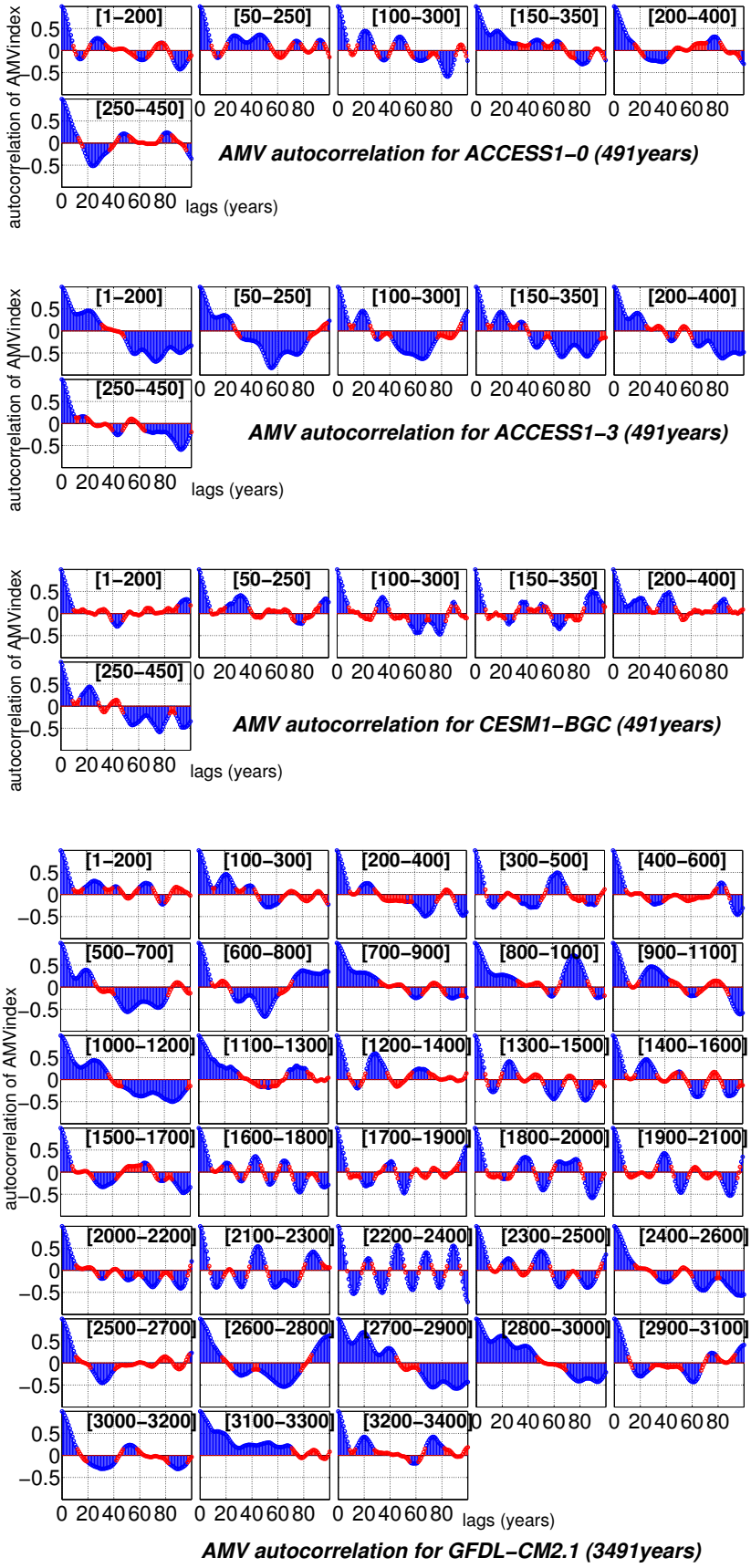

Figure 5.13: *As in Figure 5.11, but for ACCESS1-0, ACCESS1-3, CESM1-BGC and GFDL-CM2.1.*

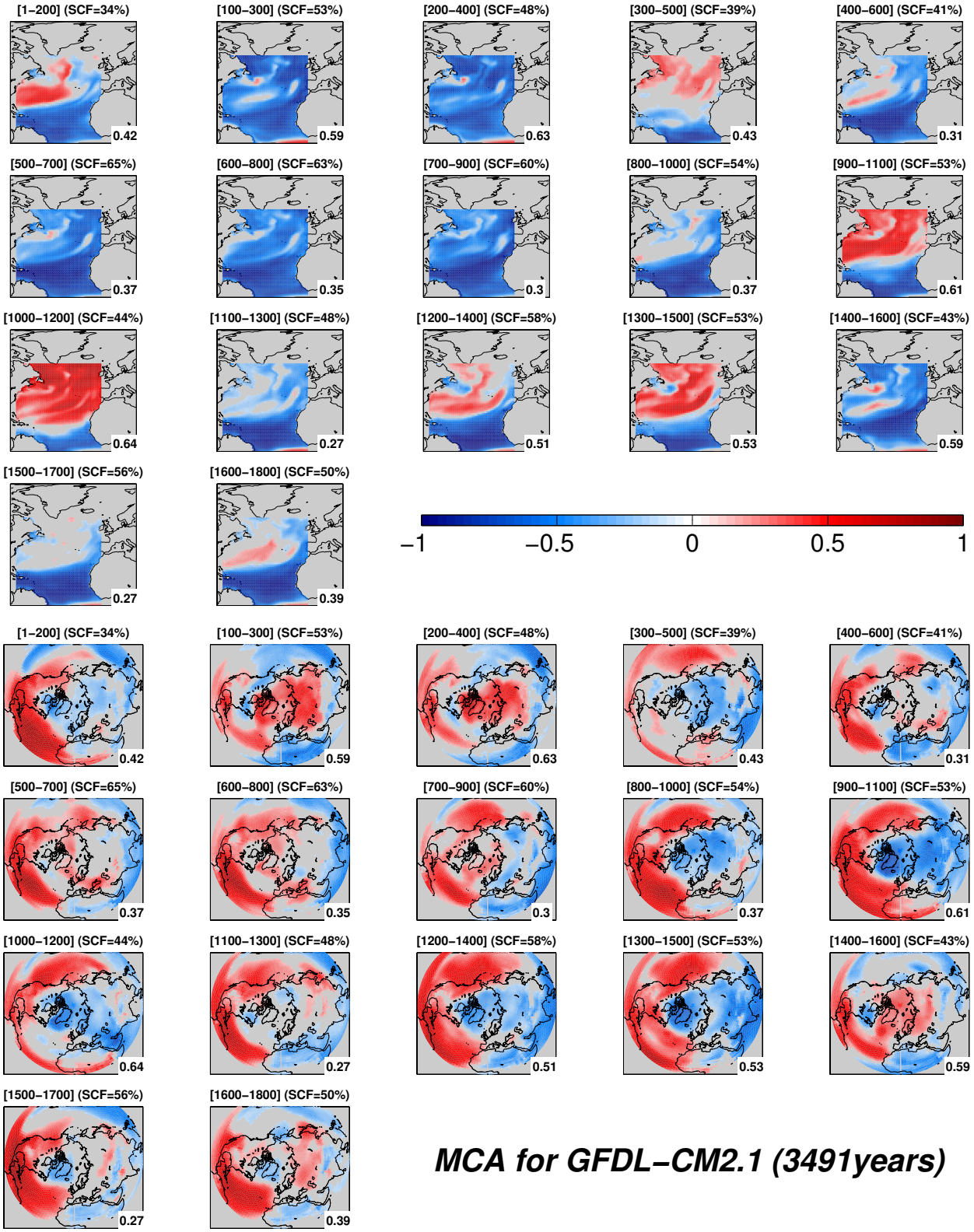

Figure 5.14: *MCA homogeneous (top) and heterogeneous (bottom) correlation maps between NA SST and global SLP, for 200-year intervals (indicated on top in square brackets), for GFDL-CM2.1. The Squared Covariance Fraction (SCF) is the percentage of explain covariance of the first MCA mode. Grey shading refers to non-significant values; the bottom right white box shows the AMV/AMOC correlation for that period.*

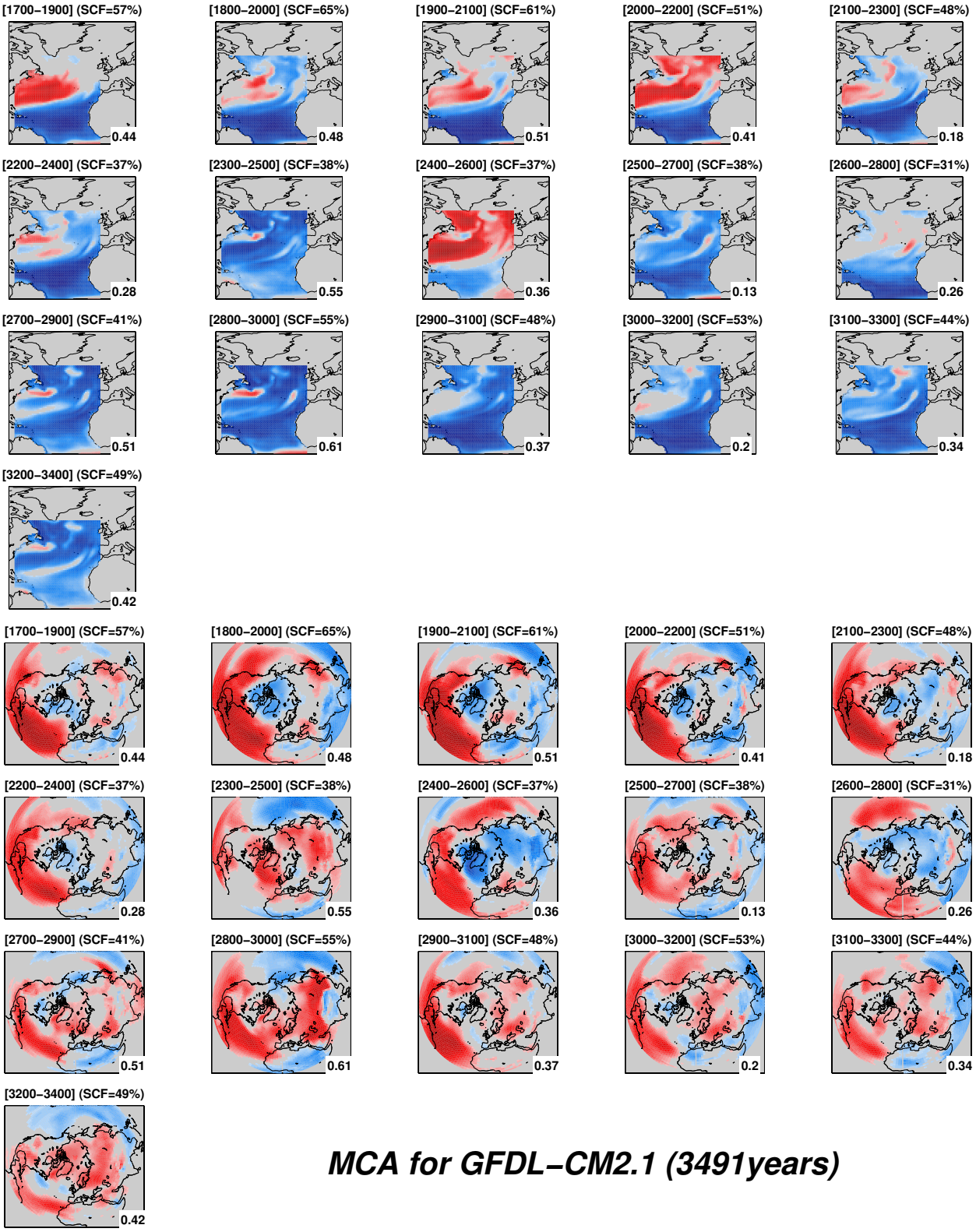

Figure 5.15: *Continue from Figure 5.14.*

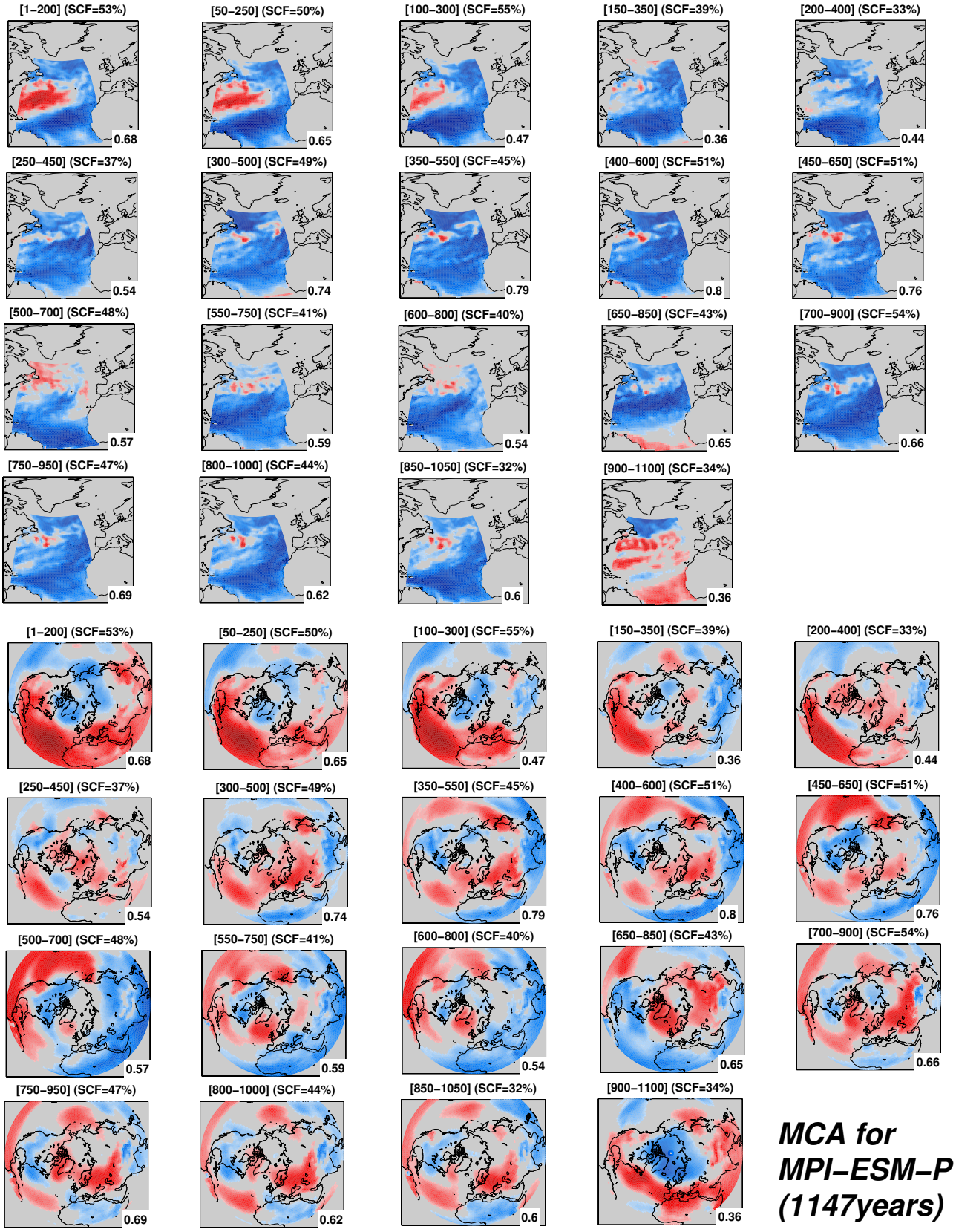

Figure 5.16: *The same as Figure 5.14, but for MPI-ESM-P model.*

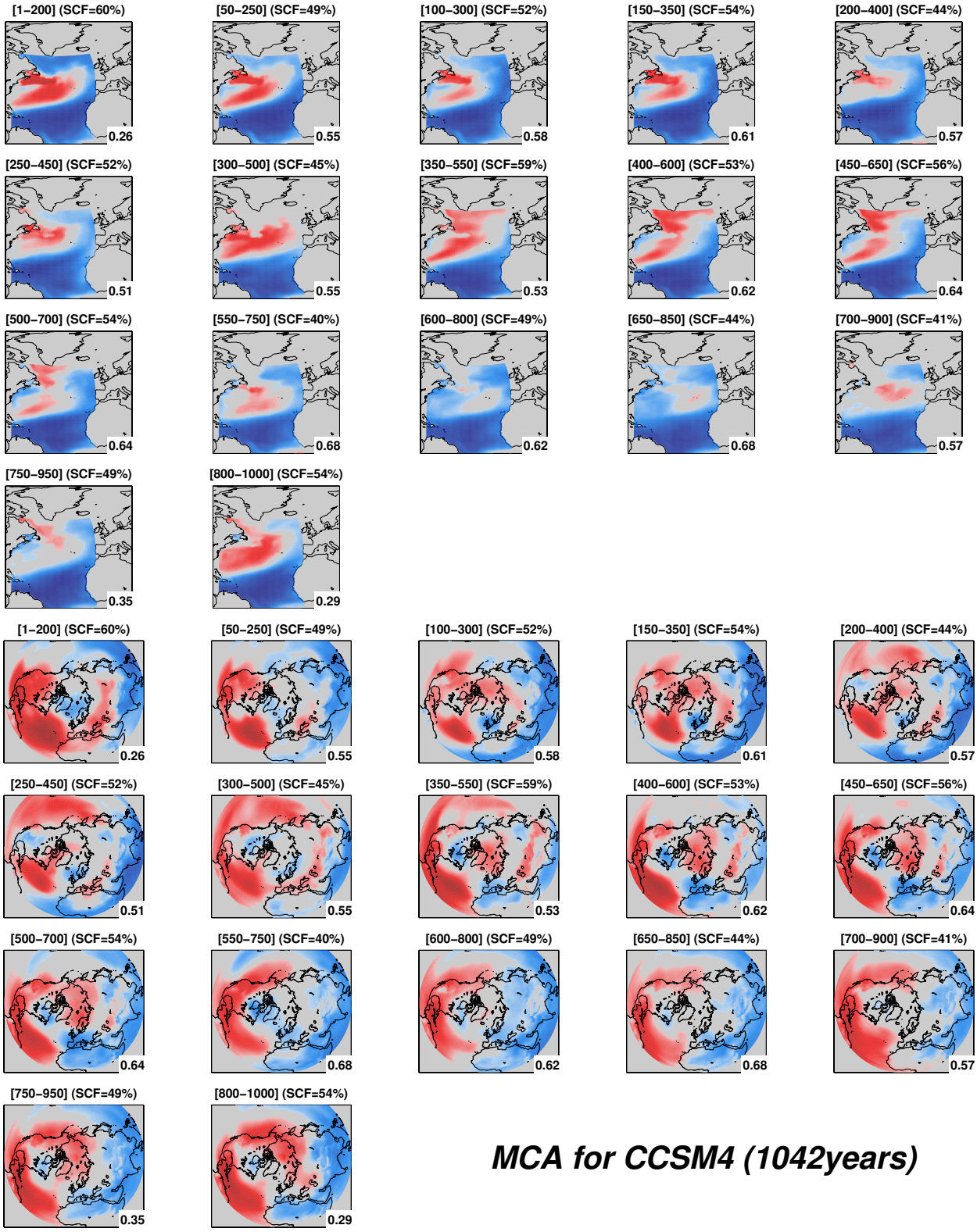

Figure 5.17: *The same as Figure 5.14, but for CCSM4 model.*

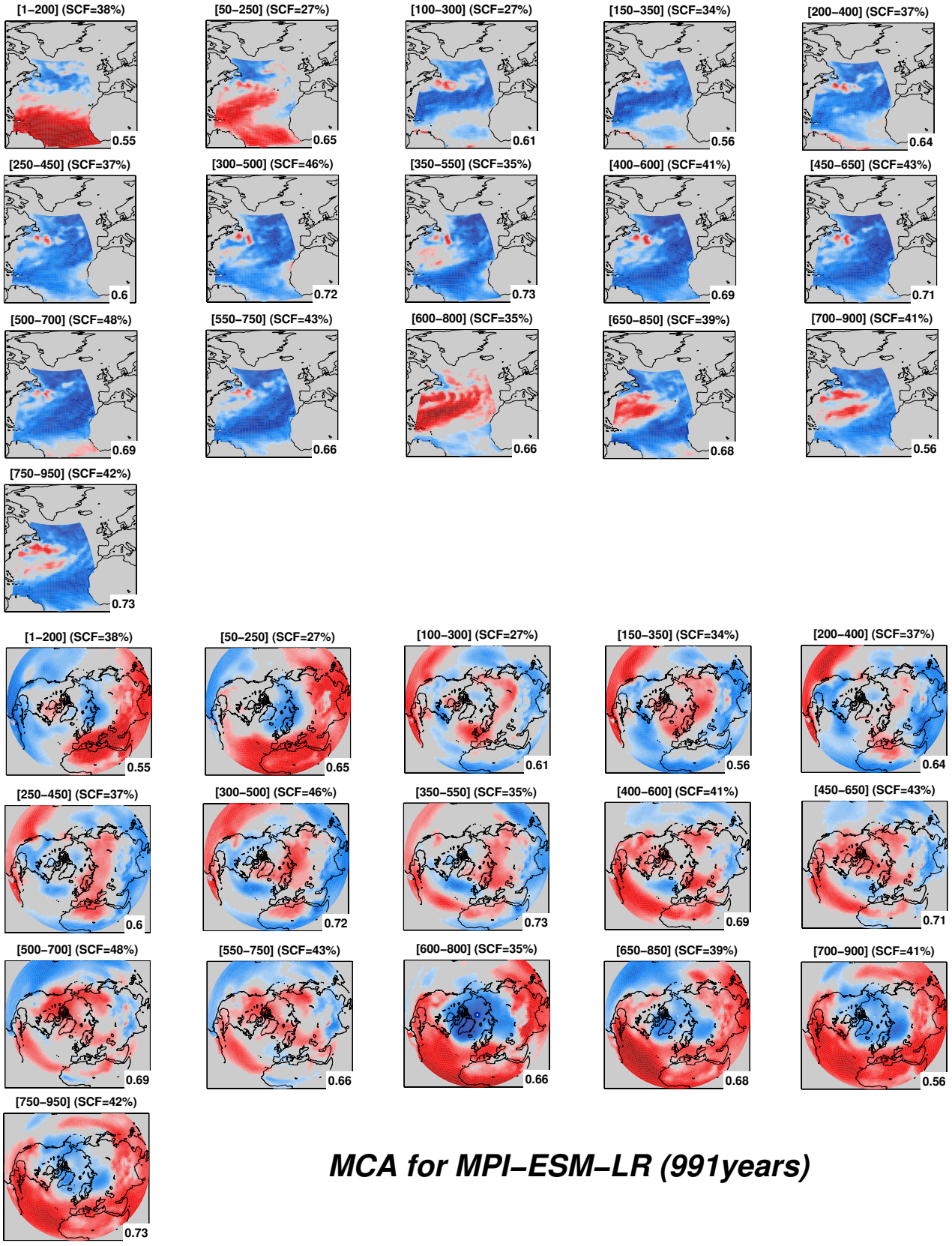

Figure 5.18: *The same as Figure 5.14, but for MPI-ESM-LR model.*

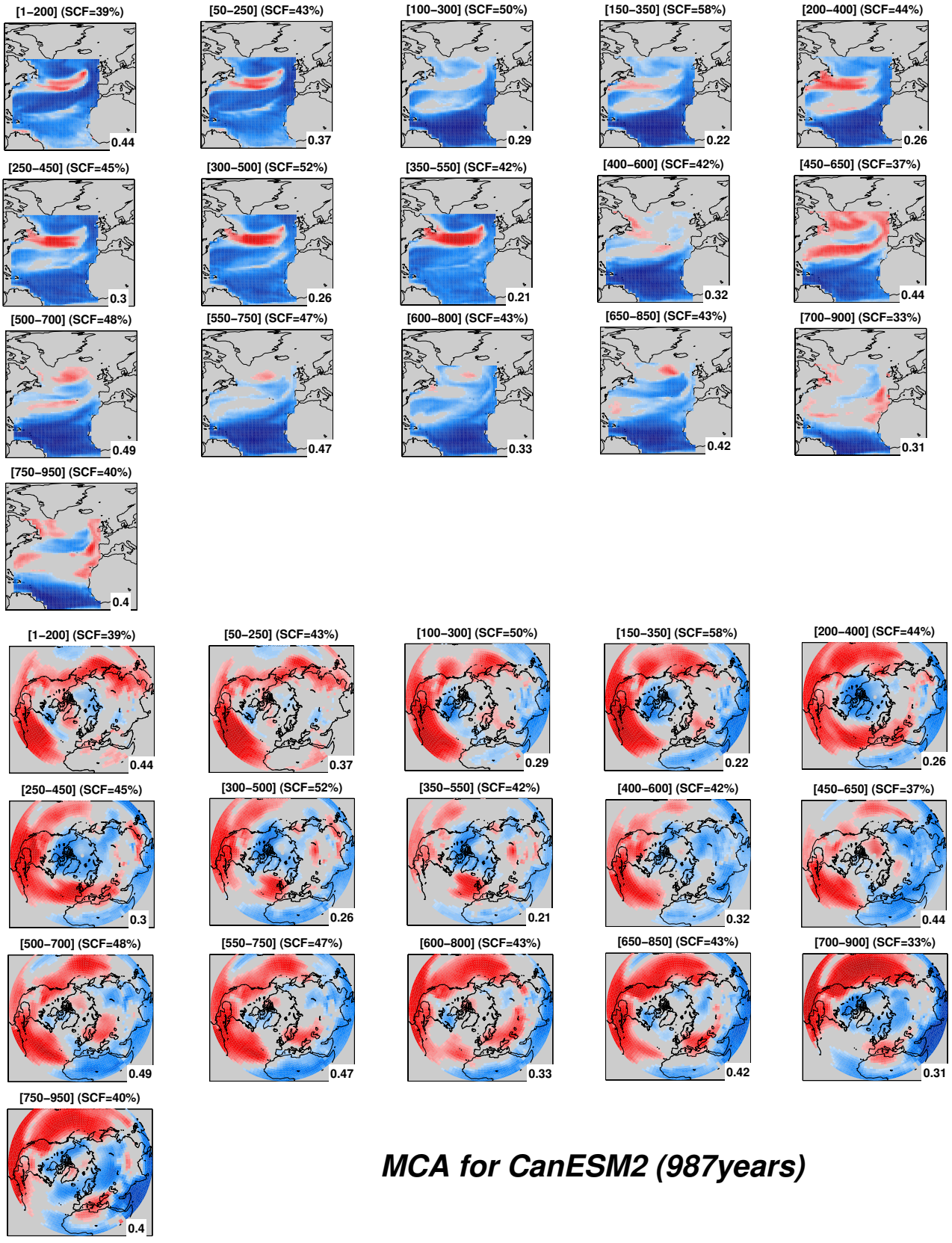

Figure 5.19: *The same as Figure 5.14, but for CanESM2 model.*

Almost in all the models, two modes of variability can be identified taking into account the homogeneous map and its corresponding heterogeneous map. They are more evident in the MPI-ESM-P model:

MODE 1: When the AMV autocorrelation undergoes a $\sim$ 20-year oscillatitory behaviour, the NA SST homogeneous map displays a tripole pattern with a region of positive correlations in the western subtropical Atlantic, surrounded by two negative lobes in the subpolar region and in the tropics. The tripole corresponds to a NAO-like dipole in the heterogeneous map. These patterns closely resemble the first EOF of winter North Atlantic SST and SLP, respectively.

MODE 2: A lower-frequency mode, with a typical $\sim$ 60-year time scale emerges at certain stages of the model evolution. This mode features a monopole for the SST, which resembles the spatial pattern associated with the AMV index. The latter is characterised by the typical comma-shaped unipolar pattern with largest values in the east and mid-latitude region. The monopole corresponds to a weaker coupling with the atmosphere, with respect to mode 1, indicating that in this case the dynamics is especially inside the ocean.

As time progresses, the central node of the tripole shrinks until it vanishes and the tripole pattern gradually transforms into the monopole, and viceversa. The competition between these two modes produces hybrid states (Figure 5.16).
The characteristics of the two identified modes are summarized schematically in Figure 5.20, taking the two most representative periods from MPI-ESM-P model as an example to describe the modes.

	MODE 1	MODE 2
AMV autocorrelation	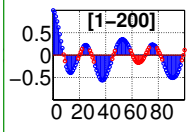 Higher frequency (∼ 20 years)	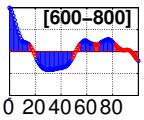 Lower frequency (∼ 60 years)
MCA homogeneous map	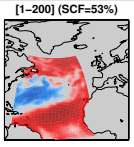 TRIPOLE	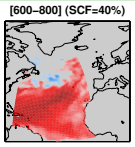 MONOPOLE (AMV-like)
MCA heterogeneous map	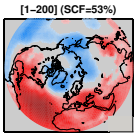 Strong signal in North Atlantic	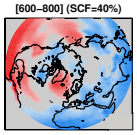 Weak signal in North Atlantic

Figure 5.20: *Shorter and longer AMV periodicities and their associated homogeneous and heterogeneous correlation maps, (left) mode 1 and (right) mode 2.*

Recent studies show the existence not only of the 50-70-year variability, but also of variability in the 20-30-year band. Frankcombe et al. [2010] find these two dominant time scales of multidecadal variability in the North Atlantic, analysing results from observational datasets (see the two peaks in Figure 5.21) and from a 500-year coupled GCM simulation. They argue that the 20-30-year variability is caused by the western propagation of subsurface temperature spatial pattern, due to internal variability of the AMOC; while the longer 50-70-year variability is related to low-frequency atmospheric forcing and Arctic-Atlantic exchange processes. The same westward propagation of large-scale temperature anomalies in the northern Atlantic is found to be responsible for a mode with a 24-year period also by Sévellec and Fedorov [2012] in an ocean GCM. Moreover, comparing CMIP3 and CMIP5 performances, Ruiz-Barradas et al. [2013] show that Atlantic multidecadal variability in the 10-20-year ranges is overestimated, whereas variability in the 70-80-year ranges is underestimated in the models.

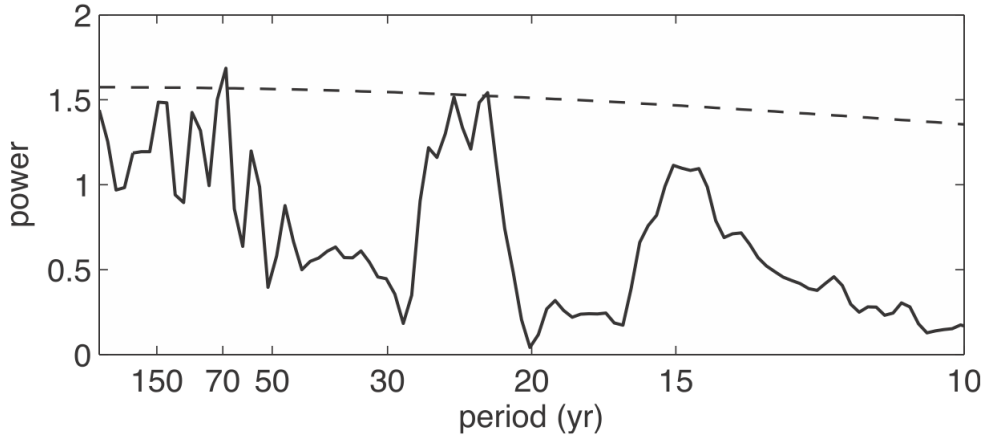

Figure 5.21: *Spectrum of the Central England Temperature (CET) record [Frankcombe et al., 2010].*

In our multi-model set, MPI-ESM-P presents two distinct peaks in its AMV spectrum, corresponding to the 20-40-year and 40-80-year bands. Therefore, in the next chapter, MPI-ESM-P model is chosen as case of study to deepen the dynamical explanation of AMV behaviour.

Chapter 6

Case study: MPI-ESM-P

Two preferential time scales (∼20 and ∼60 years) of AMV behaviour emerge across most of the models, as shown in the previous chapter. We have seen how these preferential time scales are linked to different MCA patterns. This is particularly evident in the MPI-ESM-P model, which presents two peaks in its NA SST spectrum at these preferential time scales, that are more clear and distinct than the other models. MPI-ESM-P is chosen here as case study. The aim is to understand what is the contribution of these two time scales to the non-stationarity of the AMV, if they really represent two distinct modes of variability and which physical mechanisms drive them.

MPI-ESM-P model [Jungclaus et al., 2012] is the longest among the ten CMIP5 models considered for this study, with 1156 years of length. It refers to the paleo (P) configuration of the Max-Planck-Institute Earth System Model (MPI-ESM), dedicated to paleo experiments and a subset of long-term core experiments in CMIP5. ECHAM6 is the atmospheric general circulation model, which is directly coupled to the JSBACH land model that describes physical and biogeochemical

aspects of soil and vegetation. MPIOM is the ocean general circulation model, which includes the HAMOCC model for the marine biogeochemistry. OASIS is the coupler program, which aggregates, interpolates, and exchanges fluxes and state variables once a day between ECHAM6+JSBACH and MPIOM+HAMOCC. The coupler exchanges fluxes for water, energy, momentum, and CO_2, see Figure 6.1.

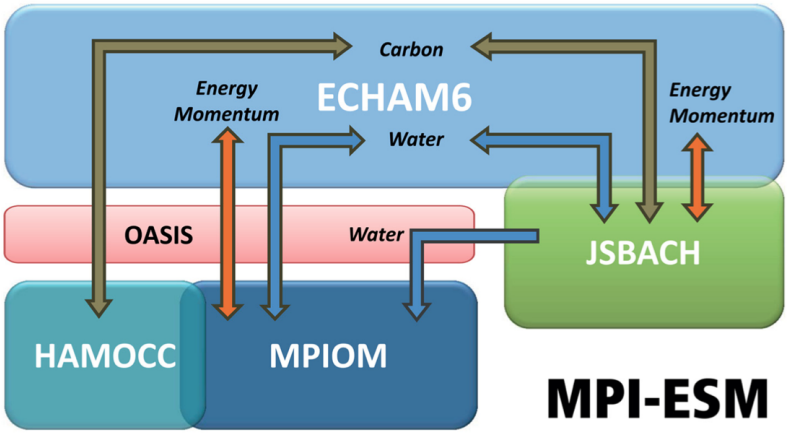

Figure 6.1: *Schematic view of MPI-ESM [Giorgetta et al., 2013].*

The P configuration is identical to the LR configuration with the exception of the orbital parameters which are prescribed, rather than calculated from the internal calendar, and of the use of a prescribed sequence of global maps for vegetation and land-use instead of using the dynamic vegetation and land use transitions. The LR and P configurations use for the atmosphere a T63/1.9° horizontal resolution and 47 hybrid sigma-pressure levels, and for the ocean a bipolar grid with 1.5° resolution (near the equator) and 40 z-levels. The poles of the ocean model are moved to Greenland and to the coast of the Weddell Sea by a conformal mapping of the geographical grid [Giorgetta et al., 2013].

6.1 What are the sources of AMV non-stationarity?

The NA SST index spectrum of MPI-ESM-P simulation shows two significant peaks at multidecadal time scale, above the red noise background, around 27- and 55-year time scales (Figure 6.2).

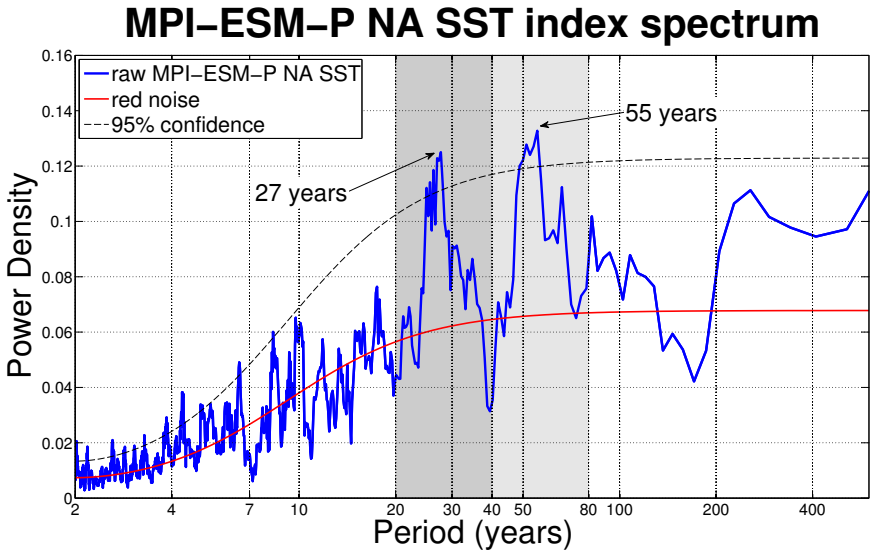

Figure 6.2: *Spectrum of AMV index for MPI-ESM-P model, computed via multi-taper method. Dark grey and light grey shading indicated the SHORT and the LONG time band, respectively.*

In order to isolate these two time scales, a 4th order Butterworth passband filter is used, selecting the following bands that include the above-mentioned peaks: we call SHORT the time band that refers to the 20-40-year range (dark grey shading in Figure 6.2), LONG the time band that refers to the 40-80-year range (light grey shading in Figure 6.2) and BOTH the time band that includes both the short and the long time bands (20-80-year range).

We use the general term NA SST index to indicate the raw unfiltered time series (only detrended), which is studied in this chapter for the 'short', 'long' and 'both'

time scales using the appropriate passband filters. Instead, AMV index only refers to the NA SST low-pass filtered by a 10-year running mean.

The aim is to understand which time scale contributes most to the non-stationarity of the entire AMV time series. Following the same procedure described in subsection 4.1.2, but now for each passband filtered time series of NA SST, final results of the count for 20 intervals are shown in Table 6.1: the long time scale contributes most to the non-stationarity of the entire time series.

time scale	**band (years)**	**points out (%)**
SHORT	[20-40]	8.83
LONG	[40-80]	15.42
BOTH	[20-80]	12.89

Table 6.1: *Number of autocovariance values that exceed the 90% confidence interval in percentage with respect to the total number of points.*

In order to see that there are intervals where the autocovariance function exceeds the confidence interval, making the entire AMV time series not-stationary, plots in Figure 6.3 are produced for the short and long time scales. Similarly to the 10-year low-pass filtered case shown in Figure 4.2, during some periods the autocovariance function (thick black line) largely departs from the average (red line).

Figure 6.4 shows what happens for the [20-80]years time scale that includes both the short and in the long time scale case. It is noticeable that the largest positive departures from the average occur when the autocovariance is above the average both in the short and in the long time scale case (e.g. during the first 200 years at lag 40 years). Viceversa, the largest negative departures from the average occurs when the autocovariance is below the average both in the short and in the long time scale case (e.g. during the interval [400-600] years at lag 40 years).

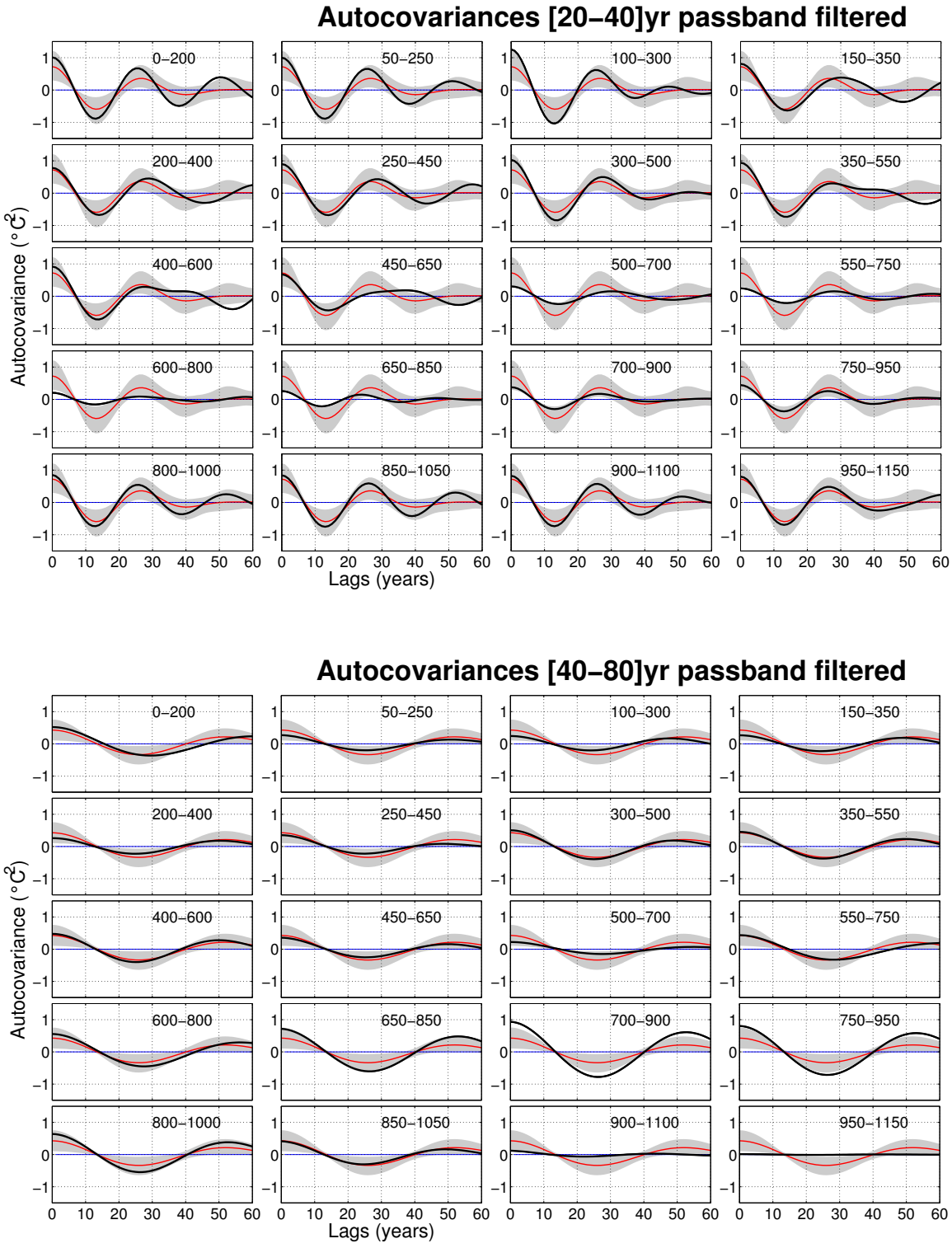

Figure 6.3: *Autocovariances for the [20-40]years (top) and [40-80]years (bottom) passband filtered time series split in 200-year-long intervals (black thick lines). The gray shading indicates the confidence interval at 90% and the red curve represents the average of the autocovariances of the the original intervals.*

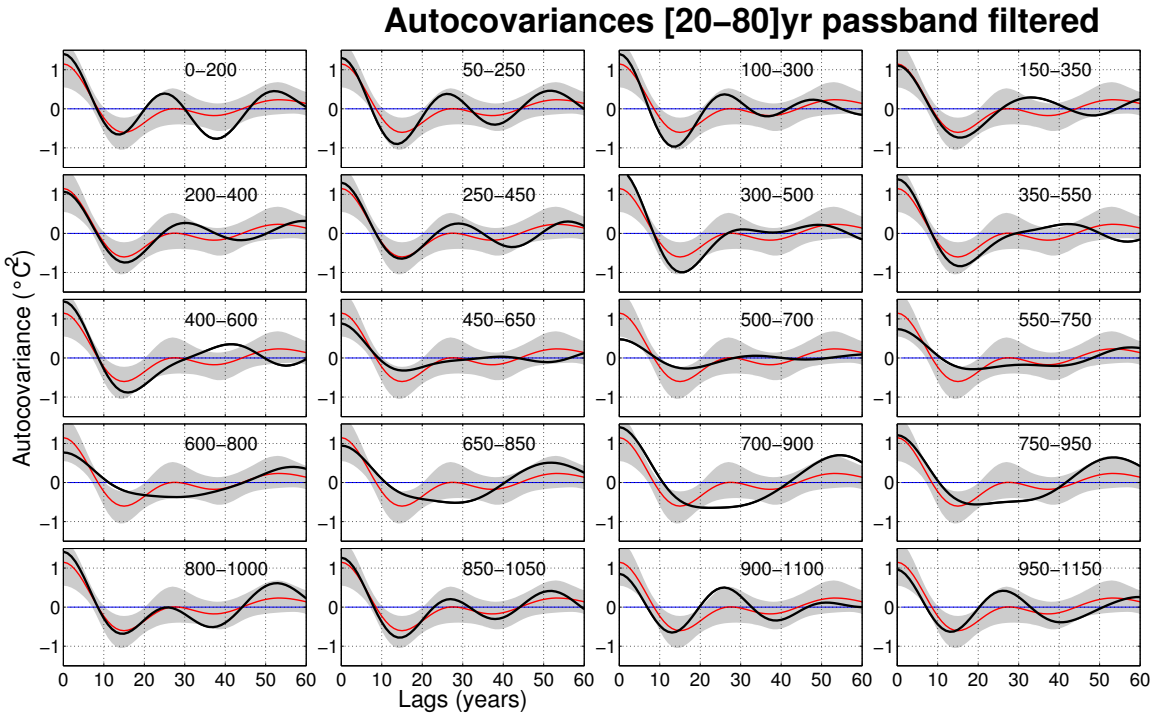

Figure 6.4: *As in Figure 6.3, but for the [20-80]years passband filtered time series.*

In other words, it seems that there are constructive and destructive interferences between the two time scales, from a statistical point of view.

Next, we explore the physical mechanisms that drives these two different time scales and that allows such interference.

6.2 Physical characterization of the two preferential multidecadal modes

This section is aimed at the description of the two preferential multidecadal time scales found in AMV spectrum (Figure 6.2): [20-40] and [40-80]-year temporal bands. Do these two time scales represent two different climate modes of variability? Here we inspect whether they represent different mechanisms, what are the processes driving the non-stationarity exhibited by the long-term AMV evolution and which of these processes is relevant to the short time scale and which to the long scale. North Atlantic sea surface temperature variability is linked to the overlying atmospheric variability and to the internal oceanic variability, therefore in Figure 6.5 the spectra of NAO and AMOC indices are shown. The temporal bands associated with the two main peaks in AMV spectrum are also shown. Both spectra present wide bands with enhanced variability that are grossly consistent with those identified in the AMV spectrum.

In order to characterise the two time scales, we analyse for both how the development of NA SST maximum is related to changes in the atmospheric surface circulation on one hand and in the internal ocean circulation on the other hand, taking winter SLP and AMOC as representatives of the two circulations, respectively. Lagged correlation analysis of winter SLP and AMOC fields onto the NA SST index is the approach followed for searching physical mechanisms responsible for the NA SST variability in the short and the long time bands. Figure 6.6 shows point-wise correlations between NA SST index and the following fields: SST (left column), winter SLP (middle column) and AMOC (right column), for negative lags in order to focus on the phase preceding the NA SST maximum, and for both the short and

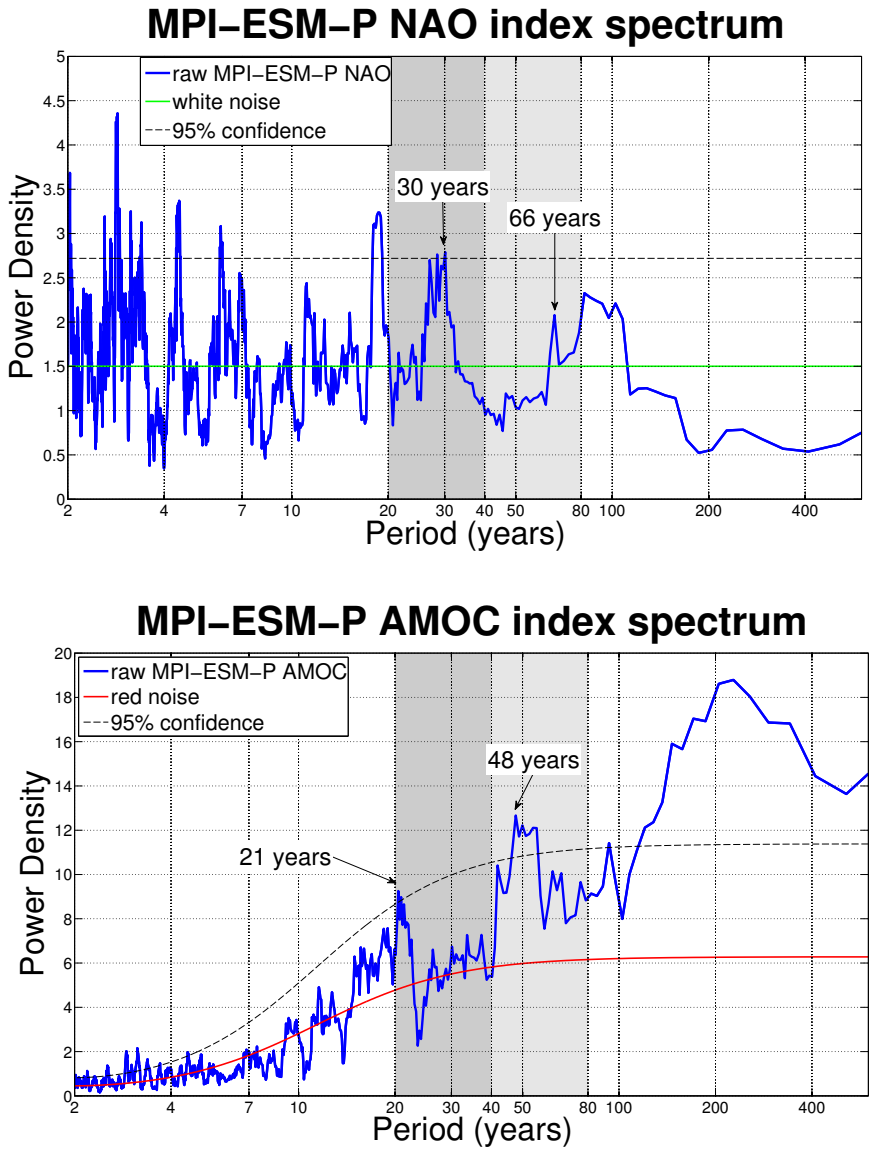

Figure 6.5: *(top) Multi-taper spectrum of NAO index, with its corresponding white noise background spectrum in green. (bottom) Multi-taper spectrum of AMOC index, with its corresponding red noise background spectrum in red. The two investigated time scales are highlighted in grey colours.*

long time scales. Significant values (at the 95% level) are enclosed within a black contour. Since all variables here are passband filtered according to the two time bands, the 95% confidence level c_i (based on t-test) for correlations between two times series X and Y with length N and with different autocorrelation sequences ρ_τ^X and ρ_τ^Y, is found following:

$$c_i = \frac{1.96}{\sqrt{df-2}} \qquad \text{where} \qquad df = \frac{N}{\sum\limits_{\tau=-(N-1)}^{N-1}(1-\frac{|\tau|}{N})\rho_\tau^X\rho_\tau^Y}$$

where df is the effective number of degrees of freedom, according to Bretherton et al.'s (1999) formula that takes into account the whole autocorrelation sequences (not only lag-one) in order to estimate the effective sample size for temporally correlated time series.

For both the two time scales, from the top to the bottom we can see the pattern evolution in time. 16 years (for the short time scale) and 24 years (for the long time scale) before the maximum of North Atlantic SST index, the correlation patterns for all the variables present a correlation of the opposite sign, this indicates an oscillatory behaviour. Atmosphere displays a NAO-like pattern when the oscillatory SST pattern turns from negative to positive basin-wide correlation area and when the area of positive AMOC/NA SST correlation originates at high North Atlantic latitudes (lag -8 for short and lag -12 for long time scale). For the long time scale, the polar negative correlation area of the NAO-like pattern intensifies strongly getting close to the zero-lag; while for the short time scale, the pattern becomes more vague. For both time scales SST variability is evidently linked to the AMOC variability. The area of positive AMOC/NA SST correlation at high latitudes refers to a clockwise overturning cell that enhances the background meridional circulation.

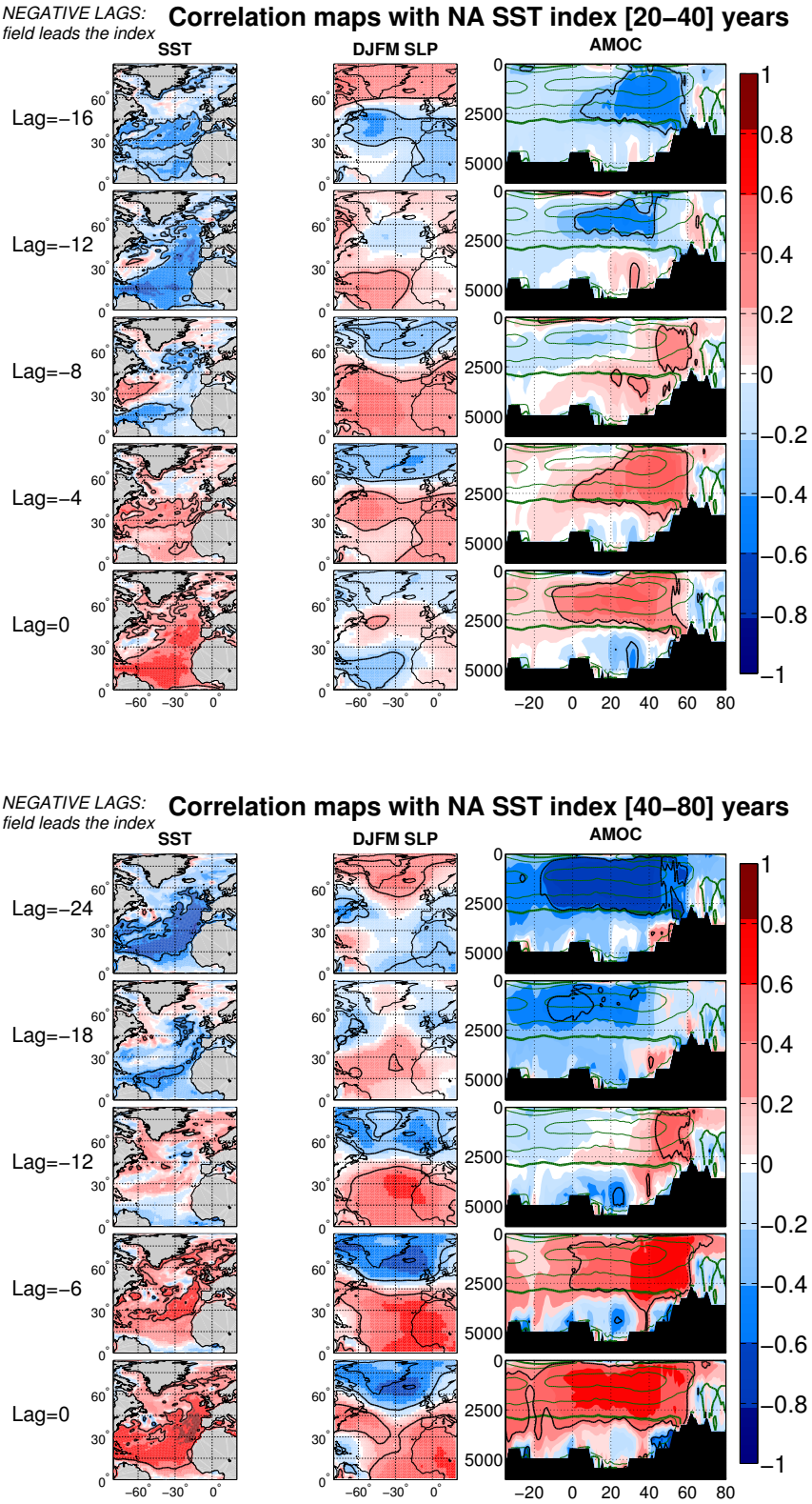

Figure 6.6: *Lagged correlation maps for both time scales: Sea Surface Temperature (SST), extended winter Sea Level Pressure (DJFM SLP) and Atlantic Meridional Overturning Circulation (AMOC) fields correlated with the North Atlantic SST index. Significant values (at the 95% level) are enclosed within a black contour and AMOC mean profile is overlapped as green contours on the right column correlation patterns.*

Then, the enhanced overturning area propagates southward up to extend beyond the equator at zero lag, when the North Atlantic SST reaches the maximum value. Short and long time scales exhibit a very similar relationship SST/AMOC, different timing considered. It seems that AMOC tends to respond similarly to any forcing pattern.

However, the strongest AMV/AMOC relationship is found for the long time scales, reaching a 0.8 correlation as shown by Figure 6.7. Moreover, AMOC leads by 2 years and by 1 year the NA SST maximum for the short and the long time scales, respectively.

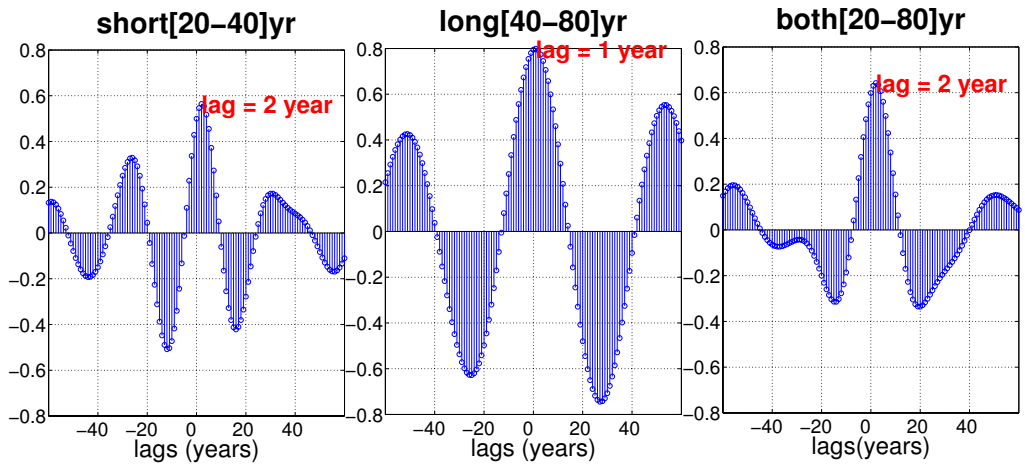

Figure 6.7: *NA SST/AMOC lagged correlations for the short time scale [20-40] years, for the long time scale [40-80] years and for both time scales [20-80] years. AMOC lags (leads) for negative (positive) lags. The year in red is the year of maximum correlation.*

In order to highlight the dynamical mechanism involved in the development of NA SST maximum, lead-lag correlations of three indices, namely AMOC, Mixed Layer Depth in the Labrador Sea (LabMLD) and NAO, with NA SST index is shown in Figure 6.8.

The same phase relationship holds for both the short and the long time scales: the NAO is in phase with the LabMLD due to the effect of the westerlies on the heat exchange at the air-sea interface, that in turn affects deep water formation in the Labrador Sea and the AMOC strength.

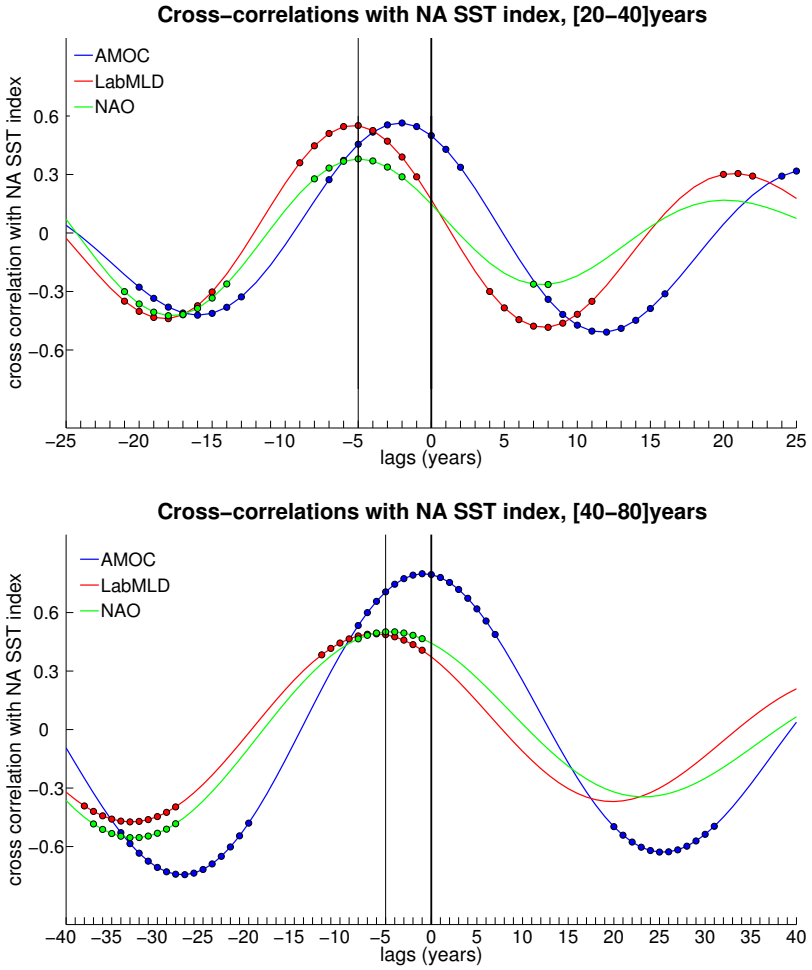

Figure 6.8: *Lead-lag correlations: Atlantic Meridional Overturning Circulation (AMOC), Labrador Sea Mixed Layer Depth (LabMLD), North Atlantic Oscillation (NAO) indices are correlated with and North Atlantic SST index. Significance at the 95% confidence level is given by filled circles.*

During a positive phase of the cycle, the NAO maximum (green curve at lag -5)

involves stronger westerlies and so bigger heat loss from the ocean surface; therefore LabMLD peaks at the same lag leading to the AMOC maximum by 3 (4) years for the short (long) time scale. Warm water is then transported into the North Atlantic basin, determining the warming of the entire basin and the maximum of NA SST index (zero-lag).

A focus on the convection sites is needed in order to understand the differences between the two time scales. Deep water formation processes, that convert surface water masses to deep water by rising their density through cooling and/or increasing salinity, set the interhemispheric shape and the strength of the overturning cell [Kuhlbrodt et al., 2007]. For both the short and the long time scale, regions of deep water formation are identified in Labrador Sea and Greenland Sea. This is indicated by regressing Mixed Layer Depth (MLD) onto the AMOC index (Figure 6.9). The main deep convection site appears to be Labrador Sea, for this model. In particular, Figure 6.9 shows a stronger convection in the Labrador Sea convection site for the longer mode with respect to the shorter mode.

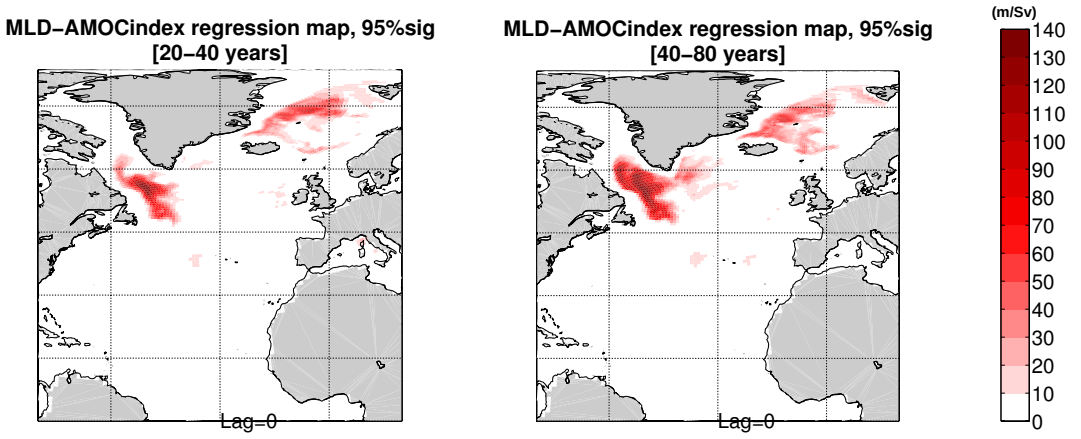

Figure 6.9: *Regression maps between Mixed Layer Depth (MLD) and AMOC index at zero-lag for both time scales.*

The Labrador Sea is an important contributor to the Meridional Overturning Circulation and a key location for the global heat and freshwater balance [Rykova et al., 2009]. This is why the averages over Labrador Sea (45°-65°N and 60°-40°W) are used in Figure 6.10, where the differences between the two modes emerge.

In Figure 6.10 we see anomalies averaged over the Labrador Sea region of deep convection correlated with NA SST index, for the two time scales. The aim of using cross-correlation plots between indices is to find what sets the time scale of NA SST oscillation for the fast and for the slow mode.

Two basic important oceanic feedbacks control sea water density variability: salinity and temperature feedbacks. Salinity is involved in a positive feedback: higher salinity in the deep water formation area enhances the circulation, and the circulation in turn transports higher salinity waters into the deep water formation regions. On the other hand, temperature is involved in a negative feedback as it stabilizes the system by bringing it back to its original state. Higher than normal temperatures over the Labrador Sea inhibit the deep water formation, weakening the circulation: a weakening of the AMOC leads to a reduction in northward ocean heat transport, causing a cooling of the high latitude North Atlantic and associated increase in density, which favours a recovery of the circulation through increased deep water formation [Boulton et al., 2014].

In Figure 6.10 (top panel) it is shown that the cooling of SST, the minimum of blue curve at lag -13, leads to the increase in density and Mixed Layer Depth. Therefore, AMOC becomes stronger and warm water is transported to the Labrador Sea region, which in turn leads to a decrease in density. Temperature feedback is negative, so this allows the oscillatory behaviour for the short time scale. However, for the long time scale (bottom panel) temperature is in phase with both density

and Mixed Layer Depth. Since warm waters prevent the deep water formation, for the long time scale the salinity (green curve), is more effective than temperature. Salinity feedback is a positive feedback so it tends to maintain the original condition. This could explain why the time scale here is longer, jointly with the fact that a temperature anomaly is rapidly damped by heat fluxes, while there is no such a feedback acting on SSS anomalies.

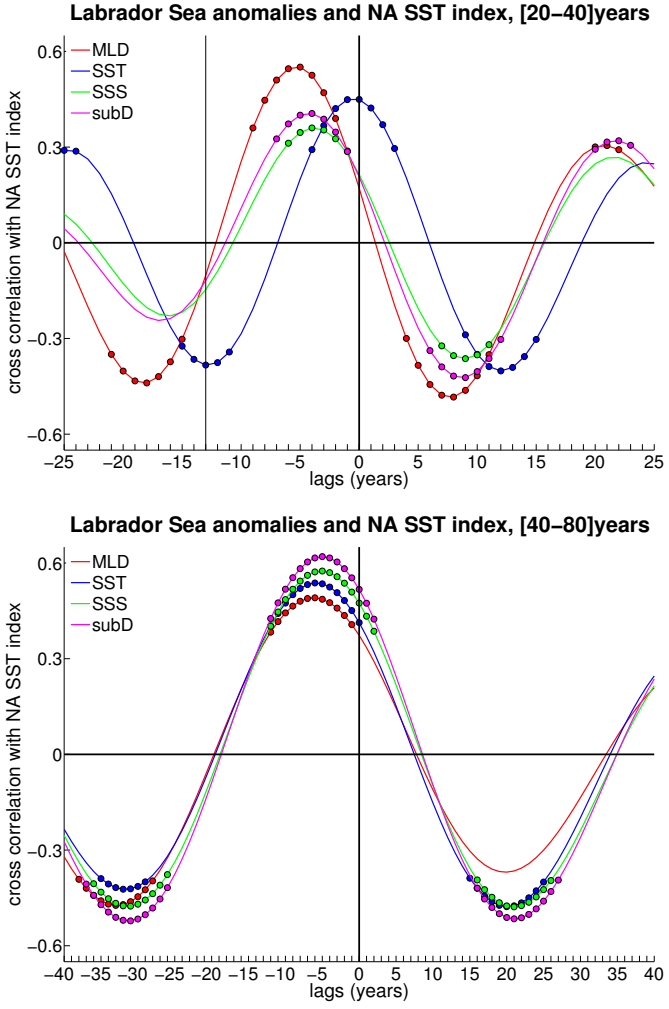

Figure 6.10: *Lead-lag correlations: Mixed Layer Depth (MLD), Sea Surface Temperature and Salinity (SST/SSS), subsurface Density (subD) indices, all averaged over Labrador Sea, are correlated with and North Atlantic SST index. Significance at the 95% confidence level is given by filled circles.*

Concluding, in MPI-ESM-P model the two preferred time scales correspond to different mechanisms: although salinity plays a role for both time scales, temperature feedback prevails at short time scale and salinity feedback prevails at long time scale.

In order to further highlight this point, in Figure 6.11 it is shown a lead-lag correlation pattern as a function of depth.

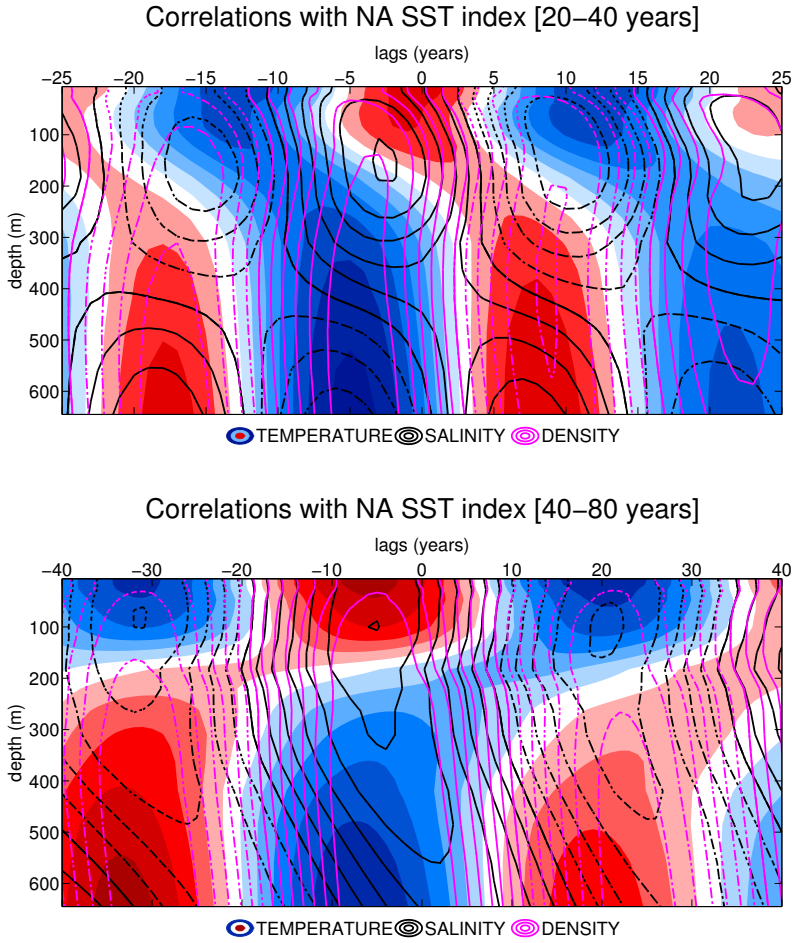

Figure 6.11: *Lead-lag correlations of temperature (filled contours), salinity (black contours) and density (magenta contours) in the Labrador Sea with NA SST index, as a function of depth. Positive (negative) correlations are red (blue) coloured areas for temperature and are solid (dashed) lines for salinity and density.*

The fast mode (top plot) shows a temperature correlation pattern that propagates with depth: the propagation below 150 m occurs once the sign of the density/NA SST correlation changes. On the other hand, it is interesting to notice the temperature correlation dipole pattern between surface and subsurface in the lagged correlation map for the slow mode (bottom plot). Since density and salinity do not show the same reversal with depth, this seems to confirm that for the slow mode temperature anomalies are not the main drivers for dense water formation.

Chapter 7

Conclusions

Aim of this study is to investigate the non-stationarity associated to internal and low-frequency variability over the North Atlantic region, in order to understand how it modulates long-term trends. The Atlantic Multidecadal Variability (AMV) is examined in a set of multi-century preindustrial climate simulations performed with different coupled general circulation models. An assessment of its spectral characteristics and its non-stationary behaviour is conducted.

Different regimes of variability (mostly warm or mostly cold, moderate or intense, nearly sinusoidal or irregular, shorter-period or longer-period, etc.) can be identified in the AMV time series. A time-evolving approach shows that the dominant variability time scales of AMV change with the selected time interval, revealing a non-stationary behaviour. In order to rigorously check this behaviour, a statistical test for AMV stationarity is developed starting from the null hypothesis of a statistically-stationary AMV, whose modulation is entirely random. Most of the models display epochs characterised by autocovariance which significantly deviates from the autocovariance of the whole time series, therefore confirming the

non-stationarity exhibited by the corresponding AMV time series. More precisely, 9 out 11 models present non-stationary unfiltered NA SST time series, while 7 out 11 models present non-stationary AMV (10-year low-pass filtered NA SST) time series. However, the models that do not pass the test are only marginally stationary because present percentages of values that exceed the confidence interval that are very close to the 10% significance level. The non-stationary behaviour identified in most models suggests that the character of the observed AMV may undergo significant changes in the future.

The relative roles played by ocean internal dynamics, through the AMOC, and changes in the ocean-atmosphere coupled interactions are inspected. For all the models, an increase in the overturning drives a warming of the North Atlantic, which reaches its maximum after 1 to 6 years. Despite the strong disagreement among the models, both in phasing and strength of the co-variability, the impact of AMV on AMOC appears to be weaker than the reverse. However, moving window AMV/AMOC cross-correlation shows periods with higher correlation that alternate with periods of lower correlation, implying that even if the AMOC does generally play an important role in the AMV variability, there are other factors that may contribute to the AMV. When the AMV/AMOC correlation is low, models show the tendency to have large positive SLP/North Atlantic SST covariances over the North Atlantic region, suggesting that in those periods the atmospheric forcing could prevail as a driver of AMV, compared to the ocean internal dynamics.

A Maximum Covariance Analysis (MCA) is applied to North Atlantic SST and global SLP, as representative of atmospheric circulation at the ocean surface, in order to understand the impact of AMV changing regimes on the ocean-atmosphere interactions. Teleconnection patterns show a largely-varying evolution in time, but

large uncertainties in the models do not allow to associate specific MCA patterns to a specific AMV regime. Nevertheless, among the models, a lower-frequency and a higher-frequency mode of variability can be identified taking into account the MCA homogeneous map and its corresponding heterogeneous map. When the AMV autocorrelation undergoes a ∼20-year oscillatory behaviour, the NA SST homogeneous map displays a tripole pattern which corresponds to a NAO-like dipole in the SLP/NA SST heterogeneous map. These patterns closely resemble the first EOF of winter North Atlantic SST and SLP, respectively. A lower-frequency mode, with a typical ∼60-year time scale emerges at certain stages of the model evolution. This mode features a monopole for the SST, which resembles the spatial pattern associated with the AMV index. The monopole corresponds to a weaker coupling with the atmosphere, with respect to the higher-frequency mode, suggesting that in this case drivers resides in the ocean. As time progresses, the tripole pattern can decay, evolving into a monopolar structure, and viceversa.

The link between the two preferential AMV time scales (∼20 and ∼60 years) and the different MCA patterns is particularly evident in the MPI-ESM-P model, which is therefore chosen as a case study to deepen the dynamical explanation of AMV behaviour: its AMV spectrum presents two distinct peaks, corresponding to a short time scale (20-40-year band) and a long time scale (40-80-year band). Results show that the non-stationarity of the entire time series is mostly due to the long time scale, according to the statistical test for AMV stationarity. For both time scales, positive NAO phase corresponds to the deepening of the ocean mixed layer in the Labrador Sea convection site, due to stronger westerlies and therefore larger heat losses in the ocean; this increases deep water formation and, consequently, the AMOC strength. More warm water is transported into the North

Atlantic basin and a few years after the AMOC maximum, the warming of the entire North Atlantic basin is reached. The difference between the two time scales in MPI-ESM-P model is due to different underlying mechanisms: although salinity plays a role for both time scales, temperature feedback prevails at short time scale and salinity feedback prevails at long time scale. Salinity feedback is a positive feedback so it tends to maintain the original condition. This could explain why the time scale here is longer, jointly with the fact that temperature anomaly is rapidly damped by heat fluxes with time than salinity. The driving role of salinity on circulation is found to depend on the time scale also by Deshayes et al. [2014]: even opposite mechanisms exist but dominate at different time scale, in fact they show that when the circulation is more intense, the subpolar gyre is fresher at interannual frequencies and saltier at longer periods.

Our study points out the large inconsistencies across models, that emerge also among the five CMIP5 models analysed by Deshayes et al. [2014], in particular in the representation of freshwater budget and circulation in the North Atlantic. Similar disagreements are found also by Ba et al. [2014] and Menary et al. [2015] who show that biases in simulated mean climate state (which differ from the observed and each other) influence the characteristics of decadal variability.

Therefore, explaining decadal variability is challenging, not only because of the lack of data and the multitude of possible processes that may be involved and that may not be limited to North Atlantic itself [Frankcombe et al., 2010], but also because of model uncertainty.

The importance of reducing model inconsistency becomes even more stressed in light of the non-stationary nature of climate variability that has emerged with this work, since in future we may expect behaviours different from the observed.

Bibliography

[Ba et al., 2014] Ba, J., Keenlyside, N. S., Latif, M., Park, W., Ding, H., Lohmann, K., Mignot, J., Menary, M., Otterå, O. H., Wouters, B., y Melia, D. S., Oka, A., Bellucci, A., and Volodin, E. (2014). A multi-model comparison of Atlantic multidecadal variability. *Clim Dyn*.

[Bellucci et al., 2008] Bellucci, A., Gualdi, S., Scoccimarro, E., and Navarra, A. (2008). NAO-ocean circulation interactions in a coupled general circulation model. *Clim Dym*, 31:759–777.

[Bjerknes, 1964] Bjerknes, J. (1964). Atlantic air-sea interaction. *Advances in Geophysics*, 10:1–82.

[Booth et al., 2012] Booth, B. B. B., Dunstone, N. J., Halloran, P. R., Andrews, T., and Bellouin, N. (2012). Aerosols implicated as a prime driver of twentieth-century North Atlantic climate variability. *Nature*, 484:228–232.

[Boulton et al., 2014] Boulton, C. A., Allison, L. C., and Lenton, T. M. (2014). Early warning signals of Atlantic Meridional Overturning Circulation collapse in a fully coupled climate model. *Nature Communications*.

[Bretherton et al., 1992] Bretherton, C. S., Smith, C., and Wallace, J. M. (1992). An Intercomparison of Methods for Finding Coupled Patterns in Climate Data. *Journal of Climate*, 5.

[Bretherton et al., 1999] Bretherton, C. S., Widmann, M., Dymnikov, V. P., Wallace, J. M., and Bladé, I. (1999). The Effective Number of Spatial Degrees of Freedom of a Time-Varying Field. *Journal of Climate*, 12.

[Collins et al., 2006] Collins, M., Botzet, M., Carril, A. F., Drange, H., Jouzeau, A., Latif, M., Masina, S., Otterå, O. H., Pohlmann, H., Sorteberg, A., Sutton, R., and Terray, L. (2006). Interannual to Decadal Climate Predictability in the North Atlantic: A Multimodel-Ensemble Study. *American Meteorological Society*, 19.

[Cunningham et al., 2010] Cunningham, S., Baringer, M., Johns, B., Toole, J., Østerhus, S., Fischer, J., Piola, A., McDonagh, E., Lozier, S., Send, U., Kanzow, T., Marotzke, J., Rhein, M., Garzoli, S., Rintoul, S., Sloyan, B., Speich, S., Talley, L., Baehr, J., Meinen, C., Treguier, A.-M., and Lherminier, P. (2010). The present and future system for measuring the Atlantic meridional overturning circulation and heat transport. *in Proceedings of OceanObs'09: Sustained Ocean Observations and Information for Society*, 2.

[Curry and Mauritzen, 2005] Curry, R. and Mauritzen, C. (2005). Dilution of the Northern North Atlantic Ocean in Recent Decades. *Science*, 308.

[Czaja and Marshall, 2001] Czaja, A. and Marshall, J. (2001). Observations of atmosphere-ocean coupling in the North Atlantic. *Q. J. R. Meteorol. SOC*, 127:1893–1916.

[Danabasoglu, 2008] Danabasoglu, G. (2008). On multidecadal variability of the Atlantic meridional overturning circulation in the community climate system model version 3. *J Clim*, 21:5524–5544.

[Delworth et al., 2006] Delworth, T. L., Broccoli, A. J., Rosati, A., Stouffer, R. J., Balaji, V., Beesley, J. A., Cooke, W. F., Dixon, K. W., Dunne, J., Dunne, K. A., Durachta, J. W., Findell, K. L., Ginoux, P., Gnanadesikan, A., Gordon, C. T., Griffies, S. M., Gudgel, R., Harrison, M. J., Held, I. M., Hemler, R. S., Horowitz, L. W., Klein, S. A., Knutson, T. R., Kushner, P. J., Langenhorst, A. R., Lee, H.-C., Lin, S.-J., Lu, J., Malyshev, S. L., Milly, P. C. D., Ramaswamy, V., Russell, J., Schwarzkopf, M. D., Shevliakova, E., Sirutis, J. J., Spelman, M. J., Stern, W. F., Winton, M., Wittenberg, A. T., Wyman, B., Zeng, F., and Zhang, R. (2006). GFDL's CM2 Global Coupled Climate Models. Part I: Formulation and Simulation Characteristics. *American Meteorological Society*.

[Delworth and Greatbatch, 2000] Delworth, T. L. and Greatbatch, R. J. (2000). Multidecadal Thermohaline Circulation Variability Driven by Atmospheric Surface Flux Forcing. *American Meteorological Society*, 13.

[Delworth et al., 1993] Delworth, T. L., Manabe, S., and Stouffer, R. J. (1993). Interdecadal variation in the thermohaline circulation in a coupled ocean-atmosphere model. *Journal of Climate*, 6:1993–2011.

[Delworth and Mann, 2000] Delworth, T. L. and Mann, M. E. (2000). Observed and simulated multidecadal variability in the Northern Hemisphere. *Clim Dym*, 16:661–676.

[Deser et al., 2010] Deser, C., Alexander, M. A., Xie, S.-P., and Phillips, A. S. (2010).

Sea Surface Temperature Variability: Patterns and Mechanisms. *Annu. Rev. Marine. Sci.*, 2:115–143.

[Deser and Blackmon, 1993] Deser, C. and Blackmon, M. L. (1993). Surface Climte Variations over the North Atlantic Ocean during Winter: 1900-1989. *American Meteorological Society.*

[Deshayes et al., 2014] Deshayes, J., Curry, R., and Msadek, R. (2014). CMIP5 Model Intercomparison of Freshwater Budget and Circulation in the North Atlantic. *Journal of Climate*, 27.

[Dijkstra et al., 2006] Dijkstra, H. A., te Raa, L., Schmeits, M., and Gerrits, J. (2006). On the physics of the Atlantic Multidecadal Oscillation. *Ocean Dynamics*, 56:36–50.

[Dong and Sutton, 2005] Dong, B. W. and Sutton, R. T. (2005). Mechanism of inter-decadal thermohaline circulation variability in a coupled ocean-atmosphere GCM. *J Clim*, 18:1117–1135.

[Ebisuzaki, 1997] Ebisuzaki, W. (1997). A Method to Estimate the Statistical Significance of a Correlation When the Data Are Serially Correlated. *American Meteorological Society.*

[Enfield et al., 2001] Enfield, D. B., Mestas-Nuñez, A. M., and Trimble, P. J. (2001). The Atlantic multidecadal oscillation and its relation to rainfall and river flows in the continental U.S. *Geophys. Res. Lett.*, 28(10):2077–2080.

[Escudier et al., 2012] Escudier, R., Mignot, J., and Swingedouw, D. (2012). A 20-year

coupled ocean-sea ice-atmosphere variability mode in the North Atlantic in an AOGCM. *Clim Dym*.

[Evan et al., 2009] Evan, A. T., Vimont, D. J., Heidinger, A. K., Kossin, J. P., and Bennartz, R. (2009). The Role of Aerosols in the Evolution of Tropical North Atlantic Ocean Temperature Anomalies. *Science*, 324(5928):778–781.

[Farneti and Vallis, 2011] Farneti, R. and Vallis, G. K. (2011). Mechanisms of interdecadal climate variability and the role of ocean-atmosphere coupling. *Clim Dyn*, 36:289–308.

[Folland et al., 2001] Folland, C. K., Colman, A. W., Rowell, D. P., and Davey, M. K. (2001). Predictability of Northeast Brazil Rainfall and Real-Time Forecast Skill, 1987–98. *Journal of Climate*, 14.

[Frankcombe et al., 2010] Frankcombe, L. M., von der Heydt, A., and Dijkstra, H. A. (2010). North Atlantic Multidecadal Climate Variability: An Investigation of Dominant Time Scales and Processes. *J Clim*, 23(13):3626–3638.

[Gastineau et al., 2013] Gastineau, G., D'Andrea, F., and Frankignoul, C. (2013). Atmospheric response to the North Atlantic Ocean variability on seasonal to decadal time scales. *Clim Dyn*, 40:2311–2330.

[Ghil, 2002] Ghil, M. (2002). Advanced spectral methods for climatic time series. *Reviews of Geophysics*, 40.

[Giorgetta et al., 2013] Giorgetta, M. A., Jungclaus, J., Reick, C. H., Legutke, S., Bader, J., Böttinger, M., Brovkin, V., Crueger, T., Esch, M., Fieg, K., Glushak, K., Gayler, V., Haak, H., Hollweg, H.-D., Ilyina, T., Kinne, S., Kornblueh, L., Matei,

D., Mauritsen, T., Mikolajewicz, U., Mueller, W., Notz, D., Pithan, F., Raddatz, T., Rast, S., Redler, R., Roeckner, E., Schmidt, H., Schnur, R., Segschneider, J., Six, K. D., Stockhause, M., Timmreck, C., Wegner, J., Widmann, H., Wieners, K.-H., Claussen, M., Marotzke, J., and Stevens, B. (2013). Climate and carbon cycle changes from 1850 to 2100 in MPI-ESM simulations for the Coupled Model Intercomparison Project phase 5. *Journal of Advances in Modeling Earth Systems*, 5:572–597.

[Goldenberg et al., 2001] Goldenberg, S. B., Landsea, C. W., Mestas-Nuñez, A. M., and Gray, W. M. (2001). The Recent Increase in Atlantic Hurricane Activity: Causes and Implications. *Science*, 293(474).

[Gray et al., 2004] Gray, S. T., Graumlich, L. J., Betancourt, J. L., and Pederson, G. T. (2004). A tree-ring based reconstruction of the Atlantic Multidecadal Oscillation since 1567 A.D. *Geophysical Research Letters*, 31.

[Gulev et al., 2013] Gulev, S. K., Latif, M., Keenlyside, N., Park, W., and Koltermann, K. P. (2013). North Atlantic Ocean control on surface heat flux on multidecadal timescales. *Nature*, 499.

[Hasselmann, 1976] Hasselmann, K. (1976). Stochastic climate models. *Tellus*, XXVIII(6).

[Huang et al., 1998] Huang, N. E., Shen, Z., Long, S. R., Wu, M. C., Shih, H. H., Zheng, Q., Yen, N.-C., Tung, C. C., and Liu, H. H. (1998). The empirical mode decomposition and the Hilbert spectrum for nonlinear and non-stationary time series analysis. *The Royal Society*, 454:903–995.

[Hurrell and Van Loon, 1997] Hurrell, J. W. and Van Loon, H. (1997). Decadal variations in climate associated with the North Atlantic Oscillation. *Climatic Change*, 36:301–326.

[Johnson and Marshall, 2002] Johnson, H. L. and Marshall, D. P. (2002). A theory for the Surface Atlantic Response to Thermohaline Variability. *American Meteorological Society*, 32.

[Jones et al., 1998] Jones, P. D., Briffa, K. R., Barnett, T. P., and Tett, S. F. B. (1998). High-resolution palaeoclimatic records for the last millennium: interpretation, integration and comparison with General Circulation Model control-run High-resolution palaeoclimatic records for the last millennium: interpretation, integration and comparison with General Circulation Model control-run temperatures. *The Holocene*, 8(4):455–471.

[Jungclaus et al., 2012] Jungclaus, J., Giorgetta, M., Reick, C., Legutke, S., Brovkin, V., Crueger, T., Esch, M., Fieg, K., Fischer, N., Glushak, K., Gayler, V., Haak, H., Hollweg, H.-D., Kinne, S., Kornblueh, L., Matei, D., Mauritsen, T., Mikolajewicz, U., Notz, W. M. D., Pohlmann, T., Raddatz, T., Rast, S., Roeckner, E., Salzmann, M., Schmidt, H., Schnur, R., Segschneider, J., Six, K., Stockhause, M., Wegner, J., Widmann, H., Wieners, K.-H., Claussen, M., Marotzke, J., and Stevens, B. (2012). *CMIP5 simulations of the Max Planck Institute for Meteorology (MPI-M) based on the MPI-ESM-P model: The piControl experiment, served by ESGF.* World Data Center for Climate (WDCC).

[Jungclaus et al., 2005] Jungclaus, J. H., Haak, H., Latif, M., and Mikolajewicz, U.

(2005). Arctic-North Atlantic Interactions and Multidecadal Variability of the Meridional Overturning Circulation. *American Meteorological Society*.

[Keenlyside et al., 2008] Keenlyside, N. S., Latif, M., Jungclaus, J., Kornblueh, L., and Roeckner, E. (2008). Advancing decadal-scale climate prediction in the North Atlantic sector. *Nature*, 453.

[Kerr, 2000] Kerr, R. A. (2000). A North Atlantic Climate Pacemaker for the Centuries. *Science*, 288(5473):1984–1985.

[Kilbourne et al., 2014] Kilbourne, K. H., Alexander, M. A., and Nye, J. A. (2014). A low latitude paleoclimate perspective on Atlantic multidecadal variability. *Journal of Marine System*, 133:4–13.

[Knight et al., 2005] Knight, J. R., Allan, R. J., Folland, C. K., Vellinga, M., , and Mann, M. E. (2005). A signature of persistent natural thermohaline circulation cycles in observed climate. *Geophys. Res. Lett.*, 32(L20708).

[Knight et al., 2006] Knight, J. R., Folland, C. K., and Scaife, A. A. (2006). Climate impacts of the Atlantic Multidecadal Oscillation. *Geophys. Res. Lett.*, 33(L17706).

[Kuhlbrodt et al., 2007] Kuhlbrodt, T., Griesel, A., Montoya, M., Levermann, A., Hofmann, M., and Rahmstorf, S. (2007). On the driving process of the Atlantic Meridional Overturning Circulation. *Reviews of Geophysics*, 45(2004RG000166).

[Kushnir, 1994] Kushnir, Y. (1994). Interdecadal Variations in North Atlantic Sea Surface Temperature and Associated Atmospheric Conditions. *American Meteorological Society*.

[Latif et al., 2006] Latif, M., Collins, M., Pohlmann, H., and Keenlyside, N. (2006). A Review of Predictability Studies of Atlantic Sector Climate on Decadal Time Scales. *American Meteorological Society*.

[Latif and Keenlyside, 2011] Latif, M. and Keenlyside, N. S. (2011). A perspective on decadal climate variability and predictability. *Deep-Sea Research*, II(58):1880–1894.

[Latif et al., 2004] Latif, M., Roeckner, E., Botzet, M., Esch, M., Haak, H., Hagemann, S., Jungclaus, J., Legutke, S., Marsland, S., Mikolajewicz, U., and Mitchell, J. (2004). Reconstructing, Monitoring, and Predicting Multidecadal-Scale Changes in the North Atlantic Thermohaline Circulation with Sea Surface Temperature. *American Meteorological Society*, 17.

[Mahajan et al., 2011] Mahajan, S., Zhang, R., and Delworth, T. L. (2011). Impact of the Atlantic Meridional Overturning Circulation (AMOC) on Arctic Surface Air Temperature and Sea Ice Variability. *American Meteorological Society*, 24.

[Mann and Emanuel, 2006] Mann, M. E. and Emanuel, K. A. (2006). Atlantic Hurricane Trends Linked to Climate Change. *EOS, Transaction, American Geophysical Union*, 87(24):233–244.

[Mann and Lees, 1996] Mann, M. E. and Lees, J. M. (1996). Robust estimation of background noise and signal detection in climate time series. *Climatic Change*, 33:409–445.

[Mann and Park, 1999] Mann, M. E. and Park, J. (1999). Oscillatory spatiotemporal signal detection in climate studies: a multiple-taper spectral domain approach. *Advances in Geophysics*, 41.

[Marini and Frankignoul, 2013] Marini, C. and Frankignoul, C. (2013). An attempt to deconstruct the Atlantic Multidecadal Oscillation. *Clim Dyn*.

[Mariotti and Dell'Aquila, 2012] Mariotti, A. and Dell'Aquila, A. (2012). Decadal climate variability in the Mediterranean region: roles of large-scale forcings and regional processes. *Clim Dyn*, 38:1129–1145.

[Marshall et al., 2001] Marshall, J., Johnson, H. L., and Goodman, J. (2001). A Study of the Interaction of the North Atlantic Oscillation with Ocean Circulation. *Journal of Climate*, 14.

[Marullo et al., 2011] Marullo, S., Artale, V., and Santoleri, R. (2011). The SST Multidecadal Variability in the Atlantic-Mediterranean Region and Its Relation to AMO. *American Meteorological Society*, 24.

[McCarthy et al., 2015] McCarthy, G., Smeed, D., Johns, W., Frajka-Williams, E., Moat, B., Rayner, D., Baringer, M., Meinen, C., Collins, J., and Bryden, H. (2015). Measuring the Atlantic Meridional Overturning Circulation at 26 °N. *Progress in Oceanography*, 130:91–111.

[McManus and Oppo, 2006] McManus, J. F. and Oppo, D. W. (2006). The Once and Future Circulation of the Ocean. Clues in seafloor sediments link ocean shifts and climate changes. http://www.whoi.edu/oceanus/feature/the-once-and-future-circulation-of-the-ocean.

[Medhaug and Furevik, 2011] Medhaug, I. and Furevik, T. (2011). North Atlantic 20th century multidecadal variability in coupled climate models: sea surface temperature and ocean overturning circulation. *Ocean Science*, 7:389–404.

[Menary et al., 2015] Menary, M. B., Hodson, D. L. R., Robson, J. I., Sutton, R. T., Wood, R. A., and Hunt, J. A. (2015). Exploring the impact of CMIP5 model biases on the simulation of North Atlantic decadal variability. *Geophysical Research Letters*, 42.

[Msadek et al., 2010] Msadek, R., Dixon, K. W., Delworth, T. L., and Hurlin, W. (2010). Assessing the predictability of the Atlantic meridional overturning circulation and associated fingerprints. *Geophysical Research Letters*, 37.

[Msadek and Frankignoul, 2009] Msadek, R. and Frankignoul, C. (2009). Atlantic multidecadal oceanic variability and its influence on the atmosphere in a climate model. *Clim Dym*, 33:45–62.

[Msadek and Frankignoul, 2010] Msadek, R. and Frankignoul, C. (2010). Mechanisms of the atmospheric response to North Atlantic multidecadal variability: a model study. *Clim Dym*.

[Otterå et al., 2010] Otterå, O. H., Bentsen, M., Drange, H., and Suo, L. (2010). External forcing as a metronome for Atlantic multidecadal variability. *Nature Geosciences*, 3.

[Park and Latif, 2005] Park, W. and Latif, M. (2005). Multidecadal and multicentennial variability of the meridional overturning circulation. *Geophys. Res. Lett.*, 35(L22703).

[Rayner et al., 2003] Rayner, N. A., Parker, D. E., Horton, E. B., Folland, C. K., Alexander, L. V., and Rowell, D. P. (2003). Global analyses of sea surface temperature, sea ice, and night marine air temperature since the late nineteenth century. *Journal of Geophysical Research*, 108(D14).

[Roberts et al., 2013] Roberts, C. D., Garry, F. K., and Jackson, L. C. (2013). A Multi-model Study of Sea Surface Temperature and Subsurface Density Fingerprints of the Atlantic Meridional Overturning Circulation. *Journal of Climate*.

[Ruiz-Barradas et al., 2013] Ruiz-Barradas, A., Nigam, S., and Kavvada, A. (2013). The Atlantic Multidecadal Oscillation in twentieth century climate simulations: uneven progress from CMIP3 to CMIP5. *Clim Dyn*, 41:3301–3315.

[Ruprich-Robert and Cassou, 2014] Ruprich-Robert, Y. and Cassou, C. (2014). Combined influences of seasonal East Atlantic Pattern and North Atlantic Oscillation to excite Atlantic multidecadal variability in a climate model. *Clim Dym*.

[Rykova et al., 2009] Rykova, T., Straneo, F., Lilly, J. M., and Yashayaev, I. (2009). Irminger Current Anticyclones in the Labrador Sea observed in the hydrographic record, 1990-2004. *Journal of Marine Research*, 67(3):361–384.

[Saenger et al., 2009] Saenger, C., Cohen, A. L., Oppo, D. W., Halley, R. B., and Carilli, J. E. (2009). Surface-temperature trends and variability in the low-latitude North Atlantic since 1552. *Nature Geosciences*, 2.

[Schlesinger and Ramankutty, 1994] Schlesinger, M. E. and Ramankutty, N. (1994). An oscillation in the global climate system of period 65-70 years. *Nature*, 367:723–726.

[Sévellec and Fedorov, 2012] Sévellec, F. and Fedorov, A. V. (2012). The Leading, Interdecadal Eigenmode of the Atlantic Meridional Overturning Circulation in a Realistic Ocean Model. *Journal of Climate*, 26.

[Smeed et al., 2015] Smeed, D., McCarthy, G., Rayner, D., Moat, B. I., Johns, W. E., Baringer, M. O., and Meinen, C. S. (2015). Atlantic meridional overturning circu-

lation observed by the RAPID-MOCHA-WBTS (RAPID-Meridional Overturning Circulation and Heatflux Array-Western Boundary Time Series) array at 26N from 2004 to 2014. *British Oceanographic Data Centre - Natural Environment Research Council, UK.*

[Srokosz et al., 2012] Srokosz, M., M. Baringer, H. B., S. Cunningham, T. D., Lozier, S., Marotzke, J., and Sutton, R. (2012). Past, Present, and Future Changes in the Atlantic Meridional Overturning Circulation. *American Meteorological Society.*

[Sutton and Dong, 2012] Sutton, R. T. and Dong, B. (2012). Atlantic Ocean influence on a shift in European climate in the 1990s. *Nature Geosciences*, 5.

[Sutton and Hodson, 2005] Sutton, R. T. and Hodson, D. L. R. (2005). Atlantic Ocean Forcing of North American and European Summer Climate. *Science*, 309(115).

[Taylor et al., 2009] Taylor, K. E., Stouffer, R. J., and Meehl, G. A. (2009). A Summary of the CMIP5 Experiment Design. *PCDMI Rep*, 33.

[Thomson, 1982] Thomson, D. J. (1982). Spectrum Estimation and Harmonic Analysis. *Proceedings of the IEEE*, 70(9):1055–1096.

[Timmermann et al., 1998] Timmermann, A., Latif, M., Voss, R., and Grötzner, A. (1998). Northern Hemispheric Interdecadal Variability: A Coupled Air–Sea Mode. *Journal of Climate*, 11.

[Ting et al., 2014] Ting, M., Kushnir, Y., and Li, C. (2014). North Atlantic Multidecadal SST Oscillation: External forcing versus internal variability. *Journal of Marine System*, 133:27–38.

[Ting et al., 2009] Ting, M., Kushnir, Y., Seager, R., and Li, C. (2009). Forced and Internal Twentieth-Century SST Trends in the North Atlantic. *American Meteorological Society*.

[Ting et al., 2011] Ting, M., Kushnir, Y., Seager, R., and Li, C. (2011). Robust features of Atlantic multi-decadal variability and its climate impacts. *Geophysical Research Letters*, 38.

[Trenberth and Caron, 2001] Trenberth, K. E. and Caron, J. M. (2001). Estimates of Meridional Atmosphere and Ocean Heat Transports. *American Meteorological Society*, 14.

[Trenberth and Shea, 2006] Trenberth, K. E. and Shea, D. J. (2006). Atlantic hurricanes and natural variability in 2005. *Geophysical Research Letters*, 33.

[Vallis, 2010] Vallis, G. K. (2010). Mechanisms of Climate Variability from Years to Decades. *Stochastic Physics and Climate Modelling*.

[Visbeck, 2002] Visbeck, M. (2002). The Ocean's Role in Atlantic Climate Variability. *Science*, 297.

[von Storch and Navarra, 1999] von Storch, H. and Navarra, A. (1999). *Analysis of Climate Variability: Applications of Statistical Techniques*. Springer Science and Business Media.

[von Storch and Zwiers, 1999] von Storch, H. and Zwiers, F. W. (1999). *Statistical analysis in climate research*. Cambridge University Press.

[Wallace et al., 1992] Wallace, J. M., Smith, C., and Bretherton, C. S. (1992). Singular

Value Decomposition of Wintertime Sea Surface Temperature and 500-mb Height Anomalies. *American Meteorological Society*.

[Wang and Zhang, 2013] Wang, C. and Zhang, L. (2013). Multidecadal Ocean Temperature and Salinity Variability in the Tropical North Atlantic: Linking with the AMO, AMOC, and Subtropical Cell. *American Meteorological Society*.

[Wang et al., 2014] Wang, C., Zhang, L., Lee, S.-K., Wu, L., and Mechoso, C. R. (2014). A global perspective on CMIP5 climate model biases. *Nature Climate Change*, 4(3):201–205.

[Wittenberg, 2009] Wittenberg, A. T. (2009). Are historical records sufficient to constrain ENSO simulations? *Geophysical Research Letters*, 36(L12702).

[Wunsch, 2002] Wunsch, C. (2002). What is the thermohaline circulation? *Science*, 298:1180–1181.

[Zanchettin et al., 2014] Zanchettin, D., Bothe, O., Müller, W., Bader, J., and Jungclaus, J. H. (2014). Different flavors of the Atlantic Multidecadal Variability. *Clim Dym*, 42:381–399.

[Zanchettin et al., 2010] Zanchettin, D., Rubino, A., and Jungclaus, J. H. (2010). Intermittent multidecadal-to-centennial fluctuations dominate global temperature evolution over the last millennium. *Geophys. Res. Lett.*, 37(L14702).

[Zhang and Wang, 2013] Zhang, L. and Wang, C. (2013). Multidecadal North Atlantic sea surface temperature and Atlantic meridional overturning circulation variability in CMIP5 historical simulations. *Journal of Geophysical Research: Oceans*, 118:5772–5791.

[Zhang, 2008] Zhang, R. (2008). Coherent surface-subsurface fingerprint of the Atlantic meridional overturning circulation. *Geophysical Research Letters*, 35.

[Zhang, 2010] Zhang, R. (2010). Latitudinal dependence of Atlantic meridional overturning circulation (AMOC) variations. *Geophysical Research Letters*, 37.

[Zhang and Delworth, 2006] Zhang, R. and Delworth, T. L. (2006). Impact of Atlantic multidecadal oscillations on India/Sahel rainfall and Atlantic hurricanes. *Geophysical Research Letters*, 33.

[Zhang et al., 2013] Zhang, R., Delworth, T. L., Sutton, R., Hodson, D. L. R., Dixon, K. W., Held, I. M., Kushnir, Y., Marshall, J., Ming, Y., Msadek, R., Robson, J., Rosati, A. J., Ting, M., and Vecchi, G. A. (2013). Have Aerosols Caused the Observed Atlantic Multidecadal Variability? *American Meteorological Society*.